Enhanced Real-Time Oscilloscopes Ready to Take on Today's Test Challenges p25

p25

Basics of Phase-Locked-Loop Operation in Modern Ultra-Low-Noise Synthesizers p36

Software Models of Resistors, Capacitors, and Inductors Eases Discrete Circuit Design p70

Microwaves & RF®
YOUR TRUSTED ENGINEERING RESOURCE FOR OVER 50 YEARS
DECEMBER 2018 mwrf.com

Fashioning CAVITY FILTERS for 5G

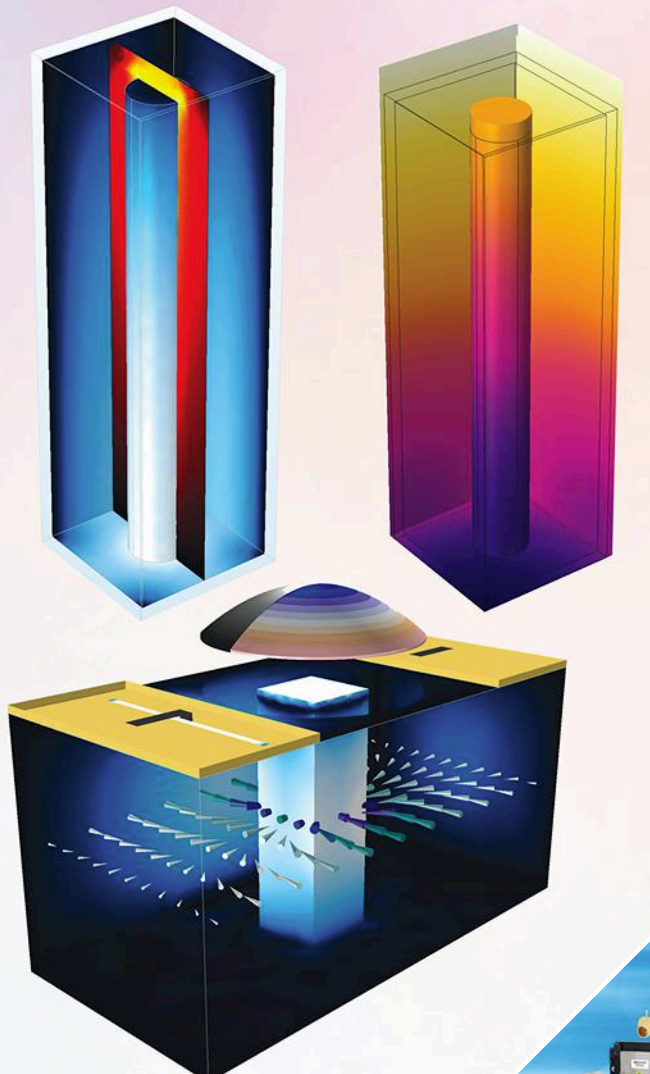

Multiphysics software brings real-world conditions into the design mix p66

$10.00

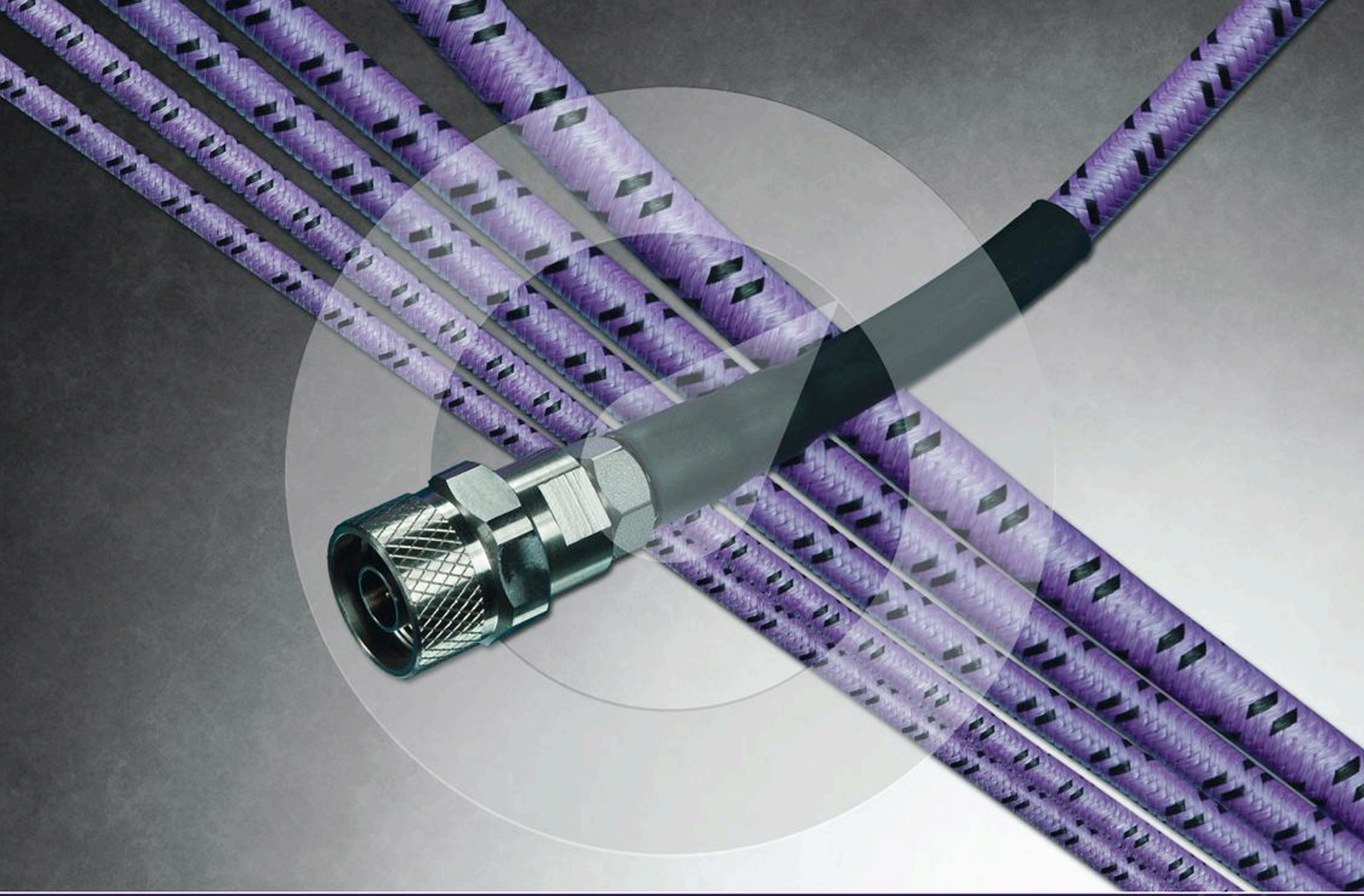

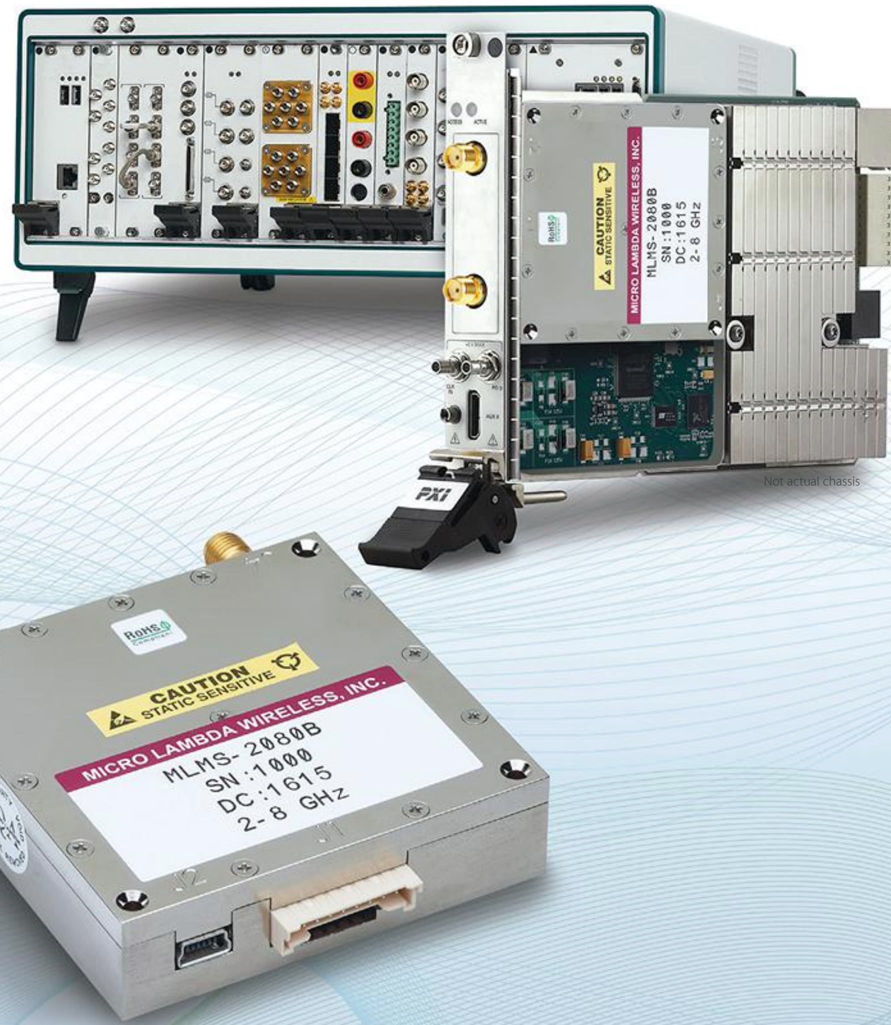

Not actual chassis

RF Amplifiers and Sub-Assemblies for Every Application

Delivery from Stock to 2 Weeks ARO from the catalog or built to your specifications!

- Competitive Pricing & Fast Delivery
- Military Reliability & Qualification
- Various Options: Temperature Compensation, Input Limiter Protection, Detectors/TTL & More
- Unconditionally Stable (100% tested)

ISO 9001:2000 and AS9100B CERTIFIED

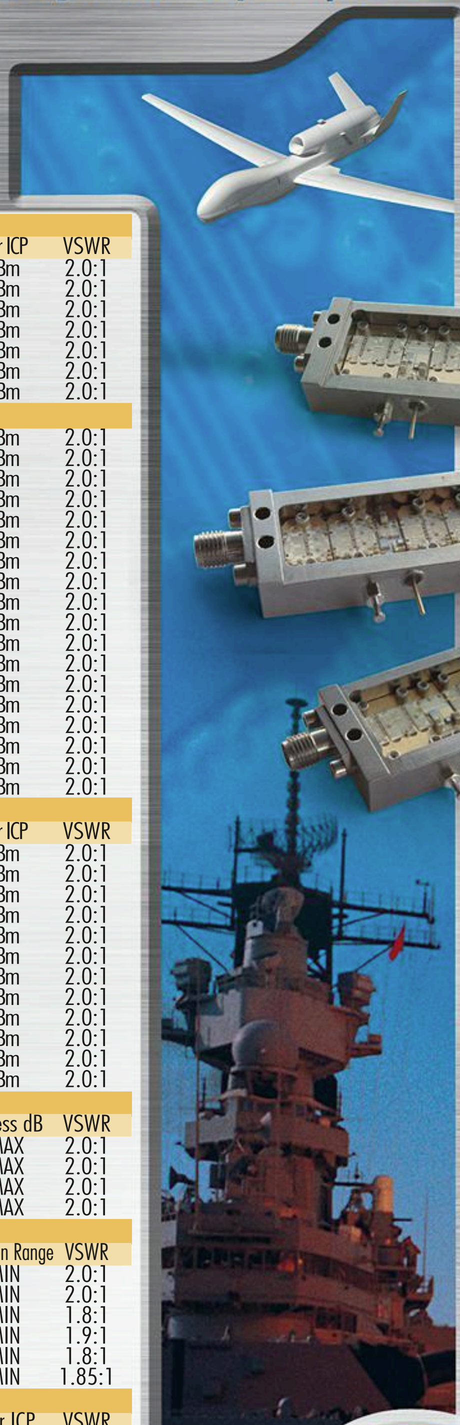

OCTAVE BAND LOW NOISE AMPLIFIERS

Model No.	Freq (GHz)	Gain (dB) MIN	Noise Figure (dB)	Power-out @ P1-dB	3rd Order ICP	VSWR
CA01-2110	0.5-1.0	28	1.0 MAX, 0.7 TYP	+10 MIN	+20 dBm	2.0:1
CA12-2110	1.0-2.0	30	1.0 MAX, 0.7 TYP	+10 MIN	+20 dBm	2.0:1
CA24-2111	2.0-4.0	29	1.1 MAX, 0.95 TYP	+10 MIN	+20 dBm	2.0:1
CA48-2111	4.0-8.0	29	1.3 MAX, 1.0 TYP	+10 MIN	+20 dBm	2.0:1
CA812-3111	8.0-12.0	27	1.6 MAX, 1.4 TYP	+10 MIN	+20 dBm	2.0:1
CA1218-4111	12.0-18.0	25	1.9 MAX, 1.7 TYP	+10 MIN	+20 dBm	2.0:1
CA1826-2110	18.0-26.5	32	3.0 MAX, 2.5 TYP	+10 MIN	+20 dBm	2.0:1

NARROW BAND LOW NOISE AND MEDIUM POWER AMPLIFIERS

Model No.	Freq (GHz)	Gain (dB) MIN	Noise Figure (dB)	Power-out @ P1-dB	3rd Order ICP	VSWR
CA01-2111	0.4 - 0.5	28	0.6 MAX, 0.4 TYP	+10 MIN	+20 dBm	2.0:1
CA01-2113	0.8 - 1.0	28	0.6 MAX, 0.4 TYP	+10 MIN	+20 dBm	2.0:1
CA12-3117	1.2 - 1.6	25	0.6 MAX, 0.4 TYP	+10 MIN	+20 dBm	2.0:1
CA23-3111	2.2 - 2.4	30	0.6 MAX, 0.45 TYP	+10 MIN	+20 dBm	2.0:1
CA23-3116	2.7 - 2.9	29	0.7 MAX, 0.5 TYP	+10 MIN	+20 dBm	2.0:1
CA34-2110	3.7 - 4.2	28	1.0 MAX, 0.5 TYP	+10 MIN	+20 dBm	2.0:1
CA56-3110	5.4 - 5.9	40	1.0 MAX, 0.5 TYP	+10 MIN	+20 dBm	2.0:1
CA78-4110	7.25 - 7.75	32	1.2 MAX, 1.0 TYP	+10 MIN	+20 dBm	2.0:1
CA910-3110	9.0 - 10.6	25	1.4 MAX, 1.2 TYP	+10 MIN	+20 dBm	2.0:1
CA1315-3110	13.75 - 15.4	25	1.6 MAX, 1.4 TYP	+10 MIN	+20 dBm	2.0:1
CA12-3114	1.35 - 1.85	30	4.0 MAX, 3.0 TYP	+33 MIN	+41 dBm	2.0:1
CA34-6116	3.1 - 3.5	40	4.5 MAX, 3.5 TYP	+35 MIN	+43 dBm	2.0:1
CA56-5114	5.9 - 6.4	30	5.0 MAX, 4.0 TYP	+30 MIN	+40 dBm	2.0:1
CA812-6115	8.0 - 12.0	30	4.5 MAX, 3.5 TYP	+30 MIN	+40 dBm	2.0:1
CA812-6116	8.0 - 12.0	30	5.0 MAX, 4.0 TYP	+33 MIN	+41 dBm	2.0:1
CA1213-7110	12.2 - 13.25	28	6.0 MAX, 5.5 TYP	+33 MIN	+42 dBm	2.0:1
CA1415-7110	14.0 - 15.0	30	5.0 MAX, 4.0 TYP	+30 MIN	+40 dBm	2.0:1
CA1722-4110	17.0 - 22.0	25	3.5 MAX, 2.8 TYP	+21 MIN	+31 dBm	2.0:1

ULTRA-BROADBAND & MULTI-OCTAVE BAND AMPLIFIERS

Model No.	Freq (GHz)	Gain (dB) MIN	Noise Figure (dB)	Power-out @ P1-dB	3rd Order ICP	VSWR
CA0102-3111	0.1-2.0	28	1.6 Max, 1.2 TYP	+10 MIN	+20 dBm	2.0:1
CA0106-3111	0.1-6.0	28	1.9 Max, 1.5 TYP	+10 MIN	+20 dBm	2.0:1
CA0108-3110	0.1-8.0	26	2.2 Max, 1.8 TYP	+10 MIN	+20 dBm	2.0:1
CA0108-4112	0.1-8.0	32	3.0 MAX, 1.8 TYP	+22 MIN	+32 dBm	2.0:1
CA02-3112	0.5-2.0	36	4.5 MAX, 2.5 TYP	+30 MIN	+40 dBm	2.0:1
CA26-3110	2.0-6.0	26	2.0 MAX, 1.5 TYP	+10 MIN	+20 dBm	2.0:1
CA26-4114	2.0-6.0	22	5.0 MAX, 3.5 TYP	+30 MIN	+40 dBm	2.0:1
CA618-4112	6.0-18.0	25	5.0 MAX, 3.5 TYP	+23 MIN	+33 dBm	2.0:1
CA618-6114	6.0-18.0	35	5.0 MAX, 3.5 TYP	+30 MIN	+40 dBm	2.0:1
CA218-4116	2.0-18.0	30	3.5 MAX, 2.8 TYP	+10 MIN	+20 dBm	2.0:1
CA218-4110	2.0-18.0	30	5.0 MAX, 3.5 TYP	+20 MIN	+30 dBm	2.0:1
CA218-4112	2.0-18.0	29	5.0 MAX, 3.5 TYP	+24 MIN	+34 dBm	2.0:1

LIMITING AMPLIFIERS

Model No.	Freq (GHz)	Input Dynamic Range	Output Power Range Psat	Power Flatness dB	VSWR
CLA24-4001	2.0 - 4.0	-28 to +10 dBm	+7 to +11 dBm	+/- 1.5 MAX	2.0:1
CLA26-8001	2.0 - 6.0	-50 to +20 dBm	+14 to +18 dBm	+/- 1.5 MAX	2.0:1
CLA712-5001	7.0 - 12.4	-21 to +10 dBm	+14 to +19 dBm	+/- 1.5 MAX	2.0:1
CLA618-1201	6.0 - 18.0	-50 to +20 dBm	+14 to +19 dBm	+/- 1.5 MAX	2.0:1

AMPLIFIERS WITH INTEGRATED GAIN ATTENUATION

Model No.	Freq (GHz)	Gain (dB) MIN	Noise Figure (dB)	Power-out @ P1-dB	Gain Attenuation Range	VSWR
CA001-2511A	0.025-0.150	21	5.0 MAX, 3.5 TYP	+12 MIN	30 dB MIN	2.0:1
CA05-3110A	0.5-5.5	23	2.5 MAX, 1.5 TYP	+18 MIN	20 dB MIN	2.0:1
CA56-3110A	5.85-6.425	28	2.5 MAX, 1.5 TYP	+16 MIN	22 dB MIN	1.8:1
CA612-4110A	6.0-12.0	24	2.5 MAX, 1.5 TYP	+12 MIN	15 dB MIN	1.9:1
CA1315-4110A	13.75-15.4	25	2.2 MAX, 1.6 TYP	+16 MIN	20 dB MIN	1.8:1
CA1518-4110A	15.0-18.0	30	3.0 MAX, 2.0 TYP	+18 MIN	20 dB MIN	1.85:1

LOW FREQUENCY AMPLIFIERS

Model No.	Freq (GHz)	Gain (dB) MIN	Noise Figure dB	Power-out @ P1-dB	3rd Order ICP	VSWR
CA001-2110	0.01-0.10	18	4.0 MAX, 2.2 TYP	+10 MIN	+20 dBm	2.0:1
CA001-2211	0.04-0.15	24	3.5 MAX, 2.2 TYP	+13 MIN	+23 dBm	2.0:1
CA001-2215	0.04-0.15	23	4.0 MAX, 2.2 TYP	+23 MIN	+33 dBm	2.0:1
CA001-3113	0.01-1.0	28	4.0 MAX, 2.8 TYP	+17 MIN	+27 dBm	2.0:1
CA002-3114	0.01-2.0	27	4.0 MAX, 2.8 TYP	+20 MIN	+30 dBm	2.0:1
CA003-3116	0.01-3.0	18	4.0 MAX, 2.8 TYP	+25 MIN	+35 dBm	2.0:1
CA004-3112	0.01-4.0	32	4.0 MAX, 2.8 TYP	+15 MIN	+25 dBm	2.0:1

CIAO Wireless can easily modify any of its standard models to meet your "exact" requirements at the Catalog Pricing.

Visit our web site at **www.ciaowireless.com** for our complete product offering.

Ciao wireless

Ciao Wireless, Inc. 4000 Via Pescador, Camarillo, CA 93012

Tel (805) 389-3224 Fax (805) 389-3629 sales@ciaowireless.com

December 2018 VOLUME 57, ISSUE 12 Microwaves&RF

IN THIS ISSUE

25

FEATURES

66

NEWS & COLUMNS

PRODUCTS & TECHNOLOGY

69

JOIN US ONLINE

follow us @MicrowavesRF

become a fan at facebook.com/microwavesRF

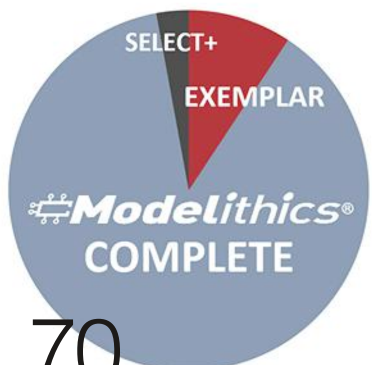

70

78

defense electronics

Starts on page **45**

10 MHz Distribution Amplifiers

- Sine wave outputs (+13dbm)
- Amplitude leveling
- Low additive phase noise
- High channel-to-channel isolation
- High return loss

***FS730 and FS735 series ... starting at $1250** (U.S. list)*

The FS730 and FS735 10 MHz distribution amplifiers from SRS provide state-of-the-art solutions to challenging signal distribution tasks.

These distribution amplifiers use an input limiter design, which removes amplitude modulation from the signal, provides fixed amplitude outputs and blocks input noise. Virtually any 10 MHz waveform with a duty cycle near 50% may be used as an input.

The FS735 model provides fourteen 10 MHz output BNC connectors on the rear panel, with status indicators on the front panel. The half-rack sized FS730 model gives seven 10 MHz outputs and is available in both bench-top and rack-mount forms.

With mix and match capability, the FS735 can also be configured with 10 MHz, 5 MHz, Broadband, and CMOS Logic distribution amplifiers side-by-side for other applications. Multiple units can be daisy-chained for easy expansion.

Please visit www.thinkSRS.com for details.

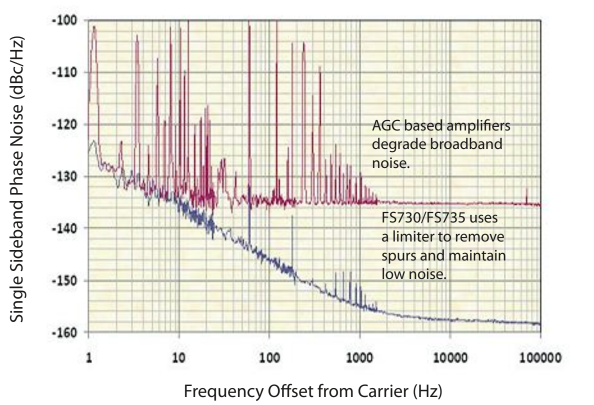

Additive phase noise in 10 MHz Distribution Amplifiers: Limiter vs. AGC Designs

SRS Stanford Research Systems

(408)744-9040
www.thinkSRS.com

Fast Pulse Test Systems from Avtech

Avtech offers over 500 standard models of high-speed pulsers, drivers, and amplifiers ideal for both R&D and automated factory-floor testing. Some of our standard models include:

AVR-E3-B: 500 ps rise time, 100 Volt pulser

AVRQ-5-B: Optocoupler CMTI tests, >120 kV/us

AVO-8D3-B: 500 Amp, 50 Volt pulser

AV-1010-B: General purpose 100V, 1 MHz pulser

AVO-9A-B: 200 ps t_r, 200 mA laser diode driver

AV-156F-B: 10 Amp current pulser for airbag initiator tests

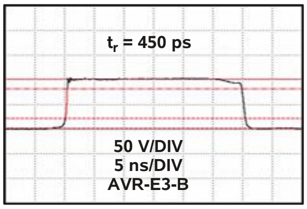

Nanosecond Electronics
Since 1975

Pricing, manuals, datasheets and test results at:
www.avtechpulse.com

AVTECH ELECTROSYSTEMS LTD.
Tel: +1-613-686-6675 Fax: +1-613-686-6679
info@avtechpulse.com

High Output - Low Risetime Pulsers from Avtech

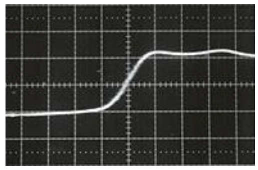

Sub-nanosecond rise time pulsers for every amplitude range!

Model AVP-3SA-C provides up to 10V with < 50 ps rise times.
← Typical waveform, 50 ps/div, 5V/div.

At the other extreme, Model AVI-V-HV2A-B provides up to 100V with < 300 ps rise times.

Ampl	t_{RISE}	Max. PRF	Model
100 V	500 ps	0.1 MHz	AVR-E3-B
100 V	300 ps	0.02 MHz	AVI-V-HV2A-B
50 V	500 ps	1 MHz	AVR-E5-B
20 V	200 ps	10 MHz	AVMR-2D-B
15 V	100 ps	25 MHz	AVM-2-C
15 V	150 ps	200 MHz	AVN-3-C
10 V	100 ps	1 MHz	AVP-AV-1-B
10 V	50 ps	1 MHz	AVP-3SA-C
5 V	40 ps	1 MHz	AVP-2SA-C

Nanosecond Electronics
Since 1975

Pricing, manuals, datasheets and test results at:
www.avtechpulse.com/

AVTECH ELECTROSYSTEMS LTD.
Tel: +1-613-686-6675 Fax: +1-613-686-6679
info@avtechpulse.com

Pulsed Laser Diode Drivers from Avtech

Each of the 19 models in the Avtech **AVO-9 Series** of pulsed laser diode drivers includes a replaceable output module with an ultra-high-speed socket, suitable for use with sub-nanosecond pulses.

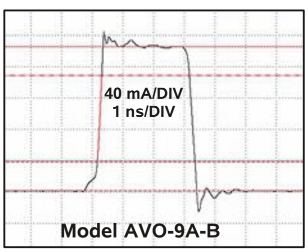

Models with maximum pulse currents of 0.1A to 10A are available, with pulse widths from 400 ps to 1 us.

GPIB, RS-232, and Ethernet control available.

Nanosecond Electronics
Since 1975

Pricing, manuals, datasheets and test results at:
www.avtechpulse.com/laser

AVTECH ELECTROSYSTEMS LTD.
Tel: +1-613-686-6675 Fax: +1-613-686-6679
info@avtechpulse.com

100 to 1000 Volt Lab Pulsers

Avtech offers a full line of 100, 200, 500, 700 and 1000 Volt user-friendly pulsers capable of driving impedances of 50 Ω and higher. The **AVR Series** is suitable for semiconductor and laser diode characterization, time-of-flight applications, attenuator testing, and other applications requiring 10, 20, or 50 ns rise times, pulse widths from 100 ns to 100 us, and PRFs up to 100 kHz. GPIB & RS-232 ports are standard, VXI Ethernet is optional.

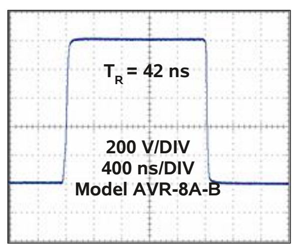

See additional test results at:
http://www.avtechpulse.com/medium

Nanosecond Electronics
Since 1975

Pricing, manuals, datasheets and test results at:
www.avtechpulse.com/medium

AVTECH ELECTROSYSTEMS LTD.
Tel: +1-613-686-6675 Fax: +1-613-686-6679
info@avtechpulse.com

ON MICROWAVES&RF.COM

Algorithms to Antenna: Waveforms for 5G, 802.11ax, and NB-IoT

System modeling and simulation for 5G, 802.11ax, and Narrowband-IoT can benefit significantly when adding waveform building blocks to the mix.

https://www.mwrf.com/systems/algorithms-antenna-waveforms-5g-80211ax-and-nb-iot

Average Power Sensors Don't Settle for Average Performance

Microwaves & RF's Chris DeMartino got his hands on a new series of average power sensors from a company that's been in the business for a long time. Did they measure up?

https://www.mwrf.com/test-measurement/average-power-sensors-don-t-settle-average-performance

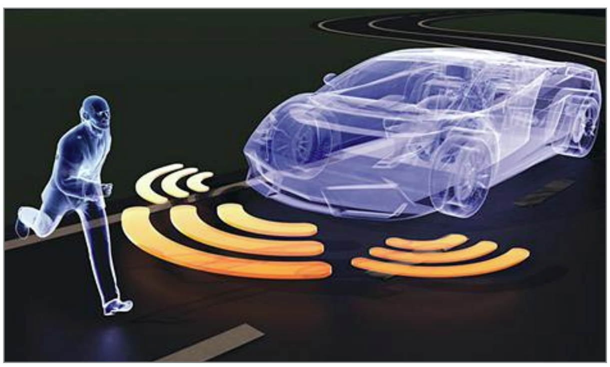

Circuit Materials Secure Automotive Safety Systems

Future automotive electronic safety systems based on radar and wireless communications will rely heavily on printed antennas, and circuit materials will play a key role in their creation.

https://www.mwrf.com/materials/circuit-materials-secure-automotive-safety-systems

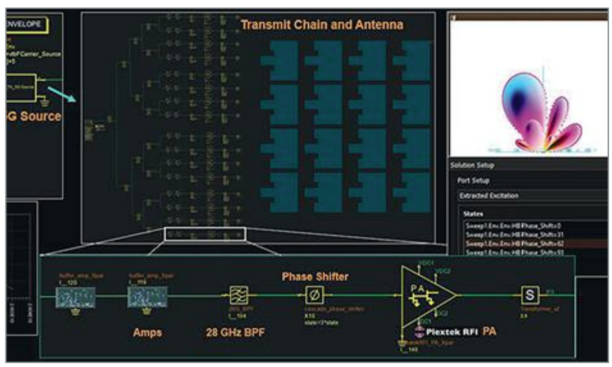

Dissecting a 5G 28-GHz Phased-Array Transmit Chain

Keysight Technologies' Jack Sifri presents the design, simulation, and analysis of a 5G 28-GHz phased-array transmit chain, implementing electromagnetic circuit excitation and co-simulation.

https://www.mwrf.com/software/dissecting-5g-28-ghz-phased-array-transmit-chain

EDITORIAL

EXECUTIVE DIRECTOR, CONTENT: **KAREN FIELD** karen.field@informa.com
TECHNICAL CONTRIBUTOR: **JACK BROWNE** jack.browne@informa.com
TECHNICAL ENGINEERING EDITOR: **CHRIS DeMARTINO** chris.demartino@informa.com
ASSOCIATE EDITOR/COMMUNITY MANAGER: **ROGER ENGELKE** roger.engelke@informa.com
ASSOCIATE EDITOR/COMMUNITY MANAGER: **JEREMY COHEN** jeremy.cohen@informa.com
ASSOCIATE CONTENT PRODUCER: **JAMES MORRA** james.morra@informa.com

ART DEPARTMENT

GROUP DESIGN DIRECTOR: **ANTHONY VITOLO** tony.vitolo@informa.com
CONTENT DESIGN SPECIALIST: **JOCELYN HARTZOG** jocelyn.hartzog@informa.com
CONTENT & DESIGN PRODUCTION MANAGER: **JULIE JANTZER-WARD** julie.jantzer-ward@informa.com

PRODUCTION

GROUP PRODUCTION MANAGER: **GREG ARAUJO** greg.araujo@informa.com
PRODUCTION MANAGER: **VICKI McCARTY** vicki.mccarty@informa.com

AUDIENCE MARKETING

USER MARKETING MANAGER: **DEBBIE BRADY** debbie.brady@informa.com

FREE SUBSCRIPTION / STATUS OF SUBSCRIPTION / ADDRESS CHANGE/ MISSING BACK ISSUES:
OMEDA **T** | 847.513.6022 **TOLL FREE** | 866.505.7173

SALES & MARKETING

MANAGING DIRECTOR: **TRACY SMITH** **T** | 913.967.1324 **F** | 913.514.6881 tracy.smith@informa.com

REGIONAL SALES REPRESENTATIVES:

AZ, NM, TX: **GREGORY MONTGOMERY** **T** | 480.254.5540 gregory.montgomery@informa.com

AK, NORTHERN CA, OR, WA, WESTERN CANADA: **STUART BOWEN** **T** | 425.681.4395 stuart.bowen@informa.com

AL, AR, SOUTHERN CA, CO, FL, GA, HI, IA, ID, IL, IN, KS, KY, LA, MI, MN, MO, MS, MT, NC, ND, NE, NV, OH, OK, SC, SD, TN, UT, VA, WI, WV, WY, CENTRAL CANADA: **JAMIE ALLEN** **T** | 415.608.1959 **F** | 913.514.3667 jamie.allen@informa.com

CT, DE, MA, MD, ME, NH, NJ, NY, PA, RI, VT, EASTERN CANADA:
ELIZABETH ELDRIDGE **T** | 917-789-3012 elizabeth.eldridge@informa.com

INTERNATIONAL SALES:

GERMANY, AUSTRIA, SWITZERLAND: **CHRISTIAN HOELSCHER** **T** | 011.49.89.95002778
christian.hoelscher@husonmedia.com

BELGIUM, NETHERLANDS, LUXEMBURG, UNITED KINGDOM, SCANDINAVIA, FRANCE, SPAIN, PORTUGAL:
JAMES RHOADES-BROWN **T** | +011 44 1932 564999 **M** | +011 44 1932 564998 james.rhoadesbrown@husonmedia.com

ITALY: **DIEGO CASIRAGHI** diego@casiraghi-adv.com

PAN-ASIA: **HELEN LAI** **T** | 886 2-2727 7799 helen@twoway-com.com

PAN-ASIA: **CHARLES LIU** **T** | 886 2-2727 7799 liu@twoway-com.com

PLEASE SEND INSERTION ORDERS TO: orders@informa.com

INFORMA REPRINTS: **WRIGHT'S MEDIA** **T** | 877.652.5295

LIST RENTALS/ SMARTREACH CLIENT SERVICES MANAGER: **MARY RALICKI** **T** | 212.204.4284
mary.ralicki@informa.com

DIGITAL

GROUP DIGITAL DIRECTOR: **RYAN MALEC** ryan.malec@informa.com

DESIGN ENGINEERING & SOURCING GROUP

EXECUTIVE DIRECTOR, CONTENT: **KAREN FIELD** karen.field@informa.com
VP OF MARKETING: **JACQUIE NIEMIEC** jacquie.niemiec@informa.com

INFORMA MEDIA INC.

605 THIRD AVENUE
NEW YORK, NY 10158 USA **T** | 212.204.4200

informa

Electronic Design | Machine Design | Microwaves & RF | Source ESB | Hydraulics & Pneumatics |
Global Purchasing | Distribution Resource | Power Electronics | Defense Electronics

MILLIMETER WAVE

MMIC

PRODUCTS

MULTI-OCTAVE BANDWIDTHS
UP TO 43.5 GHz

Attenuators | Couplers | Mixers
Multipliers | Reflectionless Filters | Splitter/Combiners

Now over 60 MMIC models *In Stock*
covering applications above 26 GHz

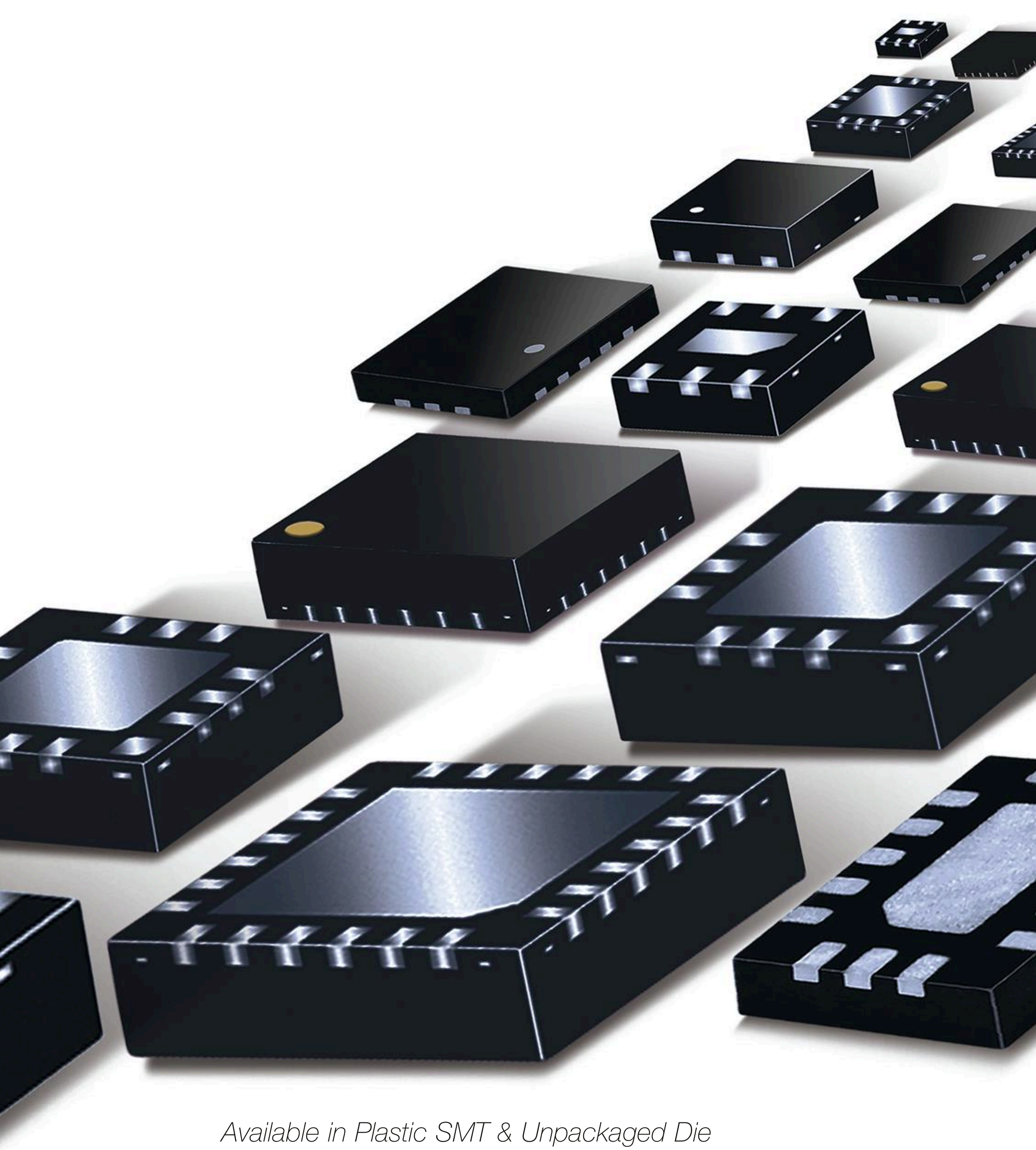

Available in Plastic SMT & Unpackaged Die

Mini-Circuits®

Editorial

CHRIS DeMARTINO | Technical Editor
chris.demartino@informa.com

Will You Own a 5G Smartphone in 2019?

As we finish 2018 and look to 2019, you're probably fully aware of the massive amount of attention geared toward 5G. Those who have been staying up-to-date surely heard plenty enough about it over the last few years. Now, though, it seems like all the hoopla is turning into reality.

So, what can we expect to see in 2019 regarding 5G? In a recent interview with *Microwaves & RF*, James Kimery, director of marketing at National Instruments (NI; *www.ni.com*) stated, "5G has unstoppable momentum and initial 5G deployments will start in 2019." He also noted, "Most initial deployments may be on sub-6-GHz bands, but there will be some fixed wireless use cases using millimeter-wave (mmWave) technologies."

The "unstoppable momentum" mentioned by Kimery is evidenced by the expected availability of 5G smartphones in 2019. Companies like Samsung, LG, Huawei, and more are expected to launch these phones. Will you be holding a 5G smartphone in your hands in 2019? If you pay attention to the news, there's a good chance of that happening (except for my colleague Jack Browne, who still refuses to own a cell phone!).

While it may be exciting to see 5G smartphones in 2019, the question is what frequencies will these devices utilize? Specifically, when will the mmWave bands that we've heard so much about really make a big impact? The answer is maybe sooner than you think.

Verizon and Samsung recently announced a successful data transmission using 800 MHz of bandwidth at 28 GHz, resulting in a maximum throughput of almost 4 Gb/s. This news certainly highlights what mmWave bands can bring to the table.

"The demonstration using a 5G New Radio (NR) compliant system for both the Samsung gNB and NI test UE demonstrates that 5G NR mmWave has much potential to realize the data-rate goals set forth by the IMT-2020 and the 3GPP for the enhanced mobile broadband (eMBB) case," said Kimery. "This real-world demonstration clearly shows that mmWave is real and that these impressive data rates are achievable."

In any case, even if we have to wait a little bit longer to see mmWave frequencies make a significant impression in this space, the thought of owning a 5G smartphone is sure to interest plenty of people out there (of course, except for Jack!). mw

News

ADVANCED SIMULATION FEATURE
Combines Best of Both Worlds

When discussing simulation software, ANSYS *(www.ansys.com)* is likely one of the first companies that comes to mind. Throughout the RF/microwave industry, engineers take advantage of ANSYS's HFSS, a well-known 3D electromagnetic (EM) simulation software tool. But HFSS is not the only entry in ANSYS's portfolio.

Another significant product is SIwave, which is a design platform that's intended to analyze printed circuit boards (PCBs) and packages. With SIwave, designers can analyze aspects like power and ground planes and long transmission lines.

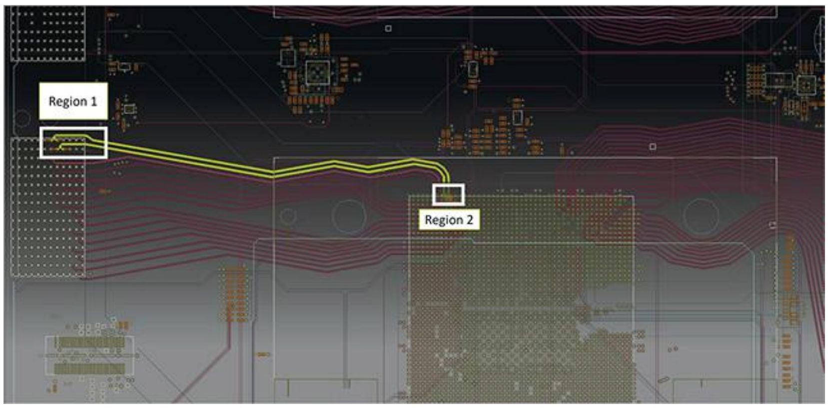

This illustration reveals two defined HFSS regions in a PCB design.

ANSYS recently introduced a new feature that combines SIwave with HFSS. With this solution, engineers can define what's known as HFSS regions inside of SIwave *(see figure)*. This hybrid technique merges SIwave's fast 2.5D solver with the HFSS 3D solver, thereby increasing the accuracy of the S-parameters of critical nets on a PCB.

"Using HFSS regions in SIwave enables engineers to define regions of a PCB," explains Denis Soldo, director at ANSYS. "These regions can be very complex—for instance, via breakouts, connector breakouts, and even bond wires in a package. So, for anything that's 3D in nature, users are able to define a region of interest.

"All necessary ports and boundaries are automatically created and assigned. The HFSS 3D finite-element-method (FEM) engine is then called upon to specifically solve for that region of interest. All the results are then automatically back-annotated into SIwave for a complete simulation."

This hybrid solution is extremely beneficial—it essentially combines accuracy with fast results. Soldo adds, "We are basically combining two different engines: full 3D FEM for 3D regions and the method-of-moments (MoM) transmission line solver in SIwave for simulating long transmission lines. In today's world, you can think of a typical server board with 30 to 40 layers with frequencies of interest ranging from 10 to 20 GHz. This is going to be an extremely large problem electrically—you're talking about thousands of wavelengths. Simulating this with even a supercomputer could take days or weeks. By combining SIwave and HFSS, we basically provide engineers with the best of both worlds. The result is fast and extremely accurate simulation results."

Thanks to advances made by ANSYS, a much more automated process can be achieved versus typical methods utilized in the past. "In the past, engineers would use a 'divide-and-conquer approach,' which is very manual in nature," says Soldo. "Of course, they would identify regions of interest. You could have a differential via pair and manually cut it out. This would be simulated to obtain results—usually in a touchstone format. Then you'd run a transmission line solver or a circuit solver for a signal net. You'd also include a connector-breakout region, run another 3D simulation, etc.

"In the end, you would end up with three, four, or five different data sets. Then, you would manually stick all of this together in a circuit simulator and run a transient simulation to look at the overall transient performance. This is a typical 'divide-and-conquer' approach. Now, that's all fully automated in SIwave with automatic region assignments and HFSS being called in the background."

ANSYS has performed extensive analysis to determine the effectiveness of this hybrid approach at higher frequencies. Soldo adds, "We have done extensive internal testing and data comparisons between SIwave-only simulations and this enhanced approach that involves SIwave combined with HFSS regions. Up to 8 GHz, we have observed that there's not much of a difference in the results. However, at higher data rates and higher frequencies (i.e., above 10 GHz), we have observed the difference in the results. Those via transitions and connector breakouts make an impact at higher frequencies—and this is why 3D accuracy is definitely required for these types of simulations." ■

THIS TOOLBOX Holds Your 5G Gear

ONE COMPANY ON the front line of wireless communications is MathWorks *(www.mathworks.com)*, demonstrated by products like the LTE Toolbox, WLAN Toolbox, and more. Now, following the completion of the 3GPP Release 15 5G New Radio (NR) standard in June 2018, MathWorks has expanded its portfolio with the recent introduction of the 5G Toolbox.

5G will differ from 4G LTE in the types of markets it will reach. "One of the big differences with 5G is that it will go beyond mobile wireless communications," says Ken Karnofsky, senior strategist for signal processing applications at MathWorks. "5G will extend to machine-to-machine (M2M) and vehicle-to-vehicle

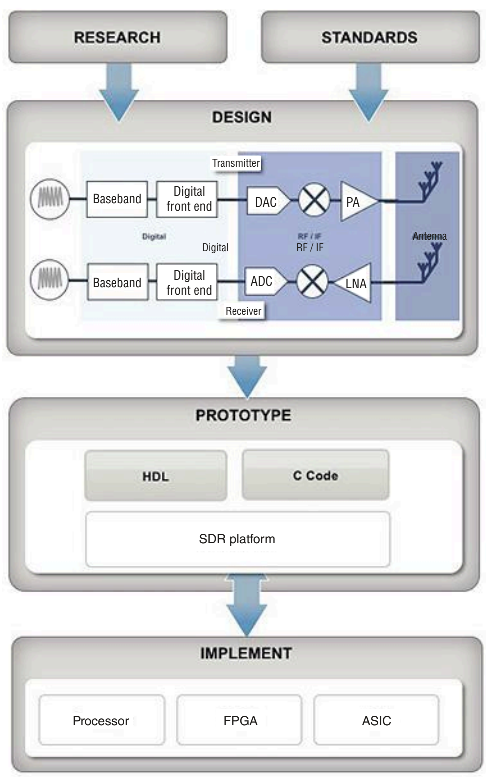

(V2V) scenarios, facilitating lower power and low latency."

Of course, other factors set 5G apart from 4G LTE, too. "The 5G standard itself really specifies the baseband processing that actually constructs the signals and handles some of the network protocols," explains Karnofsky. "The baseband physical layer is quite different than LTE in many ways. And we really see a lot of differences in the radio front-end architectures. That includes the RF components along with the antennas and antenna arrays. With aspects like massive MIMO and millimeter-wave (mmWave) operation, we're hearing from customers that the design approach is really changing."

INTRODUCING THE 5G TOOLBOX

The points mentioned highlight some of the challenges associated with creating and verifying 5G prototype systems. To help designers overcome these hurdles, MathWorks developed the 5G Toolbox. The 5G Toolbox comes equipped with standard-compliant functions and reference examples to help designers model, simulate, and verify 5G systems. It supports end-to-end link-level simulation, waveform generation and analysis, and golden reference-design verification and conformance testing.

Designers can take advantage of the 5G Toolbox to generate standard-compliant waveforms for 5G NR specifications based on NR subcarrier spacings and frame numerologies. Link-level simulations can be performed with transmitter, channel model, and receiver operations. And designers are able to analyze link performance by computing bit-error-rate (BER) and throughput metrics.

In addition, the 5G Toolbox allows for the configuration and generation of 5G NR downlink signals and channels. It also enables users to perform end-to-end block-error rate (BLER) simulations with the help of 5G NR clustered delay line (CDL) and tapped delay line (TDL) propagation-channel models. Another feature is open, customizable algorithms, which can be used as golden references for design verification. On top of that, it's possible to generate C code from open MATLAB algorithms. ■

The tools in MathWorks' 5G Toolbox can form the foundation of a workflow for designing and testing 5G products.

WAVEGUIDE SOURCE GENERATES 160- to 210-GHz Noise

Growing use of millimeter-wave (mmWave) frequencies for wireless communications is a highly touted part of 5G wireless communications systems, notably at 28, 60, and 77 GHz. But at even higher frequencies, mmWave and sub-mmWave remote sensing techniques are vital to atmospheric measurements due to the water-vapor absorption line around 183 GHz. This makes the G-band range from 160 to 210 GHz of interest to scientists and researchers with an eye to the weather.

In support of those scientists, circuit/device designers at NASA Goddard Space Flight Center (Greenbelt, Md.) developed a waveguide mmWave noise source for use at G-band frequencies. The noise source, with a center frequency of 183 GHz, was designed onto a quartz substrate implemented by means of microstrip and waveguide transmission-line technologies. It combines a Schottky-diode chip noise source within a waveguide package. It features a lowpass filter as part of the biasing of diodes without high-frequency interference, a back-short designed at the center frequency of 183 GHz with viaholes, and a longitudinal chip/waveguide probe.

The back-short structure is included in the microstrip circuitry because of the nature of how Schottky diodes generate noise. When reverse-biased, a Schottky diode will generate noise from both terminals and in both directions of the connected microstrip circuitry, thus requiring something to direct all of the noise in the desired direction.

The back-short structure accomplishes this by reflecting all noise in the unwanted direction and adding it in phase with the outgoing noise to achieve a higher output noise level from the noise source. For this noise source design, the RF back-short consists of a capacitive delay transmission line with phase delays of 180 deg. at 184 GHz, 160 deg. at 191 GHz, and −160 deg. at 176 GHz. The back-short is constructed with multiple viaholes to support heat flow away from the diodes, so that continuous operation of the diodes (and not just pulsed operation) is possible.

Measurements were made in a 50-Ω test environment, comparing results with the noise diode powered on and looking at a room-temperature target as well as a cold target, and with the noise diode turned off with the same parameters. The calculated excess noise ratio (ENR) of the noise diode was found to be about 10 dB at 200 GHz, although with proper impedance matching, it was felt that the noise output could be improved by another 3 dB.

The technology has obvious merit for generating usable noise outputs at mmWave and sub-mmWave frequencies for deep-space exploration. NASA is seeking licensees to commercialize this technology. For more information, contact the Goddard Strategic Partnerships Office at techtransfer@gsfc.nasa.gov or (301) 286-5810.

See: "A Robust Waveguide Millimeter-Wave Source," *Tech Briefs*, November 2018, Vol. 42, No. 11, p. 44.

ADDING ANTENNAS Without Penalties

MOBILE COMMUNICATIONS DEVICES are carrying more of the loads of each user's voice, video, and data information, even as those devices continue moving while in service. Several researchers examined the long-standing paradox of how to continue to add antennas for different purposes to mobile devices, even as those devices continued to be made smaller and lighter. The researchers suggest the need for a new approach to antenna design, one that does not limit the number of antennas to a placement around a mobile device or because of the small size of a mobile device.

Current 4G Long Term Evolution (LTE) cell-phone handsets are equipped with as many as six to eight different antennas to handle 4G LTE in addition to wireless signals from Bluetooth, Wi-Fi, and Global Positioning System (GPS) equipment. With the coming of 5G mobile devices and their extensions to mmWave frequency bands, even more antennas will be needed per mobile device. This creates design challenges on where to position the antennas so that they provide high-performance levels without interfering with the antenna or antennas alongside them.

Such a growing variety of functions in 4G LTE handsets has created a need for creative antenna design and placement to serve the many functions. It will become even more challenging in 5G handsets and other compact wireless products, such as Internet of Things (IoT) devices. Researchers from Smart Antennas Technologies (Birmingham, England) have sought to avoid interference by using filtering, directional antennas, and pointing them away from each other; they also employ antenna polarization where practical to minimize interference among closely spaced antennas. The researchers have also found that by using precise manufacturing methods, such as laser direct structuring, it's possible to create complex plastic shapes and fabricate the antenna circuits on top of those plastic structures to achieve small size and efficiency, helping to fit multiple antennas into small handset packages.

See "Solving the Antenna Paradox," *IEEE Spectrum*, November 2018, p. 40.

BRIG ASAY | Director Strategic Planning, Internet Infrastructure Group, Keysight Technologies
www.keysight.com

Real-Time Oscilloscopes Bridge the Measurement Gap

Technology improvements to real-time oscilloscopes, such as 110-GHz bandwidths, have given rise to their significance in terms of meeting today's test challenges.

Today's technologies continue to reach higher frequencies and wider bandwidths. Take, for instance, 5G in the U.S.—it will utilize 28- and 39-GHz frequency bands with 1.2 GHz of bandwidth. The IEEE 802.11ay standard makes use of frequencies between 60 and 70 GHz with 2-GHz bandwidths. Satellite-communication (satcom) systems routinely extend beyond 70 GHz with bandwidths greater than 5 GHz. The list of these emerging high-frequency and high-bandwidth technologies grows every year.

While it's exciting to think about the possibilities surrounding millimeter-wave (mmWave) frequencies and above, advances such as these stress the overall capabilities of today's test-and-measurement equipment. To truly show that the technology is working, one must measure it. Test-and-measurement instrument classes such as spectrum analyzers have limitations above 50 GHz, which necessitates finding another option to test at these high frequencies.

One class of instrument that's gaining traction is the real-time oscilloscope. While rarely considered in the past, real-time oscilloscopes continue to make major strides in terms of both bandwidth and signal integrity performance, and thus could be an excellent choice for emerging markets among RF instruments.

1. Keysight's UXR0134A Infiniium UXR-Series oscilloscope is a four-channel model with a bandwidth of 13 GHz.

THE EASY SPECIFICATION TO CONSIDER: BANDWIDTH

The first and most important specification centers around having the bandwidth to make measurements at very high frequencies (i.e., above 50 GHz). As recently as 2010, oscilloscope bandwidths were limited to just 30 GHz. Of course, that bandwidth spans dc to 30 GHz, so even as early as 2010 one could measure very wide bands with an oscilloscope. Unfortunately, reaching frequencies greater than 30 GHz required a downconverter. Extra calibration was also needed to remove loss and maintain a flat magnitude.

Over the last decade, though, things have changed. Around 2015, both 70- and 100-GHz oscilloscopes were introduced. And in 2018, Keysight introduced the 110-GHz bandwidth UXR-Series oscilloscope *(Fig. 1)*. With the UXR-Series, it's possible to directly digitize frequencies as high as 110 GHz. One notable point concerning the UXR-Series is that it's the first real-time oscilloscope to employ full-bandwidth preamplifier and sampling chip designs, which is attributed to Keysight's proprietary indium-phosphide (InP) technology. Other oscilloscopes must use a form of time interleaving to achieve high bandwidths, but this comes with signal-integrity tradeoffs.

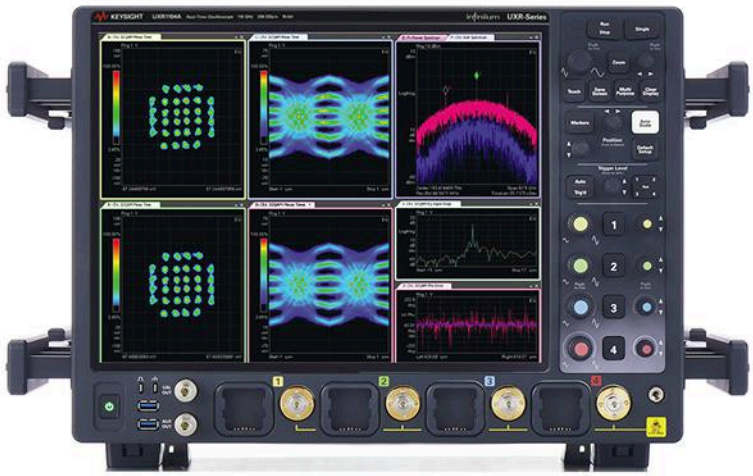

2. Shown is a UXR1104A Infiniium UXR-Series oscilloscope performing a 32-QAM optical signal analysis.

THE GROWING IMPORTANCE OF MIMO

Consumers are demanding seamless integration between mobile networks and Wi-Fi networks, with an insatiable demand for more bandwidth and faster throughput. Consumers want better performance in crowds and densely populated centers. To address these needs, technologies such as multiple-input, multiple-output (MIMO) and beamforming are making their way to the market in an accelerated fashion. MIMO, by definition, means more than one input and more than one output. The latest technology news has mentioned channel densities as high as 64 channels. However, the need for a four-channel density exists right now.

Suddenly, the real-time oscilloscope becomes important: One of its major advantages is that it naturally comes with more than one channel. Real-time oscilloscopes are typically found as two- or four-channel models. Even more crucial than the channel count is the fact that real-time oscilloscopes offer channel-to-channel calibrations as standard features. As an example, UXR-Series instruments attain channel-to-channel skew inside the box of less than 75 fs. This capability contrasts with tying multiple individual instruments together using a local oscillator (LO).

Other instruments employ a modular form factor, offering the ability to tie as many as 32 channels together. The UXR-Series oscilloscopes offer the same capability—but in a more standard box format. Thus, oscilloscopes can now meet the needs for high-frequency coverage, wide bandwidths, and multiple channels in a single box.

THAT'S GREAT—BUT WHAT ABOUT SPURIOUS AND OTHER KEY MEASUREMENTS?

Real-time oscilloscopes have always been a natural fit when it comes to bandwidths and channel count. However, their problem is linked to RF performance, which has never been good enough. Specifications like error vector magnitude (EVM), spurious-free dynamic range (SFDR), and effective number of bits (ENOB) have paled in comparison to other RF instruments. However, real-time oscilloscopes continue to improve in terms of RF performance, which begins with the analog-to-digital converters (ADCs) they employ.

For the last 20 years or so, 8-bit ADCs have dominated the real-time oscilloscope world. This limits the overall dynamic range of the scope in comparison to the 12- and 14-bit ADCs exploited by other RF instruments. In 2014, Keysight introduced the S-Series oscilloscope family, which marked the first time the company employed a 10-bit ADC in a real-time scope. Unfortunately, the scope was limited in bandwidth to only 8 GHz. However, the company had a 10-bit platform that could be leveraged above 8 GHz.

The recently introduced UXR-Series oscilloscopes now take that 10-bit ADC technology to 110-GHz bandwidths and 256-Gsample/s sampling rates. While 10 bits is better than eight bits, it still doesn't reach the performance of historical RF instrumentation. Enter oversampling to the mix.

Today's real-time oscilloscopes have sampling rates as high as 256 Gsamples/s. Typical RF frequency bands are less than 5 GHz, meaning that the oscilloscope can look at the specific band of interest and massively oversample the data, lowering the effective noise of the instrument. The oversampling allows the real-time oscilloscope to look like a 12- or 14-bit instrument at the targeted bandwidth.

When the oversampling is coupled with higher-performance ADCs, SFDR measurements range somewhere in the 60s for dBc. Historically, the same measurements have fallen in the mid-30 dBc range. Add in the fact that real-time oscilloscopes have always been extremely flat in both magnitude and phase, it's clear that these instruments have now closed the measurement performance gap *(Fig. 2)*.

SPEED

Quickly performing RF measurements is the final real hurdle that real-time instruments must overcome. Typically, oscilloscopes use non-native software to analyze high-frequency signals, which means that the software must import all of the data into the software to analyze it. Even if a measurement, such as a fast Fourier transform (FFT), is completed on the scope, it's completed in software and can be very slow. Moving forward, as oscilloscope field-programmable-gate-array (FPGA) and custom application-specific-integrated-circuit (ASIC) performance continues to increase in capability, one can expect the speed of an oscilloscope to increase, and that limit will be addressed.

CONCLUSION

The world's data demands are moving today's data communications to higher frequencies, wider bandwidths, and multiple channels. For developers of these new technologies, finding the right instrument to perform measurements is becoming an increasingly difficult challenge.

Fortunately, today's test-and-measurement vendors continue to upgrade their instrumentation. This is especially evident in the improvements made to real-time oscilloscope technology. Real-time oscilloscopes now offer up to 110 GHz of bandwidth, multiple phase-coherent channels, and specification performance that can be good enough to meet the testing challenges of today's markets. mw

BRIG ASAY manages strategic planning for Keysight Technologies' Internet Infrastructure group. Brig joined Keysight in 2005. During his time with the company, he has held the following positions: Infiniium Oscilloscope Marketing Manager, Marketing Operations Manager, and Marketing Product Manager. Prior to Keysight, Brig worked at Micron Technologies Inc. as a Test Engineer. Brig holds an MBA from Northwest Nazarene University and a BS in electrical engineering from the University of Wyoming. He has published numerous articles.

KENNETH PUGLIA | E × H Consulting Services

A Brief Tutorial on Microstrip Antennas (Part 2)

The second installment of this series dives into microstrip antenna feed lines before moving on to a microstrip antenna design example.

Picking up from where Part 1 left off, this article explores the single-element, rectangular microstrip antenna. Antenna arrays will be examined later in the series.

MICROSTRIP ANTENNA FEED LINE

The resonant input resistance at the edge of the microstrip conductor is generally greater than the feed-line characteristic impedance and requires an impedance-matching structure to reduce the mismatch loss and thereby improve the antenna efficiency. Two common feed-line techniques can facilitate the impedance matching required to achieve an efficient rectangular microstrip antenna *(Fig. 1)*.

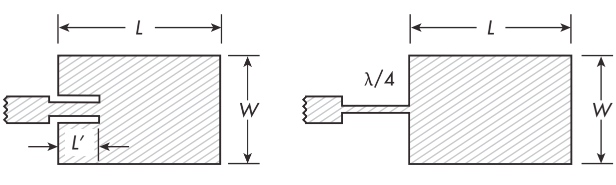

1. Shown are the inset-feed (left) and quarter-wavelength (right) techniques for impedance matching.

The inset feed technique utilizes the reduction in electric-field strength to effectively "tap" a lower impedance drive point. The quarter-wave transformer uses the transmission line formula, which provides the geometric mean of the input resistance and the characteristic impedance of the quarter-wave transmission line. Coaxial probes beneath the conductor or a vertically offset feed along the width are also used on occasion.

A useful equation to achieve the optimum inset length, y_o, is available:[1]

$$R_{in}(y = y_o) = \frac{1}{2(G_1 + G_{12})} \cdot cos^2\left(\frac{\pi}{L} y_o\right) = R_{in}(y_o = 0) \cdot cos^2\left(\frac{\pi}{L} y_o\right) \quad (1)$$

Although quite convenient and easily implemented, the inset feed distorts the equivalent slot radiation due to the change in geometry. The quarter-wavelength feed minimizes the equivalent slot field distortion due to the narrower, high-impedance line required for impedance matching. The simple formula for the impedance of the quarter-wavelength transmission line may be written as:

$$Z_{in} = \frac{Z_o^2}{R_{in}} \quad (2)$$

For a typical value of $R_{in} = 200\ \Omega$ and $Z_{in} = 50\ \Omega$:

$$Z_o = \sqrt{R_{in} \cdot Z_{in}} = \sqrt{200 \cdot 50} = 100\ \Omega \quad (3)$$

RADIATION INTENSITY PATTERNS

The two-slot radiation model is used to predict the *E*-plane and *H*-plane radiation patterns. The radiation intensity of the rectangular microstrip antenna of width *W*, length *L*, and height *h*, may be calculated using the following equations:[2]

For the *E*-plane radiation pattern: $\phi = 0$ and $-\pi/2 < \theta < \pi/2$ (planes have been redefined to comply with reference)

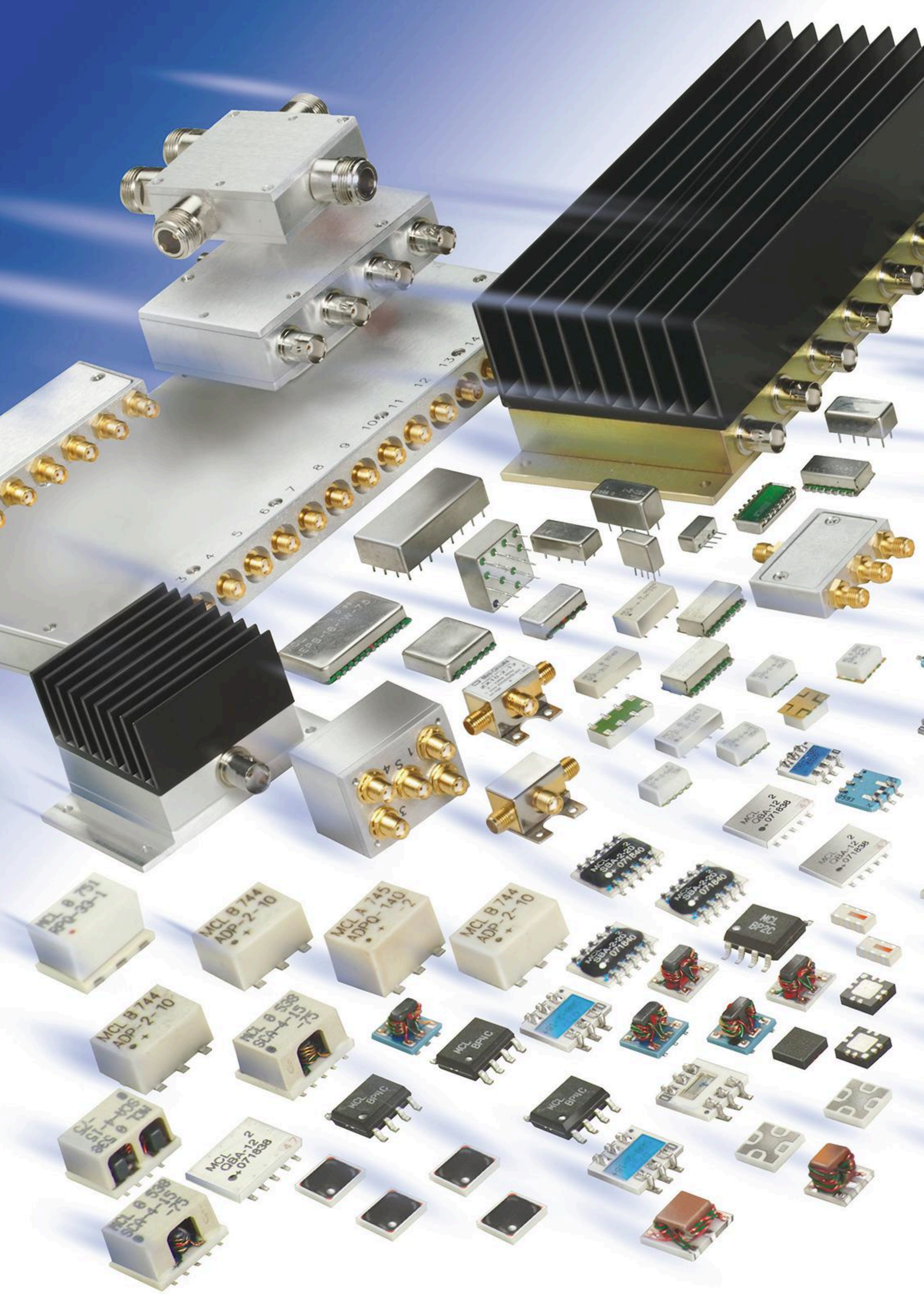

MCL B 744
ADP-2-10
MCL
QBA-12
071838
SBA-2-20
071840
BP4C
BP2C

$$P_E(\theta,\phi=0)=cos\left(\frac{k_o h}{\sqrt{\varepsilon_r}}\cdot cos(\theta)\right)\cdot\frac{sin\left(\frac{k_o W}{2}\cdot sin(\theta)\cdot sin(\phi)\right)}{\frac{k_o W}{2}\cdot sin(\theta)\cdot sin(\phi)}$$
$$\cdot cos\left(\frac{k_o L}{2}\cdot sin(\theta)\cdot cos(\phi)\right)\cdot cos(\phi),\ k_0=\frac{2\pi}{\lambda_0} \quad (4)$$

For the H-plane radiation pattern: $\phi = \pi/2$ and $-\pi/2 < \theta < \pi/2$ (planes have been redefined to comply with reference)

$$P_H\left(\theta,\phi=\frac{\pi}{2}\right)=cos\left(\frac{k_o h}{\sqrt{\varepsilon_r}}\cdot cos(\theta)\right)\cdot\frac{sin\left(\frac{k_o W}{2}\cdot sin(\theta)\cdot sin(\phi)\right)}{\frac{k_o W}{2}\cdot sin(\theta)\cdot sin(\phi)}$$
$$\cdot cos\left(\frac{k_o L}{2}\cdot sin(\theta)\cdot cos(\phi)\right)\cdot cos(\theta)\cdot sin(\phi),\ k_0=\frac{2\pi}{\lambda_0} \quad (5)$$

Bancroft[3] provides reduced complexity expressions for the E-plane and H-plane radiation patterns. However, accuracy is modestly compromised due to elimination of the height, h, as a dependent variable.

MICROSTRIP ANTENNA DIRECTIVITY

The two-slot radiation model is also utilized to predict the directivity of the rectangular microstrip antenna. *Figure 5* in Part 1 represents graphic definition in conjunction with the microstrip antenna dimensions as previously defined.

E-PLANE AND H-PLANE RADIATION PATTERN

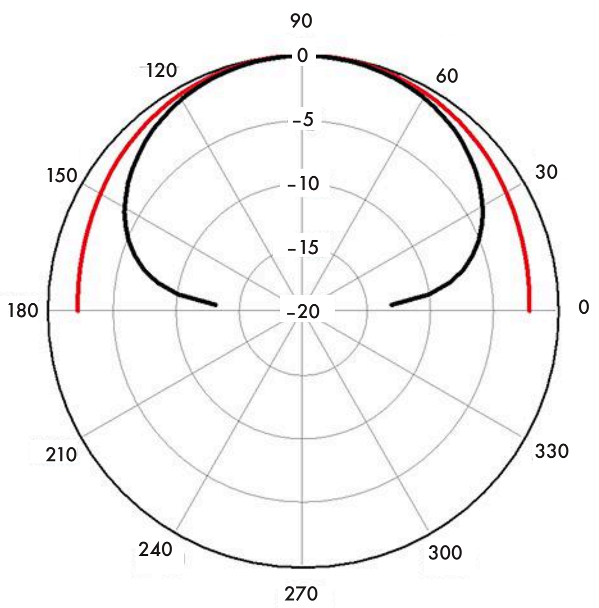

2. E-Plane (red) and H-Plane (black) radiation patterns are detailed.

Although the equation for directivity of a single slot requires the condition $k_o h << 1$, the expression provides reasonable accuracy upon comparison with actual measurement if the condition is moderately violated.

The directivity of a single slot may be written:[4]

$$D_1=\left(\frac{2\pi W}{\lambda_o}\right)^2\cdot\frac{1}{I_1}\quad\text{where}\quad I_1=\int_0^{\pi}\left[\frac{sin\left(\frac{k_o W}{2}\cdot cos\,\theta\right)}{cos\,\theta}\right]^2\cdot sin^3(\theta)d\theta \quad (6)$$

The directivity of a two-slot array, i.e., the microstrip antenna, may be written using the following expression:[5]

$$D_2=\left(\frac{2\pi W}{\lambda_o}\right)^2\cdot\frac{\pi}{I_2}$$
$$\text{where}\quad I_2=\int_0^{\pi}\int_0^{\pi}\left(\frac{sin\left(\frac{k_o W}{2}\cdot cos(\theta)\right)}{cos(\theta)}\right)^2\cdot sin^3(\theta)\cdot cos^2\left(cos\left(\frac{k_o L_{eff}}{2}\cdot sin(\theta)\cdot sin(\phi)\right)\right)d\theta d\phi \quad (7)$$

MICROSTRIP ANTENNA DESIGN

Although the previous text and equations have indicated a significant performance dependence on the width of the microstrip conductor, the astute reader may recognize that no guidelines or formulae have been offered for the width calculation. A practical starting point has been suggested by Bancroft in the following equation:[6]

$$W=\frac{c}{2f_o}\cdot\sqrt{\frac{2}{\varepsilon_r+1}} \quad (8)$$

The procedure for the design of a single-element, rectangular microstrip antenna is summarized in *Table 1*.

MICROSTRIP ANTENNA DESIGN EXAMPLE

To summarize the rectangular microstrip antenna tutorial content at this point:

- Operational parameters and principles have been established.
- Design parameters and equations have been presented and references identified.
- Design procedure has been outlined.

To further explore the rectangular microstrip antenna, a design example[7] is documented in *Table 2* using the procedure of *Table 1*. The example illustrates the design procedure for a 5.8-GHz, direct-coupled microstrip antenna on 0.062-in.-thick Rexolite *(www.rexolite.com)* substrate. Rexolite is a dimensionally stable, cross-linked polystyrene plastic with a frequency-independent dielectric constant of 2.55 and low loss tangent (typically less than 0.001 to 100 GHz).

Fig. 2 represents the E-plane and H-plane radiation patterns of the 5.8-GHz, rectangular microstrip antenna. Note that the beamwidth of the E-plane radiation pattern is somewhat greater than the H-plane beamwidth. It should also be noted that the H-plane radiation pattern is independent of the slot separation length, L. This is not evident from Equation 5 until one cautiously considers the equation under the condition, $\phi = \pi/2$.

The E-plane and H-plane radiation patterns of *Fig. 2* were calculated with MathCad using the equations of Reference 4 from Part 1. Similar patterns are produced using the other cited references.

EM SIMULATION OF DIRECT-COUPLED MICROSTRIP ANTENNA

Although the design equations provide the initial dimensional data and radiation patterns for the microstrip antenna design, an electromagnetic (EM) simulation is generally required to reduce the number of prototype iterations and achieve the available performance objectives. To that end, an EM simulation of the 5.8-GHz, direct-coupled microstrip antenna was executed using the AXIEM 3D planar EM simulator within the NI AWR Design Environment.[9]

Results of the direct-coupled microstrip antenna EM simulation are summarized within the graphics of *Table 3* and represent a degree of dimensional optimization of the initial design values as previously indicated.

In addition to providing the ability to optimize antenna performance, the AXIEM simulation software also enables dimensional sensitivity analysis; e.g., as one might expect, the length of the microstrip conductor *(L)* was found to significantly influence input impedance and center

Table 1: Microstrip Antenna Design Procedure

Procedure Number	Design Procedure Description	Note – Comment – Reference
1.	Specify: A. substrate dielectric constant – ε_r B. operational frequency – f_o C. substrate height – h	A. Preferred values of dielectric constant $2.0 < \varepsilon_r < 6$. Higher dielectric constants reduce efficiency B. Desired center frequency C. substrate height should be compatible with achievable line width and impedance levels Bancroft recommends: $h_{max} < \frac{0.3c}{2\pi f_o \sqrt{\varepsilon_r}}$
2.	Calculate the width – W	Equation 8
3.	Calculate the effective dielectric constant – ε_{eff}	Part 1, Equation 1
4.	Calculate the length extension – ΔL	Part 1, Equation 2
5.	Calculate the actual length – L	Part 1, Equation 4. Note the terms must be rearranged to solve for L. L is nominally a half-wavelength in the effective dielectric medium.
6.	Calculate the input impedance at resonance – R_{in}	Part 1, Equation 5 – note + sign for TM_{010} mode
7.	Use either inset feed or quarter-wavelength transmission line for impedance matching to the desired input impedance	Equation 1 or Equation 2. A coaxial probe beneath the substrate with center conductor extending to the inset feed point may also be appropriate on occasion.
8.	Calculate the directivity	Equations 6 and 7
9.	Calculate the radiation patterns	Equations 4 and 5
10.	Simulate antenna design using an EM simulator and compare results	EM simulation tools have provided accurate performance predictions, and in many cases have expedited the design cycle time by limiting the prototype fabrication stage to a single iteration.
11.	Fabricate antenna and compare measured results with design and simulation	

Table 2: Microstrip Antenna Design Example

Design Parameter	Symbol	Design Value	Note – Comment
Center Frequency	f_o	5.8 GHz	Operational frequency
Dielectric Constant	ε_r	2.55	Specified substrate parameter
Substrate Height	h	1.575 mm (0.062 in)	Specified parameter
Conductor width	W	19.41 mm (0.764 in)	Equation 8 (optimized value 0.750 in)
Effective dielectric constant	ε_{eff}	2.327	Part 1, Equation 1
Length extension	ΔL	0.79 mm (0.031 in)	Part 1, Equation 2
Conductor length	L	15.38 mm (0.605 in)	Part 1, Equation 4 (optimized value 0.615 in)
Resonant input resistance	R_{in}	228 Ω	Part 1, Equation 5
Inset feed length	y_o	5.41 mm (0.213 in)	Equation 1
Quarter-Wave transformer	Z_o	111 Ω	Equation 2 (optimized value 105 Ω)
Quarter-Wave transformer	$L_{\lambda/4}$	8.48 mm (0.334 in)	Microstrip calculator[8] (optimized value 0.265 in)
Quarter-Wave transformer, width	$W_{\lambda/4}$	1.05 mm (0.040 in)	Microstrip calculator (optimized value 0.035 in)
Directivity	D	7.0 dB	Equation 7 (EM simulation 6.9 dB)
Radiation pattern E-plane	P_E	Figure 2	Equation 4
Radiation pattern H-plane	P_H	Figure 2	Equation 5

frequency. The microstrip conductor width *(W)* was found to have influence on the directivity and was useful in optimizing the input impedance. The substrate thickness *(h)* was found to be the principal determinant to bandwidth and efficiency.

The value of EM antenna simulation is manifest in the ability to optimize performance as well as to provide physical insight to antenna operation using conductor current and electric-field annotation capabilities. Note specifically the current density at the conductor edges. One might correctly consider that the radiation properties of the microstrip antenna may also be explored using the current density. In fact, the radiation patterns of the microstrip antenna could also be calculated using the vector

(Continued on page 43)

Table 3: Electromagnetic Simulation Results

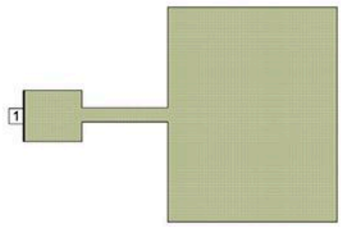

Microstrip Antenna Conductor Pattern

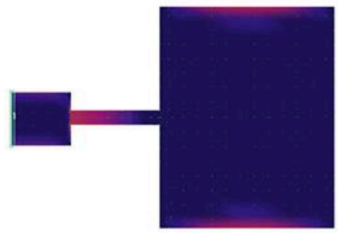

Conductor Current Distribution
(note the concentration of current at the top edges of the conductor)

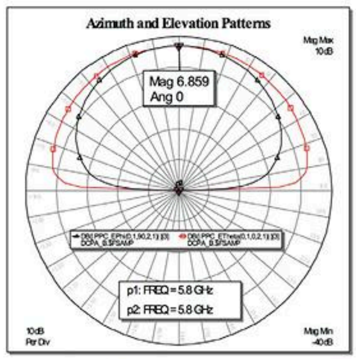

Azimuth (E-Plane) and Elevation (H-Plane) Radiation Patterns

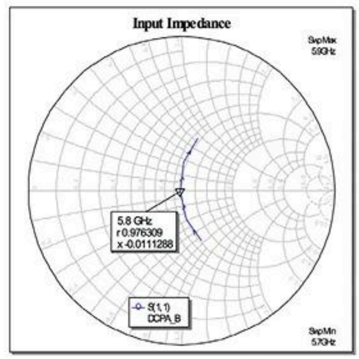

Direct-Coupled Microstrip Antenna Input Impedance

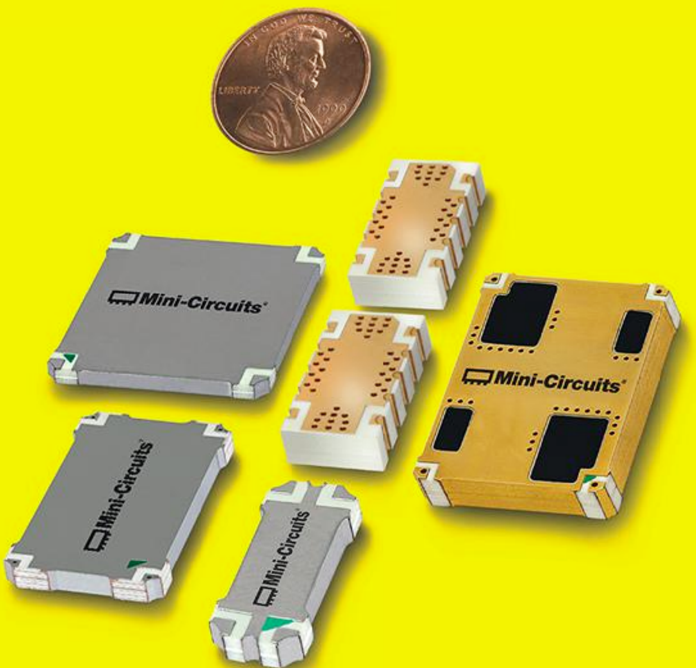
Mini-Circuits
Mini-Circuits
Mini-Circuits
Mini-Circuits

FARRON L. DACUS | RF Design Consultant, Longwing Technology
www.longwingtech.com

Design Methods of Modern Ultra-Low-Noise Synthesizers

This first article in a multi-part series on modern synthesizers describes basic phase-locked-loop operation along with various topologies.

Recent years have seen major changes in frequency-synthesis art. Ultra-low-noise discrete voltage-controlled oscillators (VCOs), the heart of low-noise synthesizers for decades, now find themselves being challenged by integrated VCOs. While the best discrete VCOs still achieve 20 to 30 dB of phase-noise superiority, integrated-circuit (IC) companies are conducting an asymmetric battle to dominate the market with full integration based not on the best VCO noise, but on architectural innovations that often render free-running VCO noise less important.

Such a goal is achieved by putting good VCOs on die, suppressing that noise down to a very low level via feedback, and then dividing down to the application band. The challenge that discrete VCO suppliers now face is to extend the outstanding phase noise they achieve in application bands to higher frequencies, where they also get the full architectural benefit of the latest synthesizer innovations.

This article, the first of a four-part series, will review modern advanced design methods. The next three articles will dive into noise, key parts and tools, and examples. Longer and more complete versions of these articles will be published online.

BASIC PLL OPERATION AND SECOND-ORDER NORMALIZED FORM

The standard second-order form of phase-locked-loop (PLL) design that's presented in most classic textbooks allows for approximate, but still useful, design and analysis equations, along with a simple description of loop operation *(Fig. 1)*.

We are accustomed to thinking primarily of voltage and current as the feedback quantities. But in addition to those, the PLL treats phase and frequency as small-signal frequency-domain variables. When seeking lock over a wide frequency range, the modern phase/frequency detector (PFD) acts as a frequency detector to steer the VCO toward lock. As frequency converges, the loop transitions to a phase-locked mode where phase as a time difference between digital edges is driven to zero.

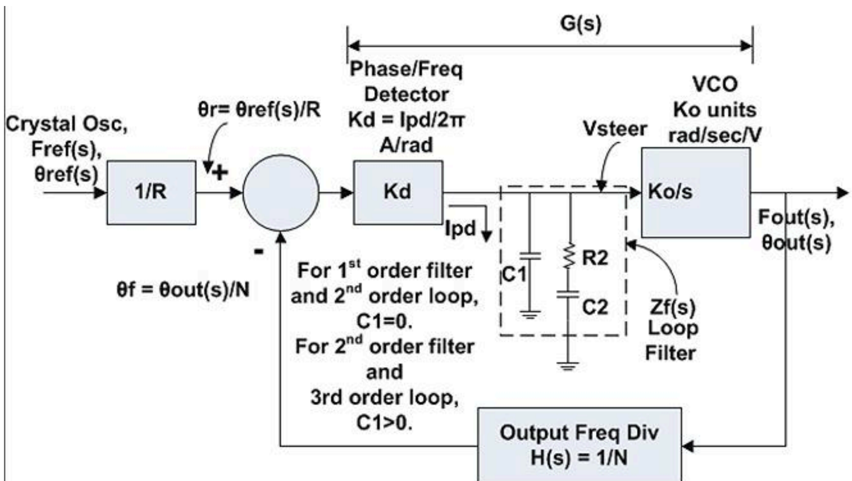

1. This is a depiction of the second- and third-order charge pump PLL synthesizer (C_1 = 0 for second-order). Frequency is set by firmware via the programmable R and N dividers.

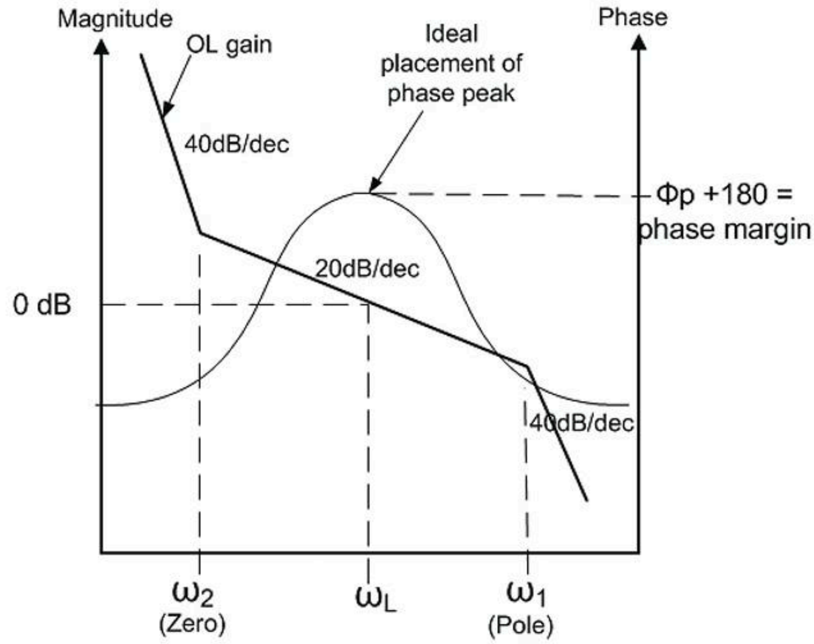

2. Shown is open-loop gain and phase in the properly designed third-order PLL. The maximum phase is forced to occur at the loop bandwidth by the design.

Since frequency is the time derivative of changing phase ($\omega = d\theta/dt$), phase is the integral of frequency. Thus, the VCO acts as an integrator of input voltage to output phase, which introduces −90 degrees of phase shift. That's why its transfer function is in the form K_o/s. Here, K_o is given in units of rad/sec/volt. VCO datasheets will normally give K_o in units of MHz/V. To be clear in this article series, we will refer to the Hz/V form of K_o as K_{Hz}. The radian form will be referred to as K_o, i.e., $K_o = 2\pi K_{Hz}$.

With the −90 deg phase shift and the −180 degrees of negative feedback, we are only allowed a maximum of 90 degrees of filtering phase shift before −360 degrees total results in instability. We normally leave a minimum of 40 degrees of "phase margin" at the loop bandwidth. This margin comes from the zero introduced by resistor R_2, as without it the charge pump driving a capacitor would also be an integrator.

From basic analysis of the loop in *Fig. 1*, we may find R_2 and C_2 as:

$$C = \frac{K_o I_{pd}}{2\pi N\omega_n^2} = \frac{K_{Hz} I_{pd}}{N\omega_n^2} \quad (1)$$

$$R = \frac{4\pi N\omega_n\zeta}{K_o I_{pd}} = \frac{2N\omega_n\zeta}{K_{Hz} I_{pd}} \quad (2)$$

The term ω_n is the "natural" frequency (settling "ring down" frequency). It's close to the open-loop bandwidth. The term ζ is the "damping factor" and must be greater than zero for stability (usually set at 0.5 to 1.0). See the online version for a derivation of the above and a more complete description.

THE THIRD-ORDER PASSIVE FILTER PLL

This third-order passive filter PLL is the simplest highly usable form. It's realized by adding another capacitor *(Fig. 1)*. Introducing another filter pole will eventually cancel out the zero. This means that there will be a frequency where phase peaks and then declines *(Fig. 2)*.

The loop filter impedance is:

$$Z(s) = \frac{1+sT_2}{s\,A_0(1+sT_1)} \quad (3)$$

A half page of circuit analysis will establish:

$$T_2 = R_2C_2 \quad (4)$$

$$T_1 = \frac{R_2C_2C_1}{A_0} \quad (5)$$

$$A_0 = C_1 + C_2 \quad (6)$$

The open-loop gain function is given by (*see figure for G and H*):

$$\mathbf{GH(j\omega)} = \frac{K_d K_o}{-N}\,\frac{1+j\omega T_2}{\omega^2 A_0(1+j\omega T_1)} \quad (7)$$

We know K_d, K_o, and N, and choose loop bandwidth ω_L and phase margin ϕ_m. To find our three unknowns A_0, T_1, and T_2, we need three equations. We get them from the magnitude of GH (which is 1 at ω_L), the phase of GH (which gives ϕ_m at ω_L), and the derivative of the phase of GH with respect to ω (which is zero at ω_L). This is the basic methodology referred to here as the modern technique.

The magnitude of GH is:

$$|GH(j\omega)| = \frac{K_d K_o}{N A_0 \omega^2}\,\frac{\sqrt{1+\omega^2 T_2{}^2}}{\sqrt{1+\omega^2 T_1{}^2}} \quad (8)$$

At $\omega = \omega_L$, this magnitude is 1, and we have:

$$A_0 = \frac{K_d K_o}{N\omega_L^2}\,\frac{\sqrt{1+\omega_L^2 T_2{}^2}}{\sqrt{1+\omega_L^2 T_1{}^2}} \quad (9)$$

The phase *margin* expressed as a positive number from 0 to 90 degrees is the difference between the open-loop phase and 180 degrees, which is:

$$\phi_m = \tan^{-1}(\omega_L T_2) - \tan^{-1}(\omega_L T_1) \quad (10)$$

Taking the derivative of phase margin with respect to variable frequency, and setting it to zero at $\omega = \omega_L$, gives:

$$\frac{T_2}{1+\omega_L^2 T_2^2} - \frac{T_1}{1+\omega_L^2 T_1^2} = 0 \quad (11)$$

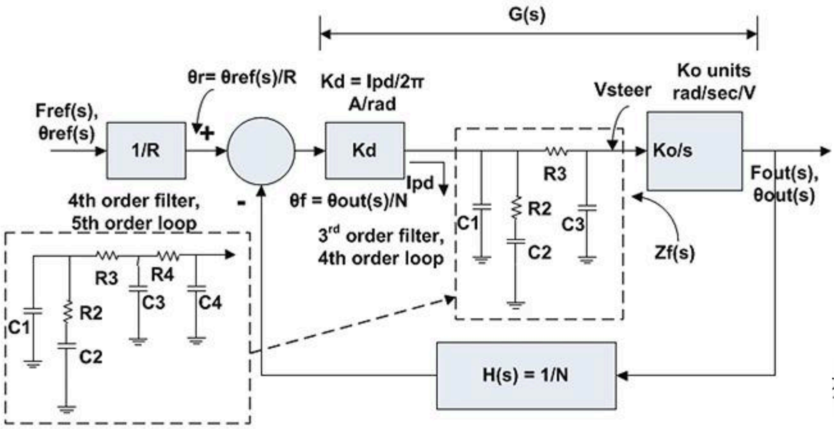

3. Here are the fourth- and fifth-order PLL forms.

We now have two nonlinear equations in the two unknowns T_1 and T_2. We may solve these numerically, but there's a closed form solution (Ref. 1, pp. 32-36):

$$T_1 = \frac{\frac{1}{\cos\phi_m} - \tan\phi_m}{\omega_L} \quad (12)$$

$$T_2 = \frac{1}{\omega_L^2 T_1} \quad (13)$$

$$\omega_L = \sqrt{\omega_1 \omega_2} \quad (14)$$

Now we may find the circuit values:

$$C_2 = A_0\left(1 - \frac{T_1}{T_2}\right) \quad (15)$$

$$C_1 = A_0 - C_2 \quad (16)$$

$$R_2 = \frac{T_2}{C_2} \quad (17)$$

The second-order filter is the lowest noise filter form. However, pushing bandwidth out typically requires additional poles of filtering to keep phase detector noise from contaminating VCO noise.

THE FOURTH-ORDER PASSIVE FILTER PLL

The fourth-order passive filter PLL form uses the third-order filter shown in *Figure 3*. It's likely the most common filter form.

The open-loop transfer function is given by:

$$\mathbf{GH}(j\omega) = \frac{K_d K_o}{-N}\,\frac{1+j\omega T_2}{\omega^2 A_0(1+j\omega T_1)(1+j\omega T_3)} \quad (18)$$

The filter (transfer) impedance that's part of the above is given by:

$$Z(s) = \frac{1+sT_2}{s\,A_0(1+sT_1)(1+sT_3)} = \frac{1+sC_2R_2}{s\,(A_2 s^2 + A_1 s + A_0)} \quad (19)$$

The coefficients A_1 and A_2 are useful abbreviations for lengthy functions of parts values.

$$A_0 = C_1 + C_2 + C_3 \quad (20)$$

Using the magnitude function of the open-loop transfer function:

$$A_0 = \frac{K_d K_o}{N\omega_L^2}\,\frac{\sqrt{1+\omega_L^2 {T_2}^2}}{\sqrt{(1+\omega_L^2 {T_1}^2)(1+\omega_L^2 {T_3}^2)}} \quad (21)$$

We next define what Banerjee (Ref. 2) calls "pole ratios," which shall be selected by the designer based on factors such as spur rejection. Technically, these would be properly referred to as time-constant ratios.

$$T_{31} = \frac{T_3}{T_1} = \frac{\omega_1}{\omega_3} = \frac{f_1}{f_3} \quad (22)$$

T_{31} determines how spaced out the added pole is. We must use $T_{31} < 1$. We find that 0.5 buys almost all of the possible spur suppression.

The phase margin of the open-loop transfer function is given by:

$$\phi_m = \tan^{-1}(\omega_L T_2) - \tan^{-1}(\omega_L T_1) - \tan^{-1}(\omega_L T_{31} T_1) \quad (23)$$

The phase margin occurs at the peak of the phase margin function. Taking this derivative with variable frequency, and then applying the first derivative test with $\omega=\omega_L$, gives:

$$\frac{T_2}{1+\omega_L^2 T_2^2} - \frac{T_1}{1+\omega_L^2 T_1^2} - \frac{T_{31}T_1}{1+\omega_L^2 T_{31}^2 T_1^2} = 0 \quad (24)$$

After selecting the pole ratio T_{31}, the above two equations may be solved numerically for T_2 and T_1, thus allowing $T_3 = T_{31}T_1$.

Now we come to the "Gamma Optimization Factor" used by Banerjee. This quantity allows for approximation, with additional information on its importance given in the online version. We may extend the earlier expressions for T_2 in approximate form to higher-order loops (Ref. 2, 5th ed., p. 309), at the same time defining γ:

$$T_2 = \frac{\gamma}{\omega_L^2 (T_1+T_3)} = \frac{\gamma}{\omega_L^2 T_1(1+T_{31})} \quad (25)$$

This parameter is normally close to 1 in practical designs—in the range of 0.7 to 1.3.

Substituting, we get this approximation (leaving the 180 deg. off to convert from phase to phase margin):

$$\phi_m = \tan^{-1}\left(\frac{\gamma}{\omega_L T_1(1+T_{31}+T_{41})}\right) - \tan^{-1}(\omega_L T_1) - \tan^{-1}(\omega_L T_{31} T_1) \quad (26)$$

The above only needs to solve for T_1. An approximation can be found using $\tan^{-1}(x) \sim x$ for small x. The result is:

$$T_1 \cong \frac{\frac{1}{\cos\phi_m} - \tan\phi_m}{\omega_L(1+T_{31})} \quad (27)$$

The other two time constants follow immediately.

$$T_3 = T_1 T_{31} \quad (28)$$

When using the approximate approach:

$$T_2 \cong \frac{\gamma}{\omega_L^2 (T_1+T_3)} \qquad (29)$$

We find A_1 and A_2 from:

$$A_1 = A_0(T_1 + T_3) = C_2C_3R_2 + C_1C_2R_2 + C_1C_3R_3 + C_2C_3R_3 \qquad (30)$$

$$A_2 = A_0T_1T_3 = C_1C_2C_3R_2R_3 \qquad (31)$$

We have the four equations for five values: C_1, C_2, C_3, R_2, and R_3. The method adopted by Banerjee to get a 5th equation is to find the largest C_3 that satisfies these equations. The above may be manipulated to find C_3:

$$C_3 = \frac{-T_2^2C_1^2+T_2A_1C_1-A_2A_0}{T_2^2C_1-A_2} \qquad (32)$$

Applying the first derivative test for the value of C_1 that peaks C_3:

$$C_1(max\, C_3) = \frac{A_2}{T_2^2}\left(1 + \sqrt{1+\frac{T_2}{A_2}(T_2A_0 - A_1)}\right) \qquad (33)$$

Everything needed to find C_1 is known, and it may be plugged into Equation 32 to find C_3. Then, the final values are found from:

$$C_2 = A_0 - C_1 - C_3 \qquad (34)$$

$$R_2 = \frac{T_2}{C_2} \qquad (35)$$

$$R_3 = \frac{A_2}{C_1C_3T_2} \qquad (36)$$

The more complex passive fourth-order filter is discussed in the online version.

OP-AMP ACTIVE FILTER PLLs

The primary reason for using an op amp is to extend the voltage range of the loop filter so that VCOs can be controlled with large tune ranges. This allows for lower K_o and lower noise. The op amp also allows for smaller, lower-noise resistors and the ability to place the lowest pole after the op amp. Several topologies exist for active loop filters, but here a single preferred version is given in full fourth-order form *(Fig. 4)*.

A low-noise dc reference voltage is provided at the positive input of the op amp, and the combination of loop action and op-amp action will keep the negative input of the op amp at this same voltage. In this form, the op-amp output will "pump up" via current flowing through Z_{for} to assume whatever voltage is needed to maintain lock. The part values can be selected so that this inverting form suffers only small noise gain.

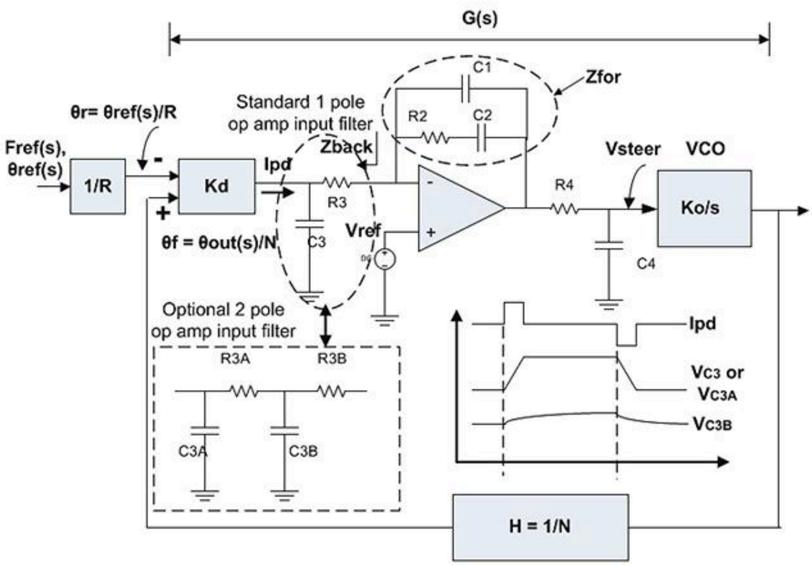

4. This is the active fourth-order filter and fifth-order PLL, with option for fifth-order filter. This filter is referred to as a "slow slew" active filter, as the input RC reduces speed requirements. Bandwidth limits of the op amp may still make it advantageous to use the two-pole input filter option (see online version).

For transfer impedance Z(f) we find:

$$Z(s) = \frac{V_{out}}{I_{pd}} = \frac{1+sT_2}{s\,A_0(1+sT_1)(1+sT_3)(1+sT_4)} \quad (37)$$

An importance point is that T_4 shall be the lowest frequency pole.

We also find:

$$A_0 = C_1 + C_2 \quad (38)$$

The open-loop gain as a function of jω is:

$$GH(j\omega) = \frac{K_d K_o}{-N}\,\frac{1+j\omega T_2}{\omega^2 A_0(1+j\omega T_1)(1+j\omega T_3)(1+j\omega T_4)} \quad (39)$$

Using the magnitude function of the open-loop transfer function (1 at loop BW), we get:

$$A_0 = \frac{K_d K_o}{N\omega_L^2}\,\frac{\sqrt{1+\omega_L^2 T_2{}^2}}{\sqrt{(1+\omega_L^2 T_1{}^2)(1+\omega_L^2 T_3{}^2)(1+\omega_L^2 T_4{}^2)}} \quad (40)$$

In order to maintain one set of equations whether or not f_1 or f_3 is lower, we refer both higher-frequency poles to the lowest pole f_4.

To evaluate A_0, we need T_4 and T_2; then we use the selected pole ratios to get T_1 and T_3. The exact equation is:

$$\phi_m = \tan^{-1}(\omega_L T_2) - \tan^{-1}(\omega_L T_4) - \tan^{-1}(\omega_L T_{14} T_4) - \tan^{-1}(\omega_L T_{34} T_4) \quad (41)$$

The max phase margin occurs at the peak of the phase-margin function, where we substitute $\omega=\omega_L$ after taking the derivative in the first derivative test:

$$\frac{T_2}{1+\omega_L^2 T_2^2} - \frac{T_1}{1+\omega_L^2 T_4^2} - \frac{T_{14}T_4}{1+\omega_L^2 T_{14}^2 T_4^2} - \frac{T_{34}T_4}{1+\omega_L^2 T_{34}^2 T_4^2} = 0 \quad (42)$$

Now these two may be solved numerically for T_2 and T_4, leading then to T_1 and T_3 via the selected pole ratios (usually around 0.5 for the lowest pole above f_4 and 0.25 for the next pole relative to T_4). The below approximations may be used as starting points for the numerical solutions, or as is.

$$\phi_m = \tan^{-1}\left(\frac{\gamma}{\omega_L T_4(1+T_{14}+T_{34})}\right) - \tan^{-1}(\omega_L T_4) - \tan^{-1}(\omega_L T_{14} T_4)\tan^{-1}(\omega_L T_{34} T_4) \quad (43)$$

We may use γ = 1 or alter the value from 1 based on the optimization criteria in Banerjee (Ref. 2, 5th ed., chapter 36). The only variable remaining is T_4, which may be solved numerically, or approximately:

$$T_4 \cong \frac{\frac{1}{\cos\phi_m} - \tan\phi_m}{\omega_L(1+T_{14}+T_{34})} \quad (44)$$

If the approximate form is used, then:

$$T_2 \cong \frac{\gamma}{\omega_L^2\,(T_1+T_3+T_4)} \quad (45)$$

In either case:

$$T_1 = T_{14} T_4 \quad (46)$$

$$T_3 = T_{34} T_4 \quad (47)$$

We now have all of the variables needed to find $A_0 = C_1 + C_2$. We may then find all of the part values in Z_{for} from:

$$C_1 = \frac{T_1 A_0}{T_2} \quad (48)$$

$$C_2 = A_0 - C_1 \quad (49)$$

$$R_2 = \frac{T_2}{C_2} \quad (50)$$

Now we select the values for R_3, C_3, R_4, and C_4, which seems easy as we have their time constants. But there are some subtle complexities at work here, including op-amp limits to consider.

On the input side of the op amp, it might seem like a smaller R_3 would help with noise. However, the opposite is actually true. The thermal noise of R_3 rises proportionally with its square root. But as R_3 increases, the noise gain decreases. Therefore, the noise of R_3 on the op-amp output decreases with its square root. So, we tend to select the

largest R_3 that other limits allow, as follows.

Banerjee gives (Ref. 2, 5th ed, p.38) the duty cycle of the phase-frequency detector in frequency-lock mode as a function of the ratio of f_{ref} and f_{out}/N as:

$$D_c = 1 - \frac{f_{lower}}{f_{upper}} \qquad (51)$$

In the above, f_{lower} is the smaller of f_{ref} and f_{out}/N. Since most VCOs do not steer far in a fractional sense from their center frequency, the duty cycle would seldom range above 10% (octave-type VCOs being the exception).

Let us define ΔV_{mC3} as the max filtered voltage change from V_{ref} that we wish to be imposed (such as to comply with op-amp input requirements) on C_3 during a frequency-lock acquisition event. We may thus write a relationship for R_{3max} as:

$$R_{3max} = \frac{\Delta V_{mC3}}{D_c I_{pd}} \qquad (52)$$

In addition, we need to beware of slew-rate limits. Banerjee offers experimental evidence (Ref. 2, 5th ed., pp. 371-372) that if the op amp is not fast enough, there will be worsening of 1/f phase noise inside the loop bandwidth (typically a few dB). Four slew rate cases are derived in the online version: two in frequency-acquisition mode (for lock speed) and two in PLL mode (for noise control). The worst case (highest) requirement on slew rate is usually the frequency-locking case toward the end of the frequency-lock process given by:

$$ReqSlewRateFLL(R_2\ limited) \cong \frac{D_{cmax} I_{pd}}{C_3} \frac{R_2}{R_3} \qquad (53)$$

Additionally, bandwidth limits of the op amp are an issue. However, this can be mitigated by the two-pole input filter option. This allows the op amp to be "cocooned" within filtering that prevents signals beyond its specified bandwidth from reaching it. This would seem to be a more logical strategy than the typical GBW > 10X loop bandwidth that's often assumed with op-amp circuits. See the online version for further discussion.

Next, we consider the op-amp output current limits on C_4. We are used to seeing strict limits on op amps, but against a capacitor (not a pure dc load), many can drive loads of 10 Ω and sometimes even less. But, with a large frequency change on the PLL, that capacitance does take large current that may exceed the op-amp max in the range of 10 to 100 mA. Fundamentally, we desire the op-amp max current I_{opmax} to be able to charge C_4 at the same rate that $D_c{*}I_{pd}$ charges C_2 during a large frequency change. Using I*t = CV:

$$C_{4max} = \frac{I_{opmax} C_2}{D_c I_{pd}} \qquad (54)$$

This maximum is sometimes more than we would like to use due to size and cost reasons, possibly leading to resistor values too small for the op amp. In that case, we select a value of R_4 that allows for thermal noise considerably less than that of the op amp. We then find $C_4 = T_4/R_4$.

WHAT'S NEXT

The transfer-function approach presented here leads to noise sources and shaping in article 2 of the series, along with revealing the key innovations driving full integration and how discrete VCO makers can fight back. Article 3 will focus on key parts and CAD tools that are the weapons of the low-noise synthesizer designer. Article 4 will put it all together with requirements and examples of integrated and discrete VCO synthesizers to meet them. mw

ACKNOWLEDGMENTS

The author expresses his appreciation for the valuable reviews, comments and information provided by Adnaan Khan, Joe Bouchez of LoneStar III Five Designs, Dean Banerjee at Texas Instruments, C.Y. Teng and Miguel Troester at Taitien, and Ulrich Rohde, Ajay Poddar, and Bill Becker at Synergy Microwave.

REFERENCES

1. *"Digital PLL Frequency Synthesizers: Theory and Design",* Ulrich L. Rohde, Prentice-Hall, 1983.

2. *"PLL Performance, Simulation, and Design",* Dean Banerjee, First Edition 1998. The 5th edition of 2017 of this outstanding reference may be freely downloaded at: http://www.ti.com/tool/pll_book.

3. *"Phaselock Techniques,"* 2nd Ed, Floyd Gardner, John Wiley and Sons, 1979.

4. *"Phase Locked Loops,"* Third Edition, Roland Best, McGraw-Hill, 1997.

(Continued from page 34)

potential associated with the conductor current.

PROTOTYPE MICROSTRIP ANTENNA

A prototype microstrip antenna was fabricated in accordance with the parameters of *Table 2* with modest dimensional revision resulting from the EM simulation to optimize the input impedance and directivity. The prototype antenna conductor dimensions are illustrated in *Figure 3*. mw

REFERENCES

1. Balanis, C. A., *Antenna Theory*, 3rd Ed., John Wiley and Sons, Hoboken, NJ, 2005, pp. 824-825.
2. Carver, K. and Mink, J., *Microstrip Antenna Technology*, IEEE Transactions, Antennas and Propagation, January 1981.
3. Bancroft, R., *Microstrip and Printed Antenna Design*, 2nd Ed., Scitech Publishing, Raleigh, NC, 2009, p. 30.
4. Balanis, C. A., *Antenna Theory*, 3rd Ed., John Wiley and Sons, Hoboken, NJ, 2005, p. 840.
5. Balanis, C. A., *Antenna Theory*, 3rd Ed., John Wiley and Sons, Hoboken, NJ, 2005, p. 841.
6. Bancroft, R., *Microstrip and Printed Antenna Design*, 2nd Ed., Scitech Publishing, Raleigh, NC, 2009, p. 60.
7. An excellent design example of a 10-GHz microstrip antenna is presented in [6], Chapter 14.
8. Online microstrip parameter calculator: *http://www.microwaves101.com/content/calculators.cfm.*
9. AXIEM technology utilizes an open-boundary, non-gridded, method-of-moments solver that supports thick metal in layered dielectric media. Additional information is available at *www.awrcorp.com/products/axiem*.

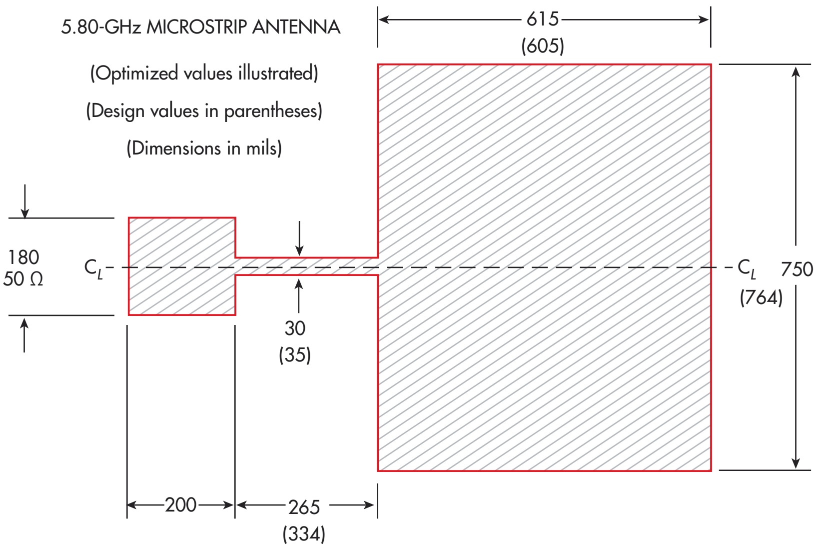

3. This is the microstrip antenna conductor pattern for the 5.8-GHz design example.

defense electronics

A Special Section to INFORMA'S DESIGN ENGINEERING & SOURCING GROUP DECEMBER 2018

NSA Certifies Airborne SDR

JACK BROWNE | Technical Contributor

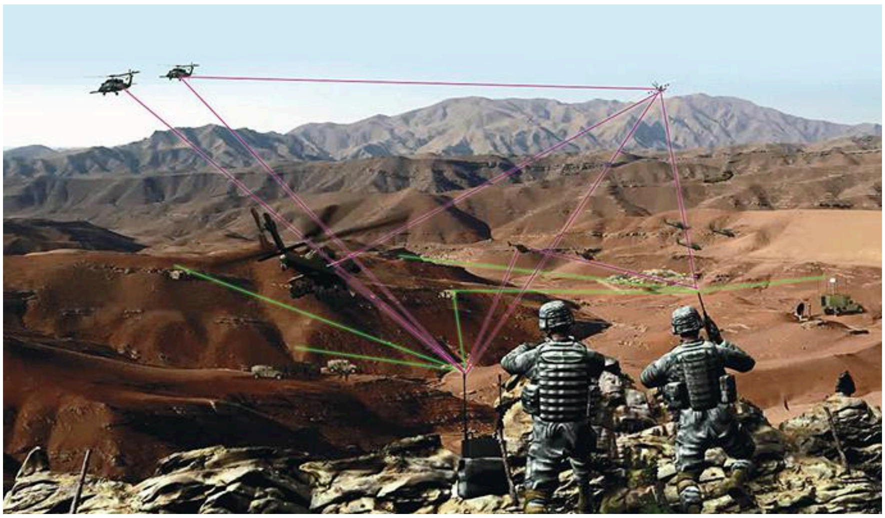

1. SDR technology provides secure reliable communications to armed forces on the ground and in the air. *(Courtesy of Rockwell Collins)*

ROCKWELL COLLINS continues to evolve its software-defined-radio (SDR) communications equipment technology, recently receiving a Type-1 top secret (TS) certification from the National Security Agency (NSA) for its latest-generation ARC-210 RT-2036(C) airborne radio. The SDR provides secure, reliable communications for warfighters on the ground and in the air *(Fig. 1)*.

"This NSA certification is one of the final steps in getting our latest-generation airborne radio technology into the field," says Troy Brunk, vice-president and general manager, Communication, Navigation and Electronic Warfare Solutions for Rockwell Collins. "With data, images, voice, and video being sent from the air to the ground in real time, warfighters will have critical information at their fingertips to gain a tactical advantage on the battlefield."

2. The ARC-210 RT-2036(C) will enable U.S. Armed Forces to tap into new communications capabilities such as the U.S. DoD's MUOS program and Second-Generation Anti-Jam Tactical UHF Radio for NATO (SATURN) program. *(Courtesy of Rockwell Collins)*

(Continued on page 48)

Lockheed Martin Builds on IR Sensor System

LOCKHEED MARTIN has been contracted for phase II of the U.S. Navy's F/A-18E/F Super Hornet Block II Infrared Search and Track (IRST) program. The contract, which is worth $108 million, was awarded by the aircraft's prime contractor, Boeing, and will have Lockheed Martin complete development, platform integration, flight test, and qualification of the IRST21 Block II sensor system. The efforts are meant to enhance the detection, tracking, and ranging capabilities of the IRST21 sensor system in radar-denied environments.

"We are continuing a long legacy of delivering unmatched sensor technologies to our customers around the globe," says Michael Williamson, vice-president of Sensors & Global Sustainment at Lockheed Martin Missiles and Fire Control. "The IRST21 sensor system provides U.S. Navy F/A-18E/F operators with superior detection and survivability capabilities." The IRST21 sensor system uses infrared (IR) search-and-track technology to passively detect and track airborne threats in environments.

The IRST21 sensor system supports both Navy and Air Force

(Continued on page 48)

MANET is Made for the Military

JACK BROWNE | Technical Contributor

COMMUNICATIONS OF ANY KIND, secure or otherwise, is vital to any armed forces hoping for a successful campaign. Without reliable messaging, troops are lost in the field. Civilians who have lost battery power for their cell phones or lost the phones themselves can understand the psychological needs for a reliable communications device.

Military radio communications technology has made great strides in recent decades. But most battlefield radio technologies have adopted link approaches much like civilian cell-phone links, where a radio communicates with a base station and tower before it connects to the listener at the other end of the link.

Some years ago, DARPA proposed Mobile Ad Hoc Networking (MANET) technology for battlefield radios, in which the need for communications system infrastructure equipment, such as cell towers, is eliminated. The radios carried by soldiers in the field or installed in military vehicles communicate with each other, without the base station, acting as nodes on a mobile network.

Of course, for over 20 years now, MANET radios have been more of a curiosity than a reality, largely due to the small number of nodes that could reliably function without any form of infrastructure—limited by the transmit power and receiver sensitivity of the radios. The internet (also created by DARPA) is a form of ready-made infrastructure for MANET radios, if radio designers can incorporate internet-protocol (IP) processing within the radios.

Most attempts at doing so have been unsuccessful, and MANET has, until now, remained yet another "dark and mysterious" technology developed by DARPA. But during a recent visit to Persistent Systems, *Microwaves & RF*'s editors were treated to a demonstration of MANET radios using IP technology—without the network size limitations of many earlier MANET radio designs. These energy-efficient MANET radio designs *(see p. 56)* are modular and scalable, allowing for creation of large mobile ad hoc networks.

DARPA has championed many innovative technologies like the internet. MANET technology has been "on the edge" of the battlefield for many years, but has long had the potential to be one of the essential defense electronic technologies. Tactical communications are vital to all troops, and they can afford no less than the best!

NSA Certifies Airborne SDR

(Continued from page 45)

The ARC-210 RT-2036(C) SDR *(Fig. 2)* provides advanced communications capabilities, such as the U.S. Department of Defense's (DoD) Mobile User Objective System (MUOS), for which it's undergoing conformance testing with the U.S. Navy. The RT-2036(C) radio also meets the requirements for the Second-Generation Anti-Jam Tactical UHF Radio for NATO (SATURN) program while maintaining interoperability with legacy radio waveforms.

Rockwell Collins recently received a five-year IDIQ contract from the Navy for production deliveries of the ARC-210 RT-2036(C) radio. The radio features an open architecture that supports legacy radio waveforms and allows for software-based upgrades as needed. It operates over an extended frequency range compared to legacy military radio designs and implements the latest NSA algorithms and modernized Electronic Counter Countermeasures (ECCM) functions. de

Lockheed Martin Builds on IR Sensor System

(Continued from page 45)

efforts. It's currently mounted in the nose of the F/A-18E/F's centerline fuel tank *(see figure)* and in Legion Pod for other fighter and on-fighter platforms. The system is in full production and has been in use for more than 300,000 flight hours on the U.S. Navy's F-14 and F/A-18E/F, international F-15 platforms, and the U.S. Air Force's F-15C and F-16 fighter aircraft. de

The IRST21 sensor system mounted on the Navy's F/A-18E/F fighter uses IR technology to detect and track threats in environments that are difficult for radar systems. *(Courtesy of Lockheed Martin)*

RAYTHEON WINS PAIR OF NGA CONTRACTS

RAYTHEON CO. HAS garnered two National Geospatial Agency (NGA) contracts to develop data automation, analytics, and artificial-intelligence (AI) capabilities. The two prime indefinite-delivery, indefinite-quantity (IDIQ) contracts have a combined potential value of as much as $600 million. The Elevation Content and Precise Imagery programs, which will be led and handled by Raytheon Intelligence, Information and Services (IIS), are part of the NGA's Janus initiative to produce systems that provide NGA partners with access to NGA's content services.

"Our advanced analytics, automation, and AI will keep NGA capabilities on the cutting edge," says Dave Wajsgras, president of Raytheon IIS. "The solutions provided by NGA to the broader user community will offer higher quality and faster delivery of mission critical information."

Raytheon will apply more than 30 years of advanced photogrammetric algorithm development experience as part of automating the NGA's data production capabilities and streamlining the NGA's production processes and workflows in aligning with the NGA's Automation, Augmentation, and Artificial Intelligence (AAA) strategy. Jane Chappel, vice president of Global Intelligence Solutions at Raytheon IIS, notes, "The Janus program is just the latest example of NGA's forward-leaning approach to technology, and we're ready to support them as a key partner in this new initiative." ■

LTCC FILTERS

- New reduced size models (0805)
- Insertion loss as low as 0.8 dB
- Higher rejection rate, up to 45 dB
- Over 230 models **in stock!**

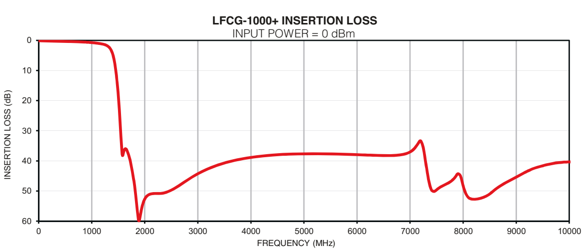

INPUT RETURN LOSS
INPUT POWER = 0 dBm

Mini-Circuits®

DARPA Calls on BAE and Smart Machines to Sort Signals

GROWING USE of RF/microwave signals may require machines and robots to keep things straight. For this reason, DARPA awarded BAE Systems a contract worth $9.2 million for its Radio Frequency Machine Learning System (RFMLS) program. DARPA is looking to BAE to develop new data-driven machine-learning algorithms to help decipher the growing number of RF/microwave signals populating an ever-more-crowded frequency spectrum. It's hoped that practical solutions can be developed to keep track of the many high-frequency wireless signals in use for commercial, industrial, and military applications.

DARPA has contracted BAE Systems to develop machine-learning solutions to help sort real from rogue RF signals.

Data-driven machine-learning research has made great strides in image and speech recognition, as well as fostering progress in developing safe autonomous vehicles. Machine-learning techniques are felt to be capable of supporting traditional RF/microwave signal-processing methods to identify and categorize high-frequency signals and separate dangerous rogue signals that could serve as jammers for an increasing number of wireless RF devices.

As the number of RF sensors increases for Internet of Things (IoT) applications as well as for such systems as unmanned aerial vehicles (UAVs) and unmanned ground vehicles (UGVs), data-driven machine learning may provide the means to quickly and effectively process many RF/microwave signals in an operating environment to prevent hacking, spooking, and disruption of desired RF-based services.

"The inability to uniquely identify signals in an environment creates operational risk due to the lack of situational awareness, inability to target threats, and vulnerability of communications to malicious attack," says Dr. John Hogan, director of the Sensor Processing and Exploitation product line at BAE Systems. "Our goal for the RFMLS program is to create algorithms that will enable a whole new level of understanding of the RF spectrum, so users can identify and react to any signals that could be putting them in harm's way."

Under this Phase 1 contract, BAE Systems' scientists intend to create machine-learning algorithms based on cognitive approaches that can identify and differentiate signals according to applications. The researchers intend to sort through signals in real time based on relative importance, so that interference and disruption of applications can be avoided.

The RFMLS program involves work on machine learning as well as artificial-intelligence (AI) research. BAE's research will build on the company's vast expertise in its autonomy technology portfolio. It adds to previous work involving machine learning and intelligence, including the DARPA Communications Under Extreme RF Spectrum Conditions (CommEX) and Adaptive Radar Countermeasures (ARC) programs. BAE Systems has also advanced to the second round of another major DARPA effort to bring machine learning and AI to the RF domain called the Spectrum Collaboration Challenge (SC2). Work on the RFMLS program will be performed at BAE's facilities in Burlington, Mass. and Durham, N.C. ■

Optical Technology Takes on NCDL Signals

TRADITIONALLY, the wide bandwidths and high frequencies required for the interchange of common-data-link (CDL) signals for communications between different intelligence, surveillance, and reconnaissance (ISR) systems operated by armed forces and government agencies has required heavy waveguide transmission lines. These lines are needed to support bidirectional microwave signals at about 14 to 16 GHz between sensors, terminals, remote antennas, and other system platforms. But Optical Zonu *(www.opticalzonu.com)* shows that it's possible to accomplish CDL communications reliably and securely using optical communications technology.

The company's OZC RFoF CDL Link, a lightweight alternative to waveguide, has been a part of secure, high-speed links for the Navy CDL (NCDL) system. It uses optical signals to transfer CDL signals over much greater distances than possible with electromagnetic (EM) signals over waveguide—as far as 50 km—with the wide bandwidths needed for CDL signals. The system, which features a broadband optical transceiver with wide dynamic range, employs fiber fault detection for enhanced reliability and suffers much less signal loss than traditional waveguide CDL solutions.

The fiber fault detection used in many of the firm's optical transceivers operates very much like a radar system over a conventional two-fiber optical communications link. When a data link fails to connect or suffers a disruption in service, the transmitter section of the transceiver switches into transmit optical-time-domain-reflectometer (TxOTDR) mode and emits optical pulses into the cable, at power levels of +13 dBm or higher. The receiver portion of the system then detects the returning reflected optical pulses at optical power levels as low as –52 dBm to determine the location of the intermittent connection or fault in the optical fiber.

Such innovative optical fiber technology protects naval data, but it's also well-suited for commercial applications and public utilities, communications network monitoring, and maintenance.

JACK BROWNE | Technical Contributor

Measuring Advances in Military Test Equipment

Increasing complexity in military electronic systems pushes test-equipment suppliers to deliver high-performance measurement solutions with as many functions as possible.

GREATER COMPLEXITY in military electronic systems requires more capabilities in the measurement equipment used to test those systems. Consequently, various market studies predict healthy growth for at least the next five years for test equipment aimed at specific markets within military electronics, such as mobile radio testing and aviation test equipment. Mobile radios are being designed smaller and lighter with multiple frequency bands and modulation formats, while aviation testing must account for the increased use of robotic and automated systems as well as RF/microwave and digital electronics systems.

In the case of mobile radios, single models are being designed with multiple modulation formats, switchable bandwidths, and increased frequency ranges that must be covered by candidate test instruments. Aviation testing involves a wide range of measurements, from characterizing communications and GPS radios to checking brakes, hydraulic systems, and vacuum integrity. Increasing use of military unmanned aerial vehicles (UAVs) is a main driver behind the expected growth in demand for electronic test equipment aimed at aviation systems. Major customers for test equipment in these two military market areas are expected to be Boeing, General Electric, Honeywell, Lockheed Martin, and Rockwell Collins.

Test equipment for evaluating the RF/microwave performance levels of mil/aero systems and their components covers a wide range of frequencies and functions due to the diversified nature of military electronic systems. An analyzer that can digitize and accurately display the key parameters of a radar pulse may not be the best choice for deciphering the characteristics of a secure radio communications system.

Leading suppliers of test equipment for military electronic applications are quite aware of the needs of military specifiers. They are continually evaluating available high-frequency technologies for what might form the basis for next-generation test equipment. Their efforts result in constantly improving test gear for the two main measurement functions needed to characterize military electronic systems: signal generation and analysis.

GENERATING SIGNALS

Signal generators for military applications must cover an enormous amount of ground in terms of frequency and waveform type, given the range of signal formats used—from radar pulses to complex modulated millimeter-wave (mmWave) signals in secure communications systems. Rather than rely on a conventional swept-frequency signal generator, military systems testers are turning more to arbitrary waveform generators (AWGs). AWGs have the capability to almost randomly program different waveform formats over a defined frequency range.

Although early AWG models were limited in frequency and functionality, newer models are providing more of the signal-generation capabilities needed for evaluating different military electronic systems. Of course, as commercial applications such as advanced driver-assistance systems (ADAS) increasingly adopt waveforms (radar pulses) like those used by the military, many of the same AWGs employed in military electronic testing will also work in commercial applications.

1. Model M3302A is an AWG that also incorporates a two-channel, 500-Msamples/s digitizer in its compact PXIe format. *(Courtesy of Keysight Technologies)*

In the case of the M3302A AWG from Keysight Technologies, it can also be used to digitize the signals that must be "imitated" by its AWG section. The PXIe modular instrument *(Fig. 1)* provides two channels at 500 Msamples/s and 16-b vertical resolution as an AWG, and two channels at 500 Msamples/s and 14-b resolution as a digitizer. Whether for signal generation or capture, it can hold as much as 2 GB of random-access memory (RAM).

The two key instrument functions are designed to work together as an integrated system, with less than 400-ns latency from input-to-output signal processing. This combination of functions within such a compact modular footprint (fitting two slots in a 3U-high PXIe chassis) makes the M3302A a good choice for testing electronic-warfare (EW) systems and radars, and performing channel emulation for even advanced software-defined-radio (SDR) systems. It can be used with software or hardware programming, or no programming, using a mechanical control interface.

The trend of adding functionality to essential instrument functions also follows in the model UHFAWG AWG from Zurich Instruments *(www.zhinstruments.com)*, which integrates signal generation and detection within the same compact instrument. As with the Keysight AWGs, it can program its own waveforms and digitize external signals via its two 600-MHz input channels. The two channels are tightly matched in terms of amplitude and phase characteristics to provide phase coherency for the most demanding multichannel test applications.

For radio and other system testing, such an AWG would inject test signals into a system's intermediate-frequency (IF) ports or add a frequency upconverter to reach the RF/microwave frequency range. In contrast to conventional swept-frequency RF/microwave test signal sources, such as those based on frequency-synthesized YIG or voltage-controlled oscillators, AWGs provide the means to define test signals by key signal characteristics.

The recently launched AFG31000 series of AFGs from Tektronix *(see Microwaves & RF, November 2018, p. 54)* provide signal bandwidth to 250 MHz. The test signal sources resemble small computers, using a 9-in. diagonal capacitive touchscreen for display and straightforward programming *(Fig. 2)*.

For wide bandwidth within a single box, there's the model N5193A UXG Agile Signal Generator from Keysight Technologies, which comes in two versions: 10 MHz to 20 GHz or 10 MHz to 40 GHz, in standard rack-mount enclosures. The test signal source can

2. The AFG31000 series of arbitrary function generators use a large capacitive touchscreen to define waveform parameters. *(Courtesy of Tektronix)*

provide as much as +10 dBm output power across the frequency range, with optional attenuators bringing output levels as low as –130 dBm. The test signal source can generate everything from CW signals to short pulses, with pulse widths as narrow as 4 ns with 40-ps typical accuracy and 10-ps delay resolution. Frequency switching speeds run from typically 1 μs in standard units to 50 ns as an option.

For even wider bandwidth, the MG3690C analog signal generator from Anritsu provides a frequency range of 0.1 Hz to 70 GHz from a single coaxial connector. With typical frequency switching speed of 5 ms, it generates pulses as narrow as 100 ns. It also comes in a rack-mount enclosure *(Fig. 3)* meant for laboratory applications.

3. The model MG3690C signal generator provides signals covering 0.1 Hz to 70 GHz from a single coaxial connector. *(Courtesy of Anritsu Co.)*

ANALYZING SPECTRUM

Spectrum and signal analyzers, important tools in any military electronics test solution, are also commonly found in rack-mount enclosures as well as in portable and modular packages. However, Signal Hound added new meaning to modularity in test equipment with its model SM200A USB spectrum analyzer, with a compact size that belies its 20-MHz-to-20-GHz real-time analysis bandwidth.

The firm recently demonstrated the analyzer at the 55th Annual Association of Old Crows (AOC) International Symposium in partnership with the Linux-based SCEPTRE signal-collection software from 3dB Labs *(Fig. 4)* for spectrum monitoring, including for intelligence, surveillance, and reconnaissance (ISR) and signal-intelligence (SIGINT) applications.

4. The SM200A USB spectrum analyzer (on left) performs ISR and SIGINT measurements when equipped with SCEPTRE software from 3dB Labs. *(Courtesy of Signal Hound)*

As spectral occupancy reaches into the mmWave range, spectrum analysis and monitoring must follow, and many suppliers have developed benchtop spectrum analyzers with coverage well above 30 GHz. One of the wider-bandwidth signal analyzers, the R&S FSW85 *(Fig. 5)*, has a dc-coupled frequency range of 2 Hz to 85 GHz and an ac-coupled frequency range of 10 MHz to 85 GHz. It has a variety of built-in filters with resolution bandwidths from 1 Hz to 10 MHz for sorting signals.

5. The R&S FSW85 signal analyzer has a dc-coupled frequency range of 2 Hz to 85 GHz and an ac-coupled frequency range of 10 MHz to 85 GHz. *(Courtesy of Rohde & Schwarz)*

The FSW85 achieves a displayed average noise level (DANL) of typically –123 dBm or better at 85 GHz with YIG preselection and no attenuation or preamplification, and much better at lower frequencies. RF/microwave input signal ports are equipped with 1.0- and 1.85-mm male coaxial connectors. Numerous software packages are available for the spectrum analyzer, including for pulse and chirp testing.

Portability is an important attribute for many test instruments meant for military electronic testing in the field, and Keysight's FieldFox handheld analyzer is well-known for its measurement power in a small package. Models are available with "just" spectrum analyzers, with vector network analyzers (VNAs), and with combination spectrum analyzers and power meters operating at frequencies to 50 GHz to meet in-field requirements for higher-frequency signal analysis. All three types of FieldFox analyzers can make pulsed measurements over their frequency ranges, with starting frequencies of 30 kHz, 100 kHz, and 2 MHz.

In terms of integrating measurement power into a small package, few instruments can match the CTS-6010 tactical radio test set from Astronics *(www.astronics.com)*. It includes an RF/microwave signal generator, audio analyzer, RF/microwave signal analyzer, RF power meter, and oscilloscope in package with upgradable modularity *(Fig. 6)*. Optimized for military radio testing, the signal generator, spectrum analyzer, and power meter all cover a frequency range of 1 MHz to 6 GHz. The two-channel oscilloscope is lower in frequency, with a bandwidth of 25 MHz and voltage range of ±40 V.

6. The CTS-6010 tactical radio test set packs more than a dozen instrument functions covering 1 MHz to 6 GHz into a handheld housing. *(Courtesy of Astronics)*

These portable analyzers represent only a small sample of the many portable instruments available for in-field radar and radio testing, including the A734 portable analyzer from ProTek and the Spectrum Master line of portable spectrum analyzers from Anritsu, with its model MS2760A-0110 and a frequency range of 9 kHz to 110 GHz and dynamic range of better than 100 dB at 110 GHz. The next issue of *Defense Electronics* will take a closer look at more mmWave-capable portable spectrum analyzers and applications that can aid military electronics testers. de

JACK BROWNE | Technical Contributor

RADIO MODULES Offer Embedded Mobility

These compact radios employ MANET technology for scalability and ease of mobility, and plug-in frequency modules to adapt to the spectrum needs of different applications.

MOBILITY IS an important part of modern communications, in both commercial and military applications. Radio users require mobility, not a fixed communications terminal, and radios that can move with them and operate reliably, often across multiple frequency bands to reach different groups of users.

Persistent Systems, with its modular radio designs and use of Mobile Ad Hoc Networking (MANET) technology, provides mobile radio solutions that are as effective for humans as for machines. These solutions deliver easily integrated radio links for frequencies in L-band (1350 to 1390 MHz), BAS (2025 to 2150 MHz), S-band (2200 to 2500 MHz), and C-band (4400 to 6000 MHz) ranges.

MANET radio technology was developed with the encouragement of DARPA, hoping to create a radio technology that would allow mobile communication anywhere in the world without relying on fixed communications infrastructure (e.g., cellular radio towers). Persistent Systems has developed several lines of MANET radios suitable for human as well as robotic users, such as the unmanned aerial vehicles (UAVs) increasingly used for defense ISR operations.

Its Wave Relay MANET technology can be scaled to create large networks by using multiple hops with high throughput and minimal latency. MANET radios apply internet-protocol (IP) communications techniques, with each radio appearing much like a relay or switch within the network. The radios can send and receive voice over IP (VoIP), video, and high-speed data under demanding conditions to meet the requirements for military applications; versions of the radio can serve a wide range of human and machine applications.

1.The MPU5 Wave Relay MANET radio can be equipped with different frequency modules for operation at L- through C-band frequencies. *(Courtesy of Persistent Systems, LLC)*

For humans, the MPU5 Wave Relay mobile radio *(Fig. 1)* is a portable, battery-powered Android computer, powered by a 1-GHz quad-core processor. The radio, equipped with 2 GB of random-access memory (RAM) and 128 GB of flash memory, can run Android applications and connect and control as many as three USB devices with three compatible ports. It has a built-in GPS radio for position information, HD video encoder, HD video decoder, 16 channels of push-to-talk voice communications, integrated radio-over-IP (RoIP) functionality, and 10/100 Ethernet connectivity for data rates approaching 100 Mb/s.

The radio's simple modular design features a chassis and plug-in frequency module that determines the operating frequency range. The RF-1100 L-band module runs 1350 to 1390 MHz, the RF-2100 S-band module operates from 2200 to 2500 MHz, and the RF-4100 lower C-band has a frequency range of 4435 to 4980 MHz. At most frequencies, the MPU5 provides as much as 6 W transmit power and is capable of 10 W transmit power at S-band frequencies.

The MPU5 uses software configurable bandwidth of 5, 10, or 20 MHz and a variety of modulation formats, including binary phase-shift keying (BPSK), quadrature phase-shift keying (QPSK), 16-state quadrature amplitude modulation (16QAM), and 64-state quadrature amplitude modulation. For optimum reception, it operates with a variety of antenna configurations, from single-input, single-output (SISO) through 3 × 3 multiple-input, multiple-output (MIMO) antenna setups.

The interchangeable frequency modules for the Embedded Module *(Fig. 2)* are available for L-band frequencies from 1350 to 1390 MHz, S-band frequencies from 2200 to 2507 MHz, BAS (broadcast) band frequencies from 2025 to 2150 MHz, lower C-band frequencies from 4400 to 5000 MHz, and upper C-band frequencies from 5100 to 6000 MHz.

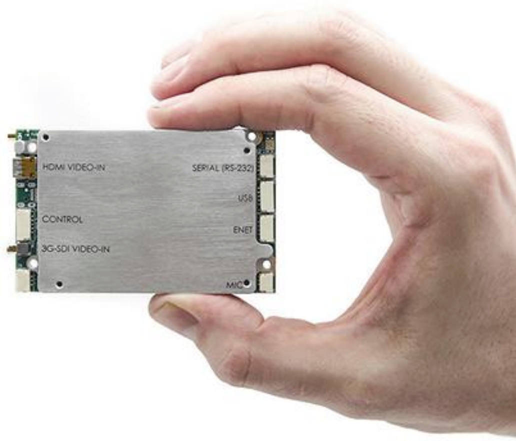

2. Embedded Modules are compact versions of the MPU5 Wave Relay radio, using many of the same frequency modules and having many of the same capabilities for UAVs and UGVs. *(Courtesy of Persistent Systems, LLC)*

The radios are RoHS-compliant and screened to IP68 for ingress protection from solid objects and liquids. They are designed for operating temperatures from –40 to +85°C.

COMPACT MODULES

For machines such as UAVs and unmanned ground vehicles (UGVs), the Embedded Module is a compact version of the MPU5 Wave Relay radio. It has the same choices in frequency bands as the MPU5, but in a format that can readily be integrated into larger systems. *(For an example of how these compact MANET radios are employed in UAVs, see "Persistent, Insitu Team on UAV MANET Radios" on www.mwrf.com.)*

The interchangeable frequency modules for the Embedded Module *(Fig. 2)* are available for L-band frequencies from 1350 to 1390 MHz, S-band frequencies from 2200 to 2507 MHz, BAS (broadcast) band frequencies from 2025 to 2150 MHz, lower C-band frequencies from 4400 to 5000 MHz, and upper C-band frequencies from 5100 to 6000 MHz. As with the frequency modules for the MPU5 Wave Relay radio, the modules for the Embedded Module are available for channel bandwidths of 5, 10, and 20 MHz. The Embedded Module radios can also operate with the same RF modulation formats as the MPU5. Both forms of the MANET radios can output 1080-pixel video.

With choice of frequency range, the software-configurable Embedded Module radios support three independent antenna chains, in configurations from SISO to 3 × 3 MIMO. The Embedded Module radios achieve radio receiver sensitivity of –98 dBm or better for a 5-MHz bandwidth, and peak data throughput of 150 Mb/s when operating at L-band frequencies with a 20-MHz channel; standard and high-power L-band modules are available. For the high-power L-band module, the transmit power can be set from +16.5 to +35.0 dBm in 0.5-dB steps. Power accuracy is ±2 dB, while worst-case frequency accuracy is ±4 ppm.

Since UAVs, UGVs, and other unmanned systems are often subject to strict requirements for electromagnetic interference (EMI) and electromagnetic compatibility (EMC), the Embedded modules are pre-certified for EMI according to MIL-STD-461 RE102 standards *(Fig. 3)*. Given the high integration of function blocks within the Embedded Module, devices such as its on-board computer, video encoders, transmitters, and command and control circuits do not need to be certified separately. To help further speed the adoption of the Embedded Module, it's available as part of an Embedded Module Development Kit, which also includes cables, an external radio mounting tray, and design documentation/software files.

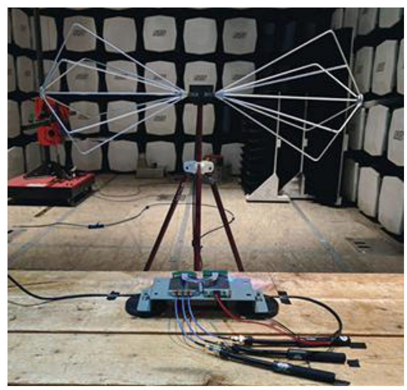

3. Pre-certification EMI testing of Embedded Modules is performed according to MIL-STD-461 RE102 standards within this well-equipped facility. *(Courtesy of Persistent Systems, LLC)*

The Embedded Module MANET radios, for such compact designs, are well-equipped with interconnections: 3G-SDI, composite, and HDMI video input connectors, RS-232 serial interconnection, USB OTG input/output connector, and 10/100 Ethernet input/output connector. Embedded Module radios have main circuit-board dimensions of 2.00 × 3.29 × 0.59 in. and weigh 3.2 oz. The Embedded Modules work with voltages of 8 to 30 V dc and draw 300-mA current from a 12-V dc supply. de

PERSISTENT SYSTEMS, LLC, 303 5th Ave., New York, NY 10016; (212) 561-5895; www.persistent.com.

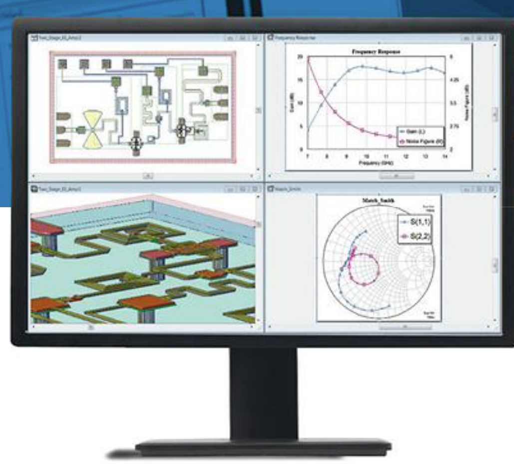

JACK BROWNE | Technical Contributor

Making DRFMs More Durable

Data is an invaluable resource in military electronic systems, and modern DRFMs provide a reliable means of protected and preserving captured information.

1. **Board-level DRFMs like that shown are powered by Virtex-5 processors/FPGAs and dedicated data converters.** *(Courtesy of Mercury Systems)*

DIGITAL RF memories (DRFMs) are critical components in many electronic-countermeasures (ECM) defense-electronics systems. They provide the means of harvesting and reusing RF/microwave signal waveforms via almost instant analog-to-digital conversion and digital signal processing, using powerful processors, mixed-signal electronics, and dedicated software packed into compact modules.

Of course, as with other markets, military specifiers are seeking smaller, lighter, and more reliable DRFMs. Design efforts embraced by DRFM designers that employ goals based on reduced size, weight, and power (SWaP) are delivering a new generation of devices that are smaller and more powerful than before and come with innovative modularity for improved reliability and ease of use.

Smaller, lighter DRFMs are important not so much for legacy military/aerospace electronic systems, but more for their expanding roles in unmanned aerial vehicles (UAVs) and unmanned marine vehicles (UMVs) used for intelligence, surveillance, and reconnaissance (ISR) missions. In unfamiliar territory, for example, U.S. Army troops often refer to surveillance drones and their DRFM-based systems as “eyes in the skies.” Some of these military drones are unmanned aerial systems (UAS), capable of carrying multiple missiles and jammers in addition to cameras, receivers, and transmitters to perform many different electronic-warfare (EW) operations under remote control from a distance.

The DRFMs within these systems are typically part of instantaneous-frequency-measurement (IFM) subsystems. DRFMs also find use in commercial and civilian applications, such as police-radar jammers and for cellular-telephone test equipment.

For ease of integration into larger systems with IFM functionality, DRFMs have traditionally been designed as printed circuit boards (PCBs). They are then installed into plug-in enclosures with board-mounted RF and digital/control connectors to facilitate interconnections with other systems.

Board-level DRFMs *(Fig. 1)* from Mercury Systems *(www.mrcy.com)*, for example, are available with analog-to-digital and digital-to-analog converters (ADCs and DACs) operating at sampling rates to 2.2 Gsamples/s, plus powerful Virtex-5 microprocessors from Xilinx *(www.xilinx.com)*. Such microprocessors rely on software-based programming to modify the delay times between the ADCs and DACs so that signals received from a threat radar system can be delayed an amount of time corresponding to a different target location, and then transmitted back to the threat radar so that the apparent location of its target is different than the actual target.

These compact board-level DRFMs rely on other system functions, such as RF/microwave frequency downconversion (receivers) and upconversion (transmitters), filtering, and amplification. However, they are available as part of IFM systems with frequency ranges from 0.5 to 2.5 GHz or 2 to 18 GHz, or as even more compact modules for airborne use.

SHRINKING SIZE

The demand for lower SWaP has been aided by using system-on-chip (SoC) semiconductor devices such as microprocessors combined with ADCs and DACs. This allows the design of extremely dense and powerful DRFM architectures into standard module formats such as OpenVPX.

For example, the first member of the Quartz line of products, the Model 5950 eight-channel signal processor from Pentek *(www.pentek.com)*, is based on a highly integrated Zynq Ultrascale+ RFSoC FPGA from Xilinx, which features eight high-speed ADCs and DACs integrated into the semiconductor circuitry with the microprocessor. As a

The demand for lower SWaP has been aided by using system-on-chip (SoC) semiconductor devices such as microprocessors combined with ADCs and DACs. This allows the design of extremely dense and powerful DRFM architectures into standard module formats such as OpenVPX.

result, the data converters are already available and do not need to be added to a board-level circuit solution.

By packing so much power into a single chip, even a compact module such as a 3U OpenVPX circuit board *(Fig. 2)* can carry much greater functionality—a GPS receiver, a large amount (18 GB) of DDR4 SDRAM memory, a PCIe interface, a gigabit serial optical interface that supports 100 Gigabit-Ethernet connections, and an on-board timing bus generator. Because of the flexibility and programmability of having an RFSoC with FPGA at the heart of the design, the Quartz Model 5950 can serve any number of applications, including as a chirp generator, a data-acquisition system, and a DRFM. In fact, Pentek offers intellectual-property (IP) programming that has been developed and refined to turn this RFSoC module into a DRFM with programmable delays from 1 to 32768 data samples.

MORE MEMORY

The same company's Talon RTX 2590 small-form-factor (SFF) module is a 250-Msample/s RF/IF signal recorder that's built for harsh environments—and for ease of data exchange after a mission *(Fig. 3)*. This SFF signal recorder provides eight phase-coherent channels of 250-MHz, 16-b ADCs, allowing users to capture as much as 100 MHz of RF/IF signal bandwidth per channel with wide dynamic range. It measures just 7.688 × 4.880 × 14.125 in., supplied in a 1/2 MIL Air Transport Rack (ATR) enclosure that can also hold as much as 30 TB of solid-state-data (SSD) memory.

The signal recorder records speeds to 4 Gb/s and can be equipped with a GPS receiver for time-stamping and positioning of recordings plus optical I/O rear-panel connections as options. The programmable recorder features the convenience of modular, removable SSD memory as well as a removing operating system (OS) drive. It employs Pentek QuickPac drive packs to make it possible to quickly remove all data storage from a recorder via the front panel. Circular connectors on the rear panel include power and computer interconnections, as well as bulkhead-mounted SMA connectors for all RF/microwave signals, GPS, clocks, and triggers. All are sealed for RF emissions and moisture protection.

In general, DRFM suppliers are facing the need to develop smaller, modular units that can be used with a great deal of flexibility in different applications. Long-time DRFM supplier Curtiss-Wright *(www.curtisswright.com)* employs commercial-off-the-shelf (COTS) devices and components in its modular DRFMs and frequency-conversion units. It also offers software-defined-radio (SDR) programming flexibility in support of UAVs for the Army and UMVs for the Navy. The firm has adopted the use of removable data storage for convenience, and in recognition of the growing amount of sensor data from both military and commercial applications, such as IoT devices.

Additional suppliers of DRFMs include Herley Whippany/Ultra Electronics *(www.ultra-herley.com)*, Israel Aerospace Industries *(www.iai.co.il)*, Mistral Solutions *(www.mistralslutions.com)*, and SA Photonics *(www.saphotonics.com)*. Also in the mix are major defense contractors, such as BAE Systems *(www.baesystems.com)*, Elbit Systems *(www.elbitsystems.com)*, Northrop Grumman Corp. *(www.northropgrumman.com)*, Raytheon Co. *(www.raytheon.com)*, and the Thales Group *(www.thalesgroup.com)*. de

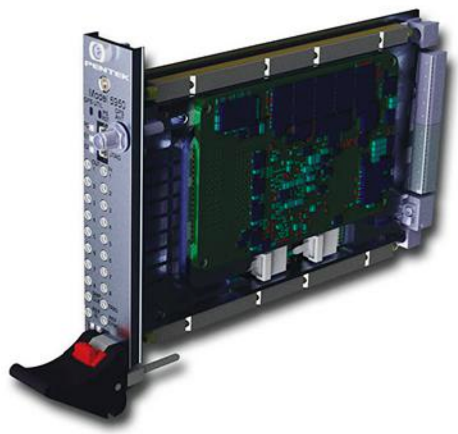

2. A highly integrated FPGA/processor with integrated data converters is at the heart of this compact programmable eight-channel signal processor. *(Courtesy of Pentek)*

3. This RF/IF signal recorder can hold as much as 30 TB of SSD memory in a 1/2 ATR MIL enclosure, with the unique QuickPac packaging technology. *(Courtesy of Pentek)*

Rugged Ethernet Cables Handle Harsh Environments

THE RAYCHEM CAT 5e cable, constructed from high-temperature fluoropolymers, provides Ethernet connectivity to 1 Gb/s in harsh military and aerospace environments. Light in weight and easy to terminate, the cables maintain flexibility even across a wide range of temperatures (–65 to +200°C). The water block variation of the cable uses highly absorbent tapes and yarns for reduced weight compared to silicon-filled water block cables. They are well-suited for many different applications, including in shipboard and satellite communications systems, avionics systems, and weapons systems.

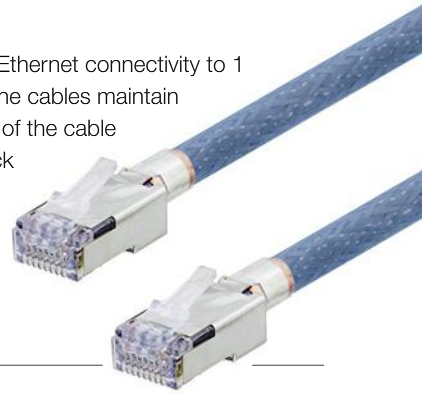

TE CONNECTIVITY

Harrisburg, PA 17106, (800) 522-6752, www.te.com

Low-Noise Amplifier Boosts 0.5 to 8.0 GHz

MODEL CMA-83LN+, a wideband, low-noise amplifier (LNA) fabricated with pHEMT MMIC technology, comes in a hermetic, nitrogen-filled, low-profile package with low-temperature-cofired-ceramic (LTCC) base. The LNA operates from 0.5 to 8.0 GHz and features 1.6-dB typical noise figure at 0.5 GHz, 1.5-dB typical noise figure at 4.0 GHz, and 1.6-dB typical noise figure at 8.0 GHz when operating from a +6-V dc supply. The typical gain is 21.2 dB at 0.5 GHz, 20.6 dB at 4.0 GHz, and 19.2 dB at 8.0 GHz. The typical output 1-dB intercept is +17.6 dBm at 0.5 GHz, +18.0 dBm at 4.0 GHz, and +16.9 dBm at 8.0 GHz. Typical output third-order intercept (IP3) is +29.4 dBm at 0.5 GHz, +28.1 dBm at 4.0 GHz, and +26.7 dBm at 8.0 GHz. The 50-Ω amplifier measures just 0.12 × 0.12 × 0.045 in. and is designed for operating temperatures from –40 to +125°C.

MINI-CIRCUITS

P.O. Box 350166, Brooklyn, NY 11235-0003, (718) 934-4500, www.mini-circuits.com

Fixed Attenuators Provide Level Control to 26.5 GHz

MODEL 9454-X (with x the attenuation value) is a line of extremely broadband fixed attenuators with standard attenuation values of 3, 6, 10, and 20 dB from DC to 26.5 GHz. They provide flat attenuation across the full frequency range, with attenuation accuracy of ±0.40 dB for attenuation values from 1 through 6 dB, ±0.60 dB for attenuation values from 7 through 20 dB, and ±0.80 dB for attenuation values from 21 through 30 dB. The attenuators, which are ideal for measurement applications as well as for precise level control in systems, handle power levels to 2 W. They are supplied with 3.5-mm coaxial connectors and are available with male-to-female, male-to-male, and female-to-female connector combinations. The typical VSWR is 1.30:1 from DC to 18.0 GHz and 1.40:1 from 18.0 to 26.5 GHz. The 50-Ω fixed attenuators, which are also available in calibrated sets with values of 3, 6, 10, and 20 dB, feature stainless-steel housings with gold-plated beryllium copper center conductors. They are rated for operating temperatures from -55 to +85°C.

ARRA, INC.

15 Harold Ct., Bayshore, NY 11706, (631) 231-8400, www.arra.com

Amplifiers Channel 100 MHz to 40 GHz

OVER 300 low-noise amplifier (LNA) models are available in the LNA series for applications in frequency bands from 100 MHz to 40 GHz and output-power levels of +10, +15, +20, or +25 dBm. For example, the lowest-power (+10 dBm) LNAs are available for frequency ranges of 1 to 2 GHz, 2 to 4 GHz, 4 to 8 GHz, 8 to 12 GHz, 12 to 18 GHz, 18 to 26.5 GHz, and 26 to 40 GHz, with minimum gain levels of 20, 30, or 40 dB. Gain flatness ranges from ±1.5 dB from 1 to 12 GHz to ±2.5 dB from 26 to 40 GHz. The worst-case noise figure is 0.6 dB from 1 to 4 GHz, 2.2 dB from 18 to 26.5 GHz, and 2.7 dB from 26 to 40 GHz. The RoHS-compliant amplifiers operate on supplies of +15 V dc and are designed for operating temperatures from -55 to +85°C. They are unconditionally stable and are impedance matched to 50 Ω at input and output ports.

L3 TECHNOLOGIES, NARDA-MITEQ

435 Moreland Rd., Hauppauge, NY 11788, (631) 231-1700, FAX: (631) 231-1711, E-mail: componentsnm@L3T.com, www.nardamiteq.com.

Military-Grade RF Cables Make Connections to 12.4 GHz

A LINE OF military-grade MIL-DTL-17 RF cable assemblies that are ideal for avionics, military electronics, satellite ground stations, and autonomous vehicles can be specified for same-day shipment in 124 basic configurations and six different cable types. The cable assemblies support operating frequencies from dc to 12.4 GHz with VSWR as low as 1.30:1 per connector. The cable assemblies are made from MIL-DTL-17 qualified cable, MIL-PRF39012 qualified connectors, AS23053 heat shrink, and J-STD solder. The COTS cable assemblies are 100% tested and shipped with a test report and material lot traceability. P&A: stock.

PASTERNACK ENTERPRISES

17792 Fitch, Irvine, CA 92614, (949) 261-1920, www.pasternack.com

Amplifier Powers 1 kW to 1 GHz

MODEL 2162 is a broadband solid-state power amplifier capable of 1000 W saturated output power from 20 to 1000 MHz. Based on silicon LDMOS power transistors, the Class AB power amplifier provides at least 500 W output power at 1-dB compression with at least 63-dB power gain. Second harmonics are –20 dBc or less while spurious content is –60 dBc or less. The amplifier is designed for a single-phase 220-V supply and consumes 6000 VA or less power at maximum output power. It comes in a rack-mount enclosure measuring 17.5 × 8.75 × 22 in. complete with forced-air cooling.

EMPOWER RF SYSTEMS INC.

316 W. Florence Ave., Inglewood, CA 90301; (310) 412-8100, www.EmpowerRF.com

Phase Shifter Adjusts DC to 18 GHz

MODEL 9426A IS a broadband phase shifter with low loss and insertion delay from DC to 18 GHz. It provides minimum phase adjustment of 60 deg./GHz, with 360-deg. phase adjustment at 6 GHz. Phase is adjusted by means of a 0.25-in. nontranslating shaft. The worst-case insertion loss is 0.50 dB to 8 GHz, 0.75 dB to 12 GHz, and 1.0 dB to 18 GHz. The worst-case VSWR is 1.30:1 to 4 GHz, 1.50:1 to 12 GHz, and 1.60:1 to 18 GHz. The rugged phase shifter is supplied in an aluminum housing with stainless-steel SMA connectors. It handles 100 W average power and 5 kW peak power.

ARRA, INC.

15 Harold Ct., Bayshore, NY 11706, (631) 231-8400, www.arra.com

Coaxial Probes Reach 40 GHz

AN EXPANDED LINE of RF coaxial probes now operates from DC to 40 GHz for high-speed communications and networking applications. The expanded line now includes four models with return loss of 10 dB or better. The RF probes are available in ground-signal (GS) and ground-signal-ground (GSG) configurations with a pitch of 800 or 1500 μm and a 2.92-mm interface. They are gold-plated and feature compliant pogo pin contacts that allow for a wide range of probing angles. The coaxial probes can be used by hand, with or without a probe positioner, and can be cable mounted or mounted with a multiaxis probe positioner. They are ideal for signal integrity measurement, coplanar waveguide, chip evaluation, substrate characterization, Gigabit SERDES, and test fixture applications.

FAIRVIEW MICROWAVE

17792 Fitch, Irvine, CA 92614, (978) 682-6936; www.fairviewmicrowave.com

Flexible Waveguide Connects 50 to 75 GHz

MODEL SWG-15020-FB-F is a 2-in. (50.8-mm) section of flexible waveguide with a WR-15 waveguide flange and UG-386/U flange. It exhibits low loss from 50 to 75 GHz and features a polysulfide rubber jacket for added robustness. The flexibility ensures that the waveguide section will provide long-term stress-free interconnections when integrated into millimeter-wave (mmWave) systems. Various standard and custom-length options of the flexible waveguide are also available.

SAGE MILLIMETER INC.

3043 Kashiwa St., Torrance, CA 90505, (424) 757-0168, FAX: (424) 757-0188, E-mail: sales@sagemillimeter.com, www.sagemillimeter.com

JIYOUN MUNN | RF Technical Product Manager, COMSOL
www.comsol.com

Designing Cavity Filters for the 5G Network

How can cavity filter designers capitalize on multiphysics software that takes real-world conditions into account?

The impending 5G network has created a race for new spectrum bands to accommodate wireless traffic. As smartphone technology continues to offer more complex solutions, the need to transmit and receive paths from a variety of sources requires multiple bands operating simultaneously through a single antenna or multiple-input, multiple-output (MIMO) systems.

Microwave cavity filters are utilized to get rid of unwanted frequency components. They are found in telecommunication infrastructures that handle signals ranging from tens of megahertz to several gigahertz.

A filter's performance may vary under severe environmental conditions. For example, a drastic rise in temperature can result in structural deformation caused by unexpected heat expansion. The physical phenomena beyond electromagnetics (EM) may not be included in a conventional EM simulation, as well as indoor laboratory measurements, despite having a large impact on the final product.

RESONANCE FREQUENCY CHANGES DUE TO THERMAL DRIFT

When a cavity filter is built with metallic materials, its performance in terms of resonant frequency can be vulnerable to severe temperature fluctuations. High-power loads or harsh environmental conditions can result in thermal drift, which makes it difficult to stabilize the high frequency of the filter. However, with the help of multiphysics simulation, it can be easy to analyze the resonant frequencies of an arbitrary shape of a structure through an eigenfrequency study.

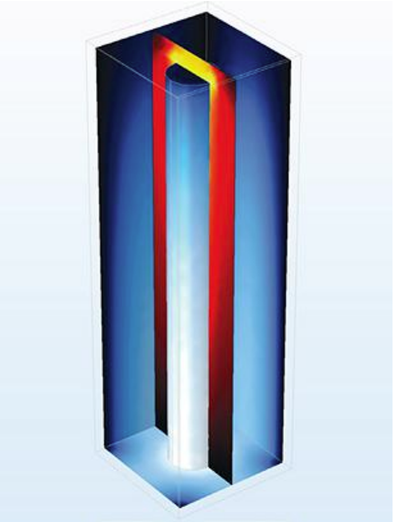

1. This is a slice plot of electric field norm and surface plot of surface current density norm.

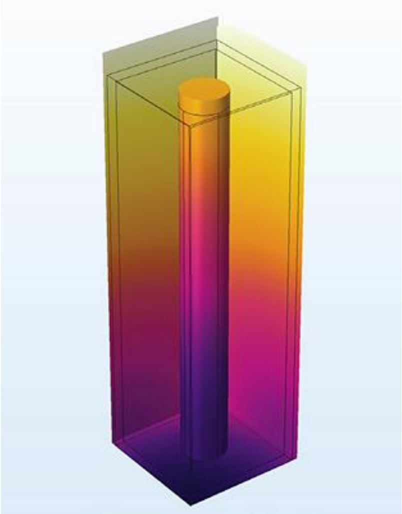

2. Here's a surface plot of total displacement due to the thermal expansion. The displacement plot is exaggerated for visualization purposes.

Consider an example model of a cavity filter that consists of a thin metallic box that's finished with copper and contains a cylindrical post *(Fig. 1)*. The simulation was conducted to determine the effect on the filter resonance when the temperature changes from 0 to +100°C. Three things we are interested in analyzing include:

- Structural mechanics
- Geometry deformation
- EM waves

These parameters capture how the temperature increase affects structural deformation and the cavity filter's resonant frequency. We found that the thermal expansion and associated drift in eigenfrequency are caused by a uniform increase in the temperature of the cavity wall and the post surface *(Fig. 2)*. Thermal drift has become a bigger concern as the frequency spectrum becomes more crowded in the race for 5G. Engineers designing cavity filters in locations that are subject to extreme conditions will want to be sure they conduct this type of analysis.

MATERIALS MAKE A BIG DIFFERENCE

Let's now look at an example made of steel iron. By adding a material with a lower thermal expansion coefficient, such as steel iron, we are able to reduce the variation of the resonant frequency caused by the temperature increases. To examine the differences between the first example, containing copper only, and this second example that contains copper and steel, we conducted another eigenfrequency analysis using multiphysics simulation *(Fig. 3)*.

We found that the reduced thermal expansion of the tuning post results in a lower capacitive coupling between the top surface of the post and the cavity, which impacts the stability of the resonance frequency. The key performance metrics for filters include minimal loss for the desired signals and adequate removal of undesired interference. Using simulation to determine the optimal combination of materials based on the environmental conditions where your cavity filter will be housed will enable a successful design.

S-PARAMETER STUDY OF TUNABLE CAVITY FILTER USING PIEZOELECTRIC ACTUATOR

In general, the resonant frequency of filter devices is a function of the electrical size of the cavity structure. By tweaking the physical shape of a structure, its corresponding resonance can be tuned. The adjusted amount of reactance, such as capacitive coupling inside of a cavity, may contribute to the lower resonant frequency obtained from a hollow cavity that's limited by electrical length.

The metallized rectangular post in the center of the cavity is not connected to the ceiling of the structure, leaving a thin gap that induces a strong capacitive coupling. The capacitance is stronger and more sensitive to the gap size variation when the gap is thinner.

To take advantage of this observation, we looked at deploying a circular disk made of a piezoelectric actuator on top of the cavity, right above the metallic post *(Fig. 4)*. The piezoelectric actuator is deformed by dc bias and controls the induced capacitive coupling between the top surface of the post and the bottom of the piezoelectric disk.

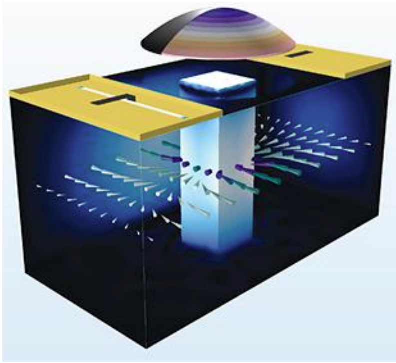

4. Shown here is surface plot of electric field norm on the cavity walls, contour plot of piezoelectric actuator displacement, and arrow plot of electric field in the middle of the cavity at 3.05 GHz with a dc bias of –300 V. The displacement plot is exaggerated for visualization purposes.

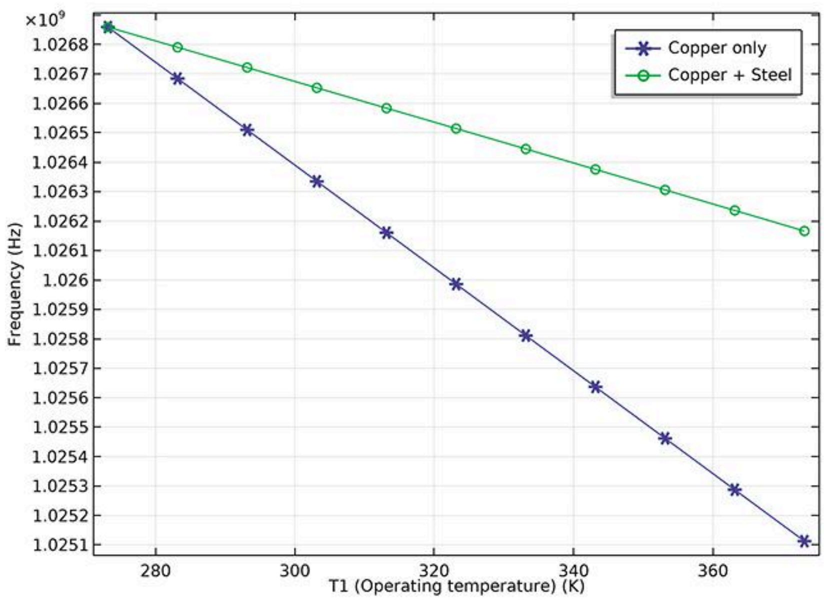

3. These plots show eigenfrequency as a function of temperature.

The filter's frequency response is tunable with the value of dc bias that generates different shape patterns of structural deformation.

The EM wave resonance behavior is affected by multiple physics phenomena. The deformation of the piezoelectric actuator with variable dc bias are numerically described in this model *(Fig. 5)*. These effects can be numerically examined through the following physics:

- Solid mechanics
- Electrostatics
- EM waves
- Moving mesh

The combination of solid mechanics and electrostatics describes how the piezoelectric actuator is mechanically deformed by a varying external electric potential. Within the same simulation environment, we evaluated the EM resonances by coupling it with the predefined Piezoelectric Effect Multiphysics node. The deformation of a piezoelectric device is captured by a moving mesh that reinitializes the numerical representation of the filter geometry for the EM analysis. Then, the cavity-resonant-mode analysis is excited by EM waves, which is analyzed in the given frequency range.

VIRTUALLY REALIZING REAL-WORLD EFFECTS ON YOUR COMPONENT DESIGN

COMSOL Multiphysics recently released updates to the RF Module that make it optimal for designing filter-type devices at conventional RF/microwave frequency ranges, as well as higher millimeter-wave (mmWave) and even terahertz (THz) bands. The software enables users to expedite the simulation process through model-order-reduction (MOR) techniques.

Traditional simulation models can be extended to include various physics phenomena that are not easily measured in the laboratory environment, such as heat effects on material properties as well as structural deformation. All of the physics are addressed in the same simulation environment, allowing for a comprehensive look into the design of your device. Whether you design cavity filters for the 5G future or not, it's imperative to include the real-world phenomena into your simulation model to achieve results that mimic the physical world we live in. mw

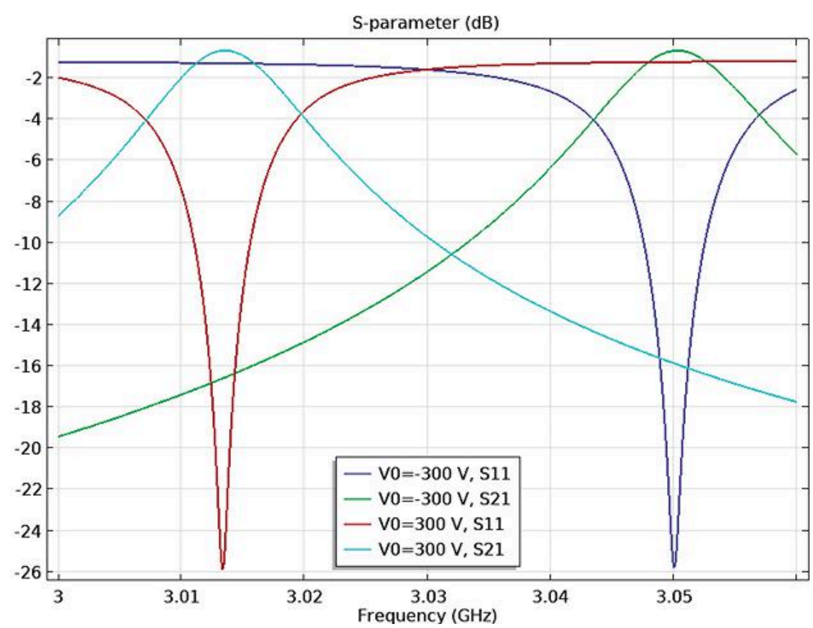

5. These S-parameter plots describe the resonant frequency change due to the different dc bias voltages applied on the piezoelectric actuator.

Product Feature

JACK BROWNE | Technical Contributor

Chip Attenuator Steps 31.5 dB to 55 GHz

This tiny flip-chip digital attenuator can control an attenuation range as wide as 31.5 dB in either 0.5- or 1.0-dB steps far into the mmWave frequency range.

Whether now as pSemi or formerly as Peregrine Semiconductor, the company has shown that its UltraCMOS silicon-on-insulator (SOI) semiconductor technology is quite capable of excellent electrical performance well into the millimeter-wave (mmWave) frequency range. Its latest demonstration is the model PE43508 digital step attenuator (DSA), a monolithic IC with 6-b digital control of a 31.5-dB attenuation range in 0.5- and 1.0-dB steps across the impressively wide frequency range of 9 kHz to 55 GHz.

With such high frequency coverage, this tiny step attenuator is well-suited for precision level control in various automotive and 5G mmWave circuits and test equipment. It maintains accurate attenuation across the attenuation and frequency ranges, with low return loss and insertion loss. In addition, it changes attenuation levels with 330-ns switching speed.

Model PE43508 is a 50-Ω IC DSA that can maintain 0.5-dB (or 1.0-dB) monotonicity across its 31.5-dB (or 31.0-dB) attenuation range. And it changes attenuation levels without positive glitches throughout the frequency range. As a result, no power spikes or attenuation errors occur even during constantly changing attenuation, as in an automatic-test-equipment (ATE) applications or satellite-communications (satcom) terminals. It's a high-performance companion to the company's two 60-GHz UltraCMOS switches (models PE42525 and PE426525) for mmWave circuit and system applications.

ACCURATE ATTENUATION

The DSA's RF performance is superior even across the wide frequency range. It's aided by the company's HaRP technology to achieve reduced gate lag and low drift in loss characteristics—the DSA suffers relatively low insertion and return losses through 55 GHz. For example, typical insertion loss is 4.7 dB from 26.5 to 45.0 GHz, 5.3 dB from 45.0 to 50.0 GHz, and 5.9 dB from 50 to 55 GHz. Typical return loss is 16 dB from 13.0 to 26.5 GHz, 14 dB from 26.5 to 45.0 GHz, and 13 dB from 45 to 55 GHz. The worst-case attenuation error is within +10% to +12% of a reading at the highest frequencies. The attenuator has a typical third-order input intercept point (IIP3) of +50 dBm.

Shown on an evaluation board as part of a development kit, the PE43508 single-chip SOI digital step attenuator provides as much as 31.5-dB attenuation from 9 kHz to 55 GHz.

The DSA supports 1.8-V control signals and has an optional VSS_EXT bypass mode. Its digital control interface allows both serial-addressable and parallel-programming modes. It can be controlled with direct-parallel, latched-parallel, and serial-addressable programming. The attenuator can also operate in normal or bypass modes. In normal mode, it runs with a single positive supply from 2.3 to 5.5 V and typically 170 µA. Bypass mode adds a negative −3-V supply (at typically 16 µA) with a positive supply from 3.1 to 5.5 V (at typically 122 µA).

The PE43508 is supplied as a flip-chip die, but it can also be mounted on ready-to-test printed circuit boards (PCBs) as part of evaluation kits *(see figure)*. It features a human-body-model (HBM) electrostatic-discharge (ESD) rating of 1 kV and an operating temperature range of −40 to +105°C. P&A: $50 (USD, 1000 qty.); samples. mw

PSEMI CORP. (formerly Peregrine Semiconductor and a Murata Co.), 9369 Carroll Park Dr., San Diego, CA 92121; (858) 731-9400, www.psemi.com.

CHRIS DeMARTINO | Technical Engineering Editor

Take the Guesswork Out of Discrete Circuit Design

A new software tool enables engineers to efficiently design circuits with models of actual vendor resistors, inductors, and capacitors, removing the need to manually determine correct part values after a design is built.

Designing circuits with discrete resistors, inductors, and capacitors can be a tricky problem for RF design engineers for several reasons. For example, consider the scenario in which a filter must be designed with discrete inductors and capacitors. In these situations, simple software tools are available that can automatically calculate the inductor and capacitor values. The software generates these values based on user-specified parameters, resulting in a filter design with an optimal frequency response.

However, these types of software tools also come with limitations. For one, they only calculate ideal inductor and capacitor values. Since real-world discrete inductors and capacitors are not ideal components, their actual performance does not entirely match the theoretical performance of ideal parts.

Specifically, real-world discrete inductors and capacitors contain parasitics that affect their performance. That means that the performance of a real filter designed with these components can differ significantly from the calculated performance of a theoretical filter designed with ideal parts of the same value.

The presence of parasitics is not the only factor that must be taken into account. With a software tool, a seemingly infinite amount of component values can be calculated to satisfy any given criteria. However, designers must keep in mind that vendors only manufacture inductors and capacitors with a finite number of values. Thus, it may not even be possible to obtain inductors and capacitors with the exact values generated by a software program. While one could simply find real parts with the closest values, this factor can nonetheless have an impact.

Another key consideration involves the physical effects of metal traces that connect the components together. This metallization impacts the overall filter performance, creating an additional challenge for designers.

When looking at all of these factors as a whole, it quickly becomes apparent that designing filters or other RF circuits (i.e., amplifiers, matching networks, diplexers, oscillators, etc.) with discrete inductors and capacitors is anything but a straightforward process. Oftentimes, obtaining desired results comes at the expense of a long and difficult trial-and-error process in the lab. Those who have experienced this can likely attest that it's a tedious operation.

To overcome these challenges, Keysight Technologies *(www.keysight.com)* added a feature to its Genesys software that can help designers save time and effort when designing and building circuits with discrete resistors, inductors, and capacitors. This feature, called Vendor Parts Synthesis (VPS), enables users to quickly design circuits using models of real vendor components. With VPS, both component parasitics and the finite number of real component values can be accounted for, provided that suitably accurate and scalable parasitic models for the components are available.

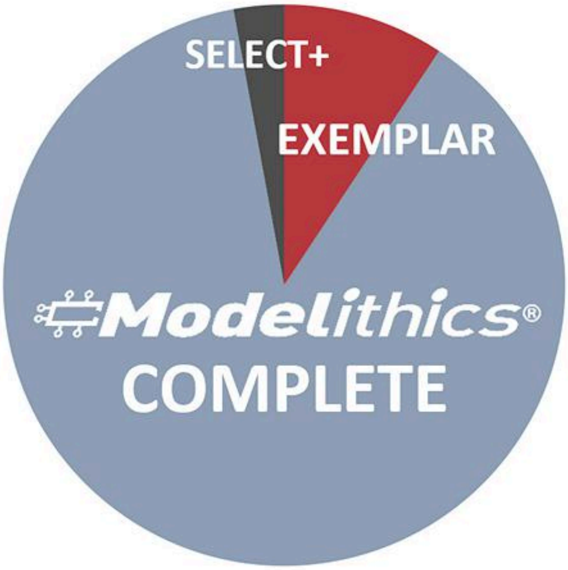

1. The Modelithics SELECT+ and EXEMPLAR Libraries are both subsets of the Modelithics COMPLETE Library.

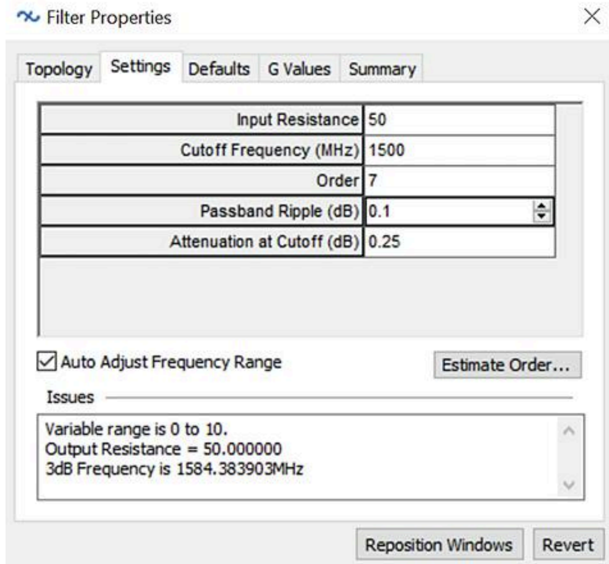

2. The filter is specified as a 7th-order lowpass filter with a cutoff frequency of 1,500 MHz.

In addition, VPS incorporates electromagnetic (EM)/circuit co-simulation to ensure accuracy. It also includes a yield analysis, which allows designers to determine the component tolerances needed to meet production requirements. This feature relies on integration of VPS with scalable parasitic models that enable statistical simulations.

VPS-enabled design flows are made possible by Modelithics *(www.modelithics.com)* Microwave Global Models, which are included in the Modelithics COMPLETE Library. These part-value scalable models accurately capture substrate-dependent parasitic behavior. They allow for optimization of part values as well as statistical simulations. The Modelithics SELECT+ Library, a subset of the COMPLETE Library *(Fig. 1)*, is now part of the Genesys software and contains the vendor part models used in the example presented in this article.

To demonstrate the VPS feature, this article focuses on a design example of a lowpass filter with a passband to 1.5 GHz. It details the design process and reveals the simulated results. Also presented is the measured data of two filters that were built, enabling a comparison between simulation and measurement results.

STARTING THE DESIGN PROCESS

Users can begin the design process by selecting *Syntheses>Passive Filter* from the Genesys workspace tree. *Figure 2* shows the resulting user interface. Clicking the *Topology* tab allows users to specify the type and shape of the filter along with the subtype. For this design, the type and shape are specified as *Lowpass* and *Chebyshev*, respectively. The subtype is set to *Minimum Inductor.*

As seen in *Fig. 2*, clicking the *Settings* tab allows users to specify the parameters. This design is a 7th-order lowpass filter with a cutoff frequency of 1,500 MHz. The passband ripple is specified to be 0.1 dB, while the attenuation at the cutoff frequency is specified at 0.25 dB. *Figure 3* shows the generated schematic based on the parameters entered. The results of the circuit simulation are given in *Figure 4*, including insertion loss and return loss plots.

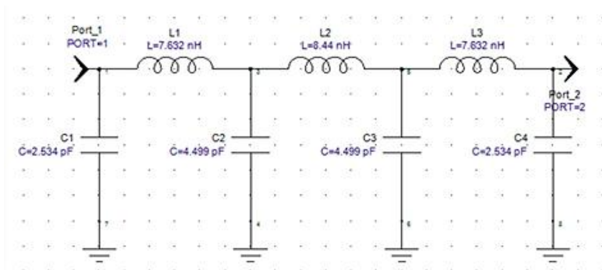

3. Shown is the filter schematic with ideal component values.

While these results clearly look acceptable, one must realize that the filter simply consists of ideal components rather than real-world parts. A closer inspection of the schematic reveals component values that are not standard manufacturer part values. On top of that, the simulation obviously does not account for the real-world physical effects of metal interconnections. Hence, the design process is still not complete at this point.

VPS TO THE RESCUE

It's at this stage in the process where VPS steps in. To start VPS, users can select *Syntheses>Vendor Parts Synthesis* from the workspace tree. Doing so will result in the *Vendor Parts Synthesis Properties* user interface *(Fig. 5)*. Clicking the *Configure Libraries* tab reveals the part libraries that are available for the design. The aforementioned Modelithics SELECT+ Library is selected here by default.

As shown in *Fig. 5*, selecting the *Defaults* tab lets users choose the part families they wish to use for the design. For this filter, the Kemet *(www.kemet.com)* CBR06 capacitor part family and Coilcraft *(www.coilcraft.com)* 0603CS inductor part family are selected. Users can also specify the component tolerances. For now, both part families are set to a tolerance of 10%, which is the default value. However, this will be examined in more detail later when a yield analysis is performed.

Clicking *Apply* will prompt users to select a substrate. For this filter, the chosen substrate is 20-mil-thick Rogers RO4350B from the Modelithics SUBSTRATE Library, which is a collection of measurement-based substrate definitions.[1]

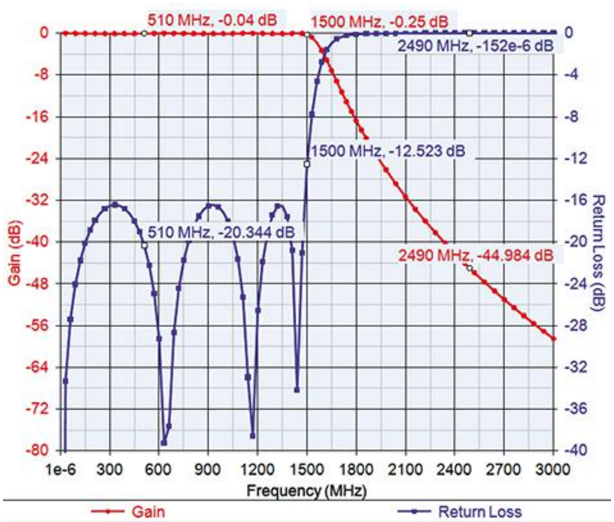

4. This is the simulated frequency response of the generated filter with ideal components.

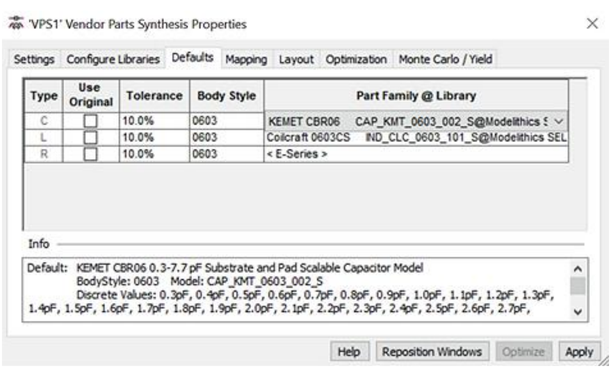

5. Designers can select the part families they wish to use in the *Vendor Parts Synthesis Properties* user interface.

The next step is to generate a layout by clicking the *Layout* tab in the *Vendor Parts Synthesis Properties* user interface *(Fig. 6)*. Note that the *Generate Momentum Analysis* checkbox must be checked so that an EM/circuit co-simulation can be performed later. Users can also specify the *Trace Width*, which is set here to 44.6 mils. *Length of C, L, and R Connections* and *Port Connection Length* are two additional parameters that users can specify. For this design, these parameters are set to 28 and 197 mils, respectively. Clicking *Apply* generates a new VPS schematic *(Fig. 7)*.

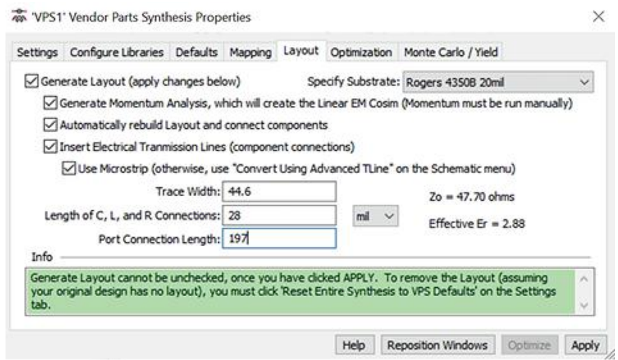

6. Layouts can be automatically generated. Users can specify *Trace Width; Length of C, L, and R Connections;* and *Port Connection Length*.

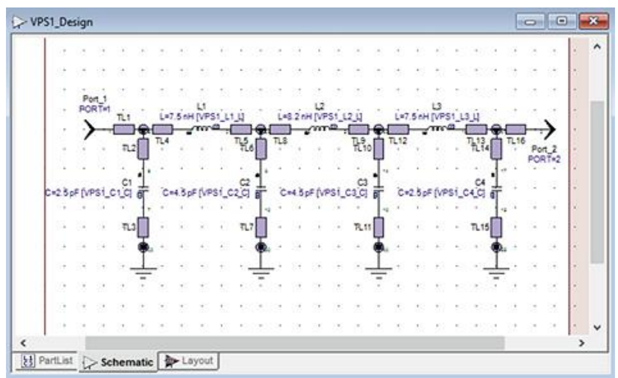

7. The VPS schematic includes components from the Kemet and Coilcraft part families along with microstrip interconnections and junction discontinuities.

The VPS schematic includes components from the selected part families with values that are as close as possible to the component values in the original, or reference, schematic. This new schematic also includes microstrip interconnections and junction discontinuities. *Figure 8* shows the results obtained from the simulation of the new VPS circuit along with the results of the original circuit simulation. The frequency response of the new VPS circuit is shifted downward by about 300 MHz in comparison to the original circuit's frequency response.

Ultra Low Phase Noise
Phase Locked Clock Translators

Model	Frequency	Ref. Input	DC Bias	Typical Phase Noise (dBc/Hz)				Package
	(MHz)	(MHz)	(VDC)	100 Hz	1 kHz	10 kHz	100 kHz	
FCTS800-10-5	800	10	+5, +12	-87	-116	-144	-158	
KFCTS800-10-5	800	10	+5, +12	-87	-116	-144	-158	
FCTS1000-10-5	1000	10	+5, +12	-75	-109	-140	-158	
FCTS1000-10-5H	1000	10	+5, +12	-84	-116	-144	-160	
FCTS1000-100-5 *	1000	100	+5, +12	-75	-109	-140	-158	
KFCTS1000-10-5 *	1000	10	+5, +12	-75	-109	-140	-158	
FCTS2000-10-5 *	2000	10	+5, +12	-80	-105	-135	-158	
FCTS2000-100-5 *	2000	100	+5, +12	-80	-105	-135	-158	
KFCTS2000-100-5 *	2000	100	+5, +12	-80	-105	-135	-158	
FSA1000-100	1000	100	+3.3, +5, +12	-105	-115	-145	-160	
KFSA1000-100	1000	100	+12	-105	-115	-145	-160	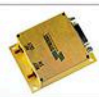
FXLNS-1000	1000	100	+5, +12	-120	-140	-149	-154	
KFXLNS-1000	1000	100	+12	-120	-140	-149	-154	

** New for 2018*

Up to 3.0 GHz

Features

- Cost Effective
- Replaces Noisy Frequency Multipliers
- No Programming Required
- Lead Free RoHS Compliant

Applications

- Scanning & Radar Systems
- ADC & DAC Fast Clocking & Sampling
- Test & Measurement Equipment
- High Performance Frequency Converters
- Base Station Applications
- Front End Converter LO's

Talk To Us About Your Custom Requirements.

SYNERGY®
MICROWAVE CORPORATION

Phone: (973) 881-8800 | Fax: (973) 881-8361
E-mail: sales@synergymwave.com | Web: www.synergymwave.com
Mail: 201 McLean Boulevard, Paterson, NJ 07504

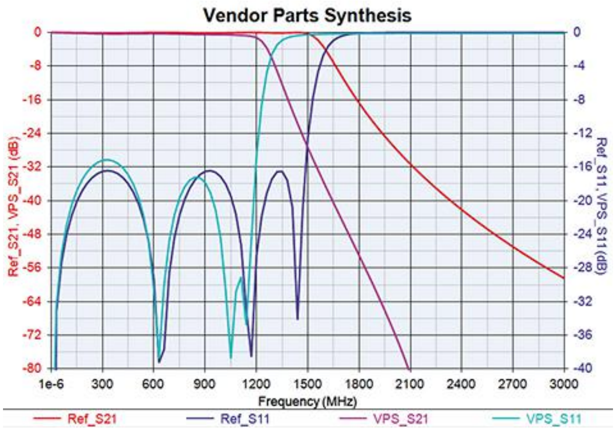

8. The simulated frequency response of the new VPS circuit is shifted downward in comparison to the simulated frequency response of the original circuit.

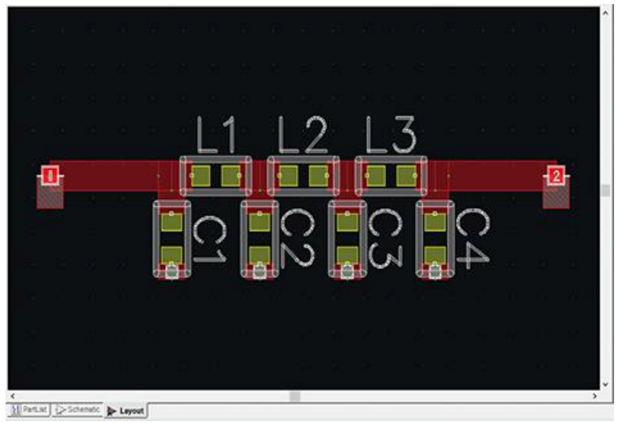

9. This is the layout of the lowpass filter.

A circuit simulation only represents part of the task at hand. To ensure accuracy, an EM/circuit co-simulation must be performed. First, the actual layout can be viewed by clicking the *Layout* tab *(Fig. 9)*. By right-clicking *VPS1_Momentum* in the workspace tree and selecting *Run (calculate now)*, users can perform an EM/circuit co-simulation *(Fig. 10)*. *Figure 11* shows the results of the EM/circuit co-simulation along with the results of the previous VPS and reference circuit simulations. One can see that the EM/circuit co-simulation deviates even further from the desired performance.

OPTIMIZING THE FILTER AND PERFORMING A YIELD ANALYSIS

Since the simulation results clearly show that the filter does not meet the required performance, the next step is to optimize the design. Users can begin the optimization process by clicking the *Optimization* tab in the *Vendor Parts Synthesis Properties* user interface *(Fig. 12)*.

As seen in *Fig. 12*, the optimization process first involves what's known as a *Continuous Optimization*. That step is followed by a *Grid Optimization*, which is a grid search of the

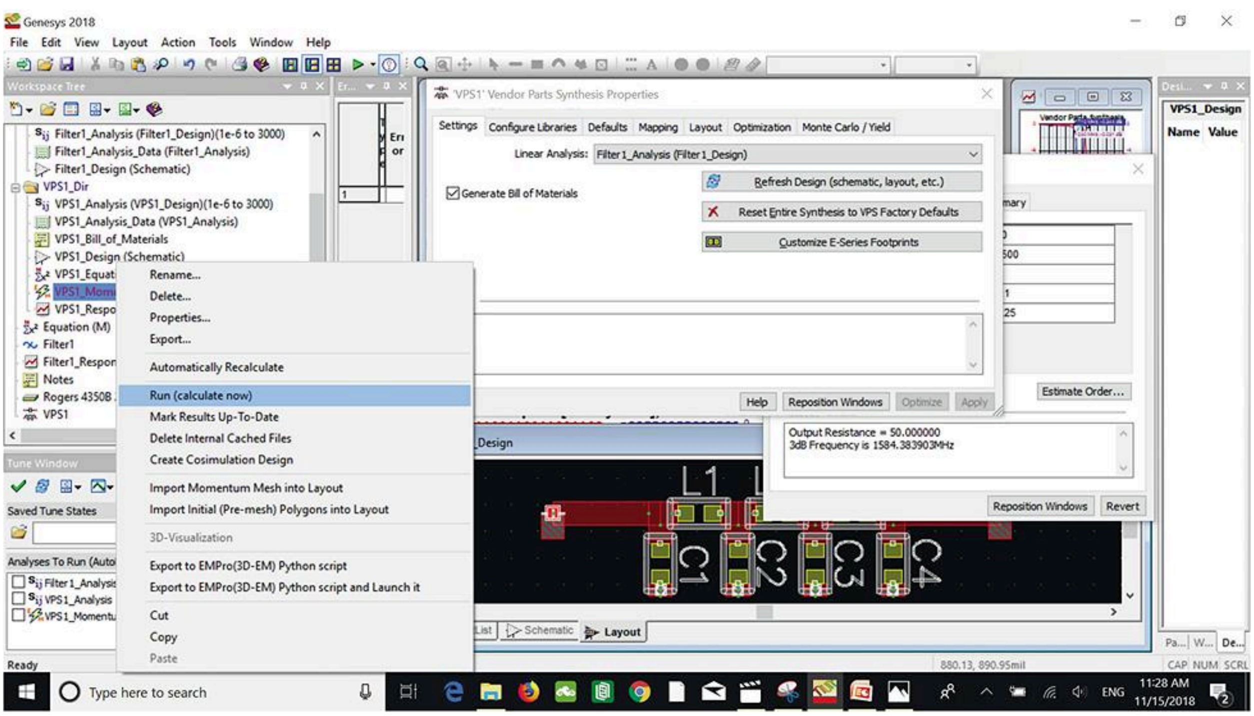

10. An EM/circuit co-simulation can be executed by right-clicking *VPS1_Momentum* in the workspace tree and selecting *Run (calculate now)*.

The VPS schematic includes components from the selected part families with values that are as close as possible to the component values in the original, or reference, schematic. This new schematic also includes microstrip interconnections and junction discontinuities. *Figure 8* shows the results obtained from the simulation of the new VPS circuit along with the results of the original circuit simulation.

nearest component values. By default, the *Grid Steps Up* and *Grid Steps Down* parameters are each set to one, meaning the software will search one step up and one step down in value. For this example, these default settings are left intact, resulting in 2,187 total grid steps.

Clicking *Apply* subsequently prompts users to specify the optimization goals. For this filter, the optimization goal is set to 1 dB for the passband transmission and 16 dB for the passband reflection. For the stopband transmission, the optimization goal is set to 25 dB. VPS automatically identifies the stopband frequency range, which in this case starts at a frequency of 1,956.31 MHz.

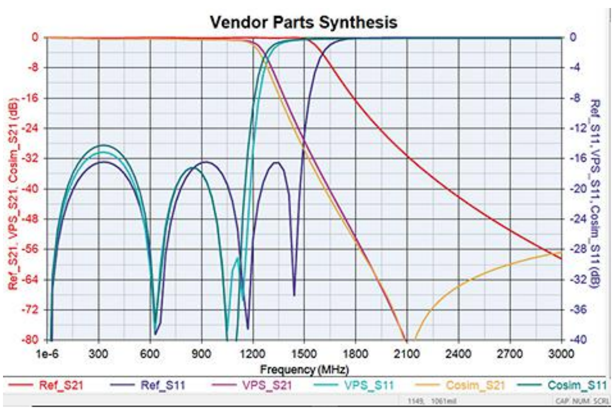

11. The EM/circuit co-simulation results stray even further from the desired performance.

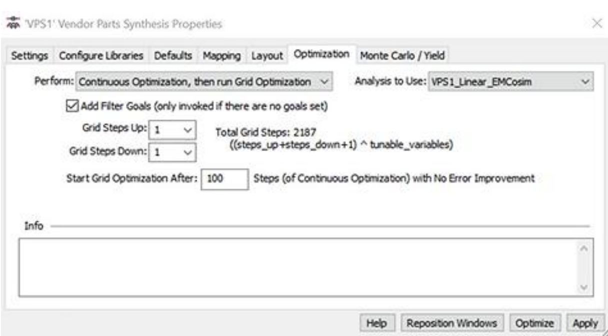

12. The optimization process involves two steps: ***Continuous Optimization*** followed by ***Grid Optimization***.

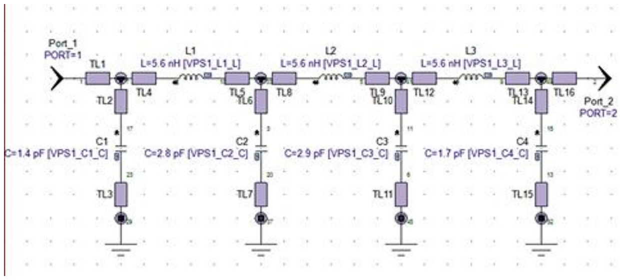

13. Following optimization, a new VPS schematic is generated with updated component values.

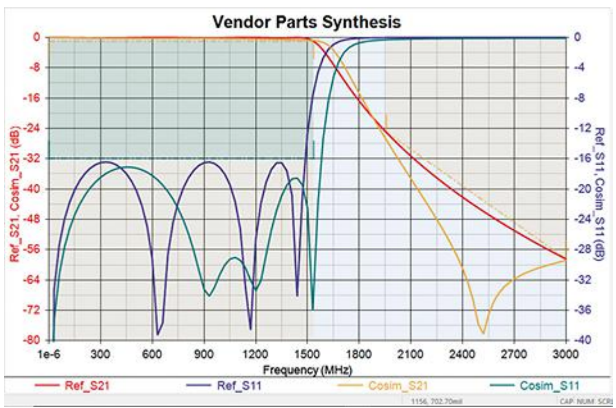

14. The new EM/circuit co-simulation results reveal a frequency response that meets the desired performance.

Performing the optimization leads to a new VPS schematic with optimized component values *(Fig. 13)*. *Figure 14* shows the EM/circuit co-simulation results of the optimized filter along with the results of the reference circuit simulation. They demonstrate that the filter now achieves the desired performance.

A yield analysis is the next and last step. It allows designers to determine if the component tolerances are sufficient for production requirements. To perform a yield analysis, users must click the *Monte Carlo / Yield* tab in the *Vendor Parts Synthesis Properties* user interface *(Fig. 15)*. All components are listed, each with a tolerance of 10% as specified earlier. After first clicking *Apply* in the interface shown in *Fig. 15*, users

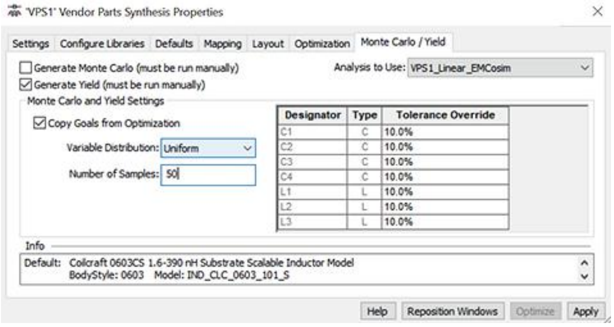

15. Shown is the user interface for performing a yield analysis. All components and their tolerances are listed.

	Original Value	Final Value
C1	2.534 pF	1.4 pF
C2	4.499 pF	2.8 pF
C3	4.499 pF	2.9 pF
C4	2.534 pF	1.7 pF
L1	7.632 nH	5.6 nH
L2	8.44 nH	5.6 nH
L3	7.632 nH	5.6 nH

Shown is a comparison of the original and final component values.

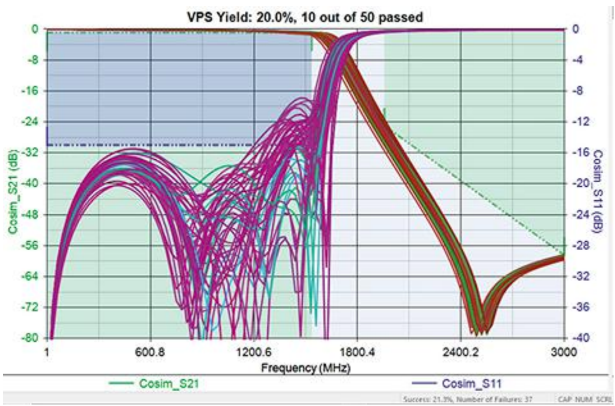

16. The yield is only 20% when all components have a 10% tolerance.

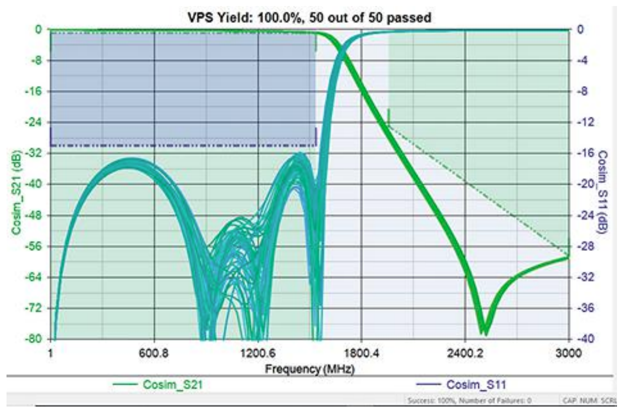

17. A 100% yield is achieved after specifying different component tolerances.

can run the yield analysis by right-clicking *VPS1_Yield* in the workspace tree and selecting *Run (calculate now)*.

The results of the yield analysis are depicted in *Figure 16*, revealing that a 10% tolerance for all components only produces a 20% yield. To increase the yield, the three inductors were each set to a tolerance of 2%; C1 and C4 were each set to a tolerance of ±0.05; and C2 and C3 were each set to a tolerance of ±0.1. Modifying the component tolerances is achieved via the previously shown user interface *(Fig. 15, again)*.

Figure 17 reveals the outcome of the new yield analysis: the new component tolerances result in a 100% yield. As a side note, while the tolerances of C2 and C3 could each have been set to ±0.05, it was determined that a tolerance of ±0.1 for each still produced a 100% yield. The design process is complete at this stage. VPS also conveniently generates a bill of materials (BOM) for the design.

The *table* compares the final component values with the component values of the original schematic.

There's quite a noticeable difference between the final and original values, thereby illustrating the difficulty of manually trying to determine the correct component values.

MEASUREMENT RESULTS AND CLOSING

To validate the simulated results presented, two filters were built and measured *(Fig. 18)*. The filters were built with the same Kemet capacitors and Coilcraft inductors included in the simulations. *Figure 19* shows the measured data of both filters along with the simulated results of the yield analysis. The measured data agrees with the simulated results, as both the measured insertion loss and return loss closely match the simulated results. Hence, the measured data validates the effectiveness of VPS.

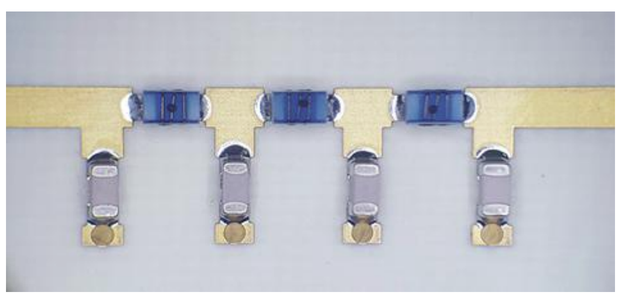

18. This is one of the filters that was built. The actual Kemet capacitors and Coilcraft inductors are shown here.

Product SPOTLIGHT

The latest product information presented by

Mini-Circuits®

www.minicircuits.com

DC Pass Directional Coupler Conquers 2.0 to 26.5 GHz

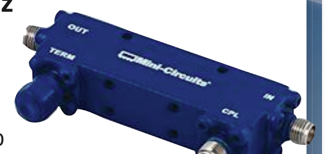

Mini-Circuits' model ZCDC20-02263S+ is a DC-pass directional coupler with broadband frequency range of 2 to 26.5 GHz. It maintains 20-dB coupling with typical coupling flatness of ±0.5 dB and typical directivity of 18 dB to 26.5 GHz. The 50-Ω directional coupler handles power levels to 20 W with mainline loss of typically only 0.3 dB from 2 to 8 GHz, 0.5 dB from 8 to 18 GHz, and 0.7 dB from 18 to 26.5 GHz. The input and output return loss is typically 39 dB from 2 to 8 GHz, 31 dB from 8 to 18 GHz, and 23 dB from 18 to 26.5 GHz. The RoHS-compliant directional coupler measures 2.25 × 0.7 × 0.5 in. (57.15 × 17.78 × 12.70 mm) with female SMA connectors. It is well suited for communications infrastructure and test applications and is designed for operating temperatures from -55 to +100°C.

8-Way Splitter/Combiner Spans 6 to 26.5 GHz

Mini-Circuits' model ZC8PD-06263+ is a wideband, eight-way, 0-deg. power splitter/combiner capable of handling as much as 20 W as a splitter from 6 to 26.5 GHz. Well suited for communications and test applications, the power splitter/combiner passes DC (as much as 530 mA) from input to output and features low insertion loss (above the 9-dB splitting loss) of typically 1.2 dB to 18 GHz and 2.1 dB to 26.5 GHz. It maintains good amplitude and phase unbalance, with typically 0.19 dB and 4.4 deg., respectively, across the full frequency range. Full-band isolation between ports is typically 28 dB. The RoHS-compliant, 50-Ω power splitter/combiner measures just 1.93 × 4.09 × 0.5 in. (49.02 × 103.89 × 12.70 mm) with female SMA connectors and is designed for operating temperatures from -55 to +100°C.

DC Block Connects 10 MHz to 65 GHz

Mini-Circuits' model BLK-E653+ is a coaxial DC block with extremely wide frequency range of 10 MHz to 65 GHz. It achieves low insertion loss of typically 0.6 dB to 50 GHz and 0.7 dB to 65 GHz, handling input voltage as high as 16 V and input power as high as +30 dBm (1 W). Suitable for test-and-measurement, defense, and communications applications, the RoHS-compliant DC block has typical return loss of 22 dB across the full frequency range. The broadband DC block features a rugged stainless-steel body and coupling nut and female 1.85-mm connectors. It is designed for operating temperatures from -55 to +100°C.

RF Transfer Switch Matrix Routes DC to 18 GHz

Mini-Circuits' model RC-2MTS-18 is an RF transfer switch matrix with wide frequency range of DC to 18 GHz. Ideal for automated test and switch matrix applications, it consists of a pair of independently controlled electromechanical transfer switches which can be operated under USB or Ethernet connection. The transfer switch matrix handles cold switching of signal power levels to 10 W with typical switching speed of 25 ms, and features high reliability, rated for 10 million switching cycles. The 50-Ω unit maintains low insertion loss of typically 0.1 dB to 8 GHz and 0.25 dB to 18 GHz, with high isolation between ports of typically 100 dB to 1 GHz, 90 dB to 8 GHz, 86 dB to 12 GHz, and 76 dB to 18 GHz. The full-band VSWR is typically 1.15:1 or better. The RF transfer switch matrix measures 6.0 × 5.5 × 2.25 in. (152.4 × 139.7 × 57.2 mm) with 8 female SMA connectors.

LNA Boosts 50 MHz to 4 GHz

Mini-Circuits' model CMA-103+ is a monolithic E-pHEMT low-noise amplifier (LNA) ideal for a wide range of applications from 50 MHz to 4 GHz. The RoHS-compliant LNA is supplied in a low-profile, nitrogen-filled, hermetically sealed ceramic case and is tested to meet MIL requirements for gross leak, thermal shock, vibration, acceleration, mechanical shock, and HTOL. It offers typical gain of 26.3 dB at 50 MHz, 16.3 dB at 1 GHz, 7.9 dB at 3 GHz, and 5.8 dB at 4 GHz, all for bias supplies of 5 and 3 V dc. The noise figure is typically 0.4 dB to 400 MHz, 0.5 dB to 1 GHz, and 1.3 dB to 4 GHz. Typical output power at 1-dB compression is +20.0 dBm at 50 MHz, +22.2 dBm at 1 GHz, and +24.2 dBm at 4 GHz. The LNA measures 0.12 × 0.12 × 0.045 in. and is designed for operating temperatures from -40 to +125°C.

Low Pass Filter Screens DC to 1 GHz

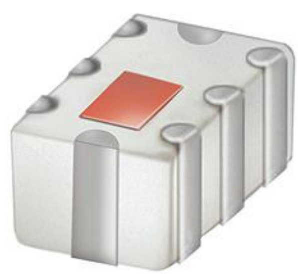

Mini-Circuits' model LFCG-1000+ is a miniature low pass filter well suited for harmonic rejection and rejection of unwanted high-frequency signals in tight PCB designs. It features 0.8-dB typical insertion loss and typical 1.20:1 VSWR across a passband of DC to 1 GHz, with high typical stopband rejection of 45 dB from 1.5 to 3.0 GHz and at least 30 dB from 1.5 to 10.0 GHz. The 50-Ω low pass filter is based on low-temperature-cofired-ceramic (LTCC) technology and delivers excellent stability with temperature, for an operating temperature range of -40 to +85°C. The filter handles input power levels to 6 W and is supplied in a compact ceramic 0805 package measuring 0.079 × 0.049 × 0.037 in. (2.00 × 1.25 × 0.95 mm).

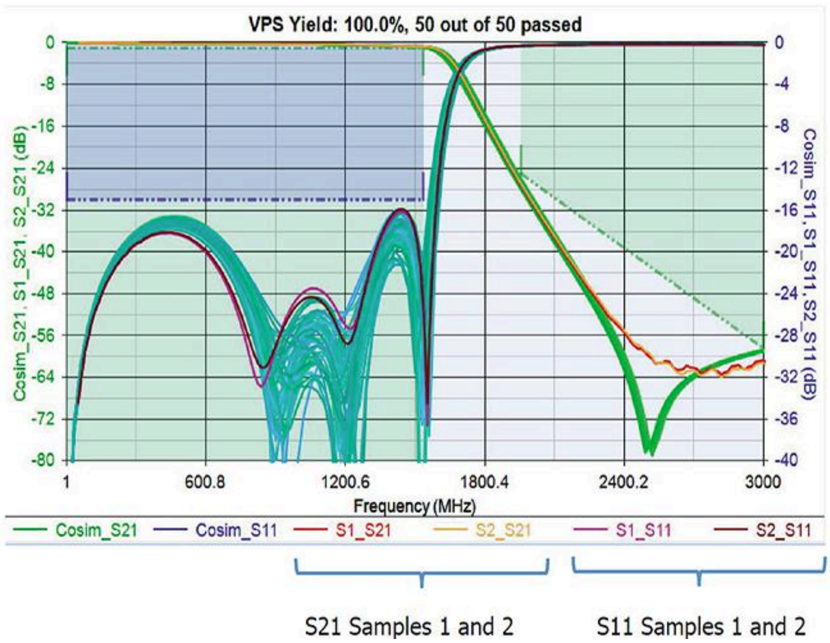

19. Both filters were measured to demonstrate that the measured data corresponded to the simulated results.

In closing, VPS is an effective tool that can rescue designers from the headaches that come with manually trying to determine correct resistor, inductor, and capacitor values when building any RF circuit in the lab. Since VPS allows designers to easily design circuits with scalable actual vendor part models from Modelithics, it effectively eliminates the process of finding the right components by guesswork. The result is a much quicker, much cheaper, and much less painful process. mw

ACKNOWLEDGEMENTS

I would like to thank How-Siang Yap from Keysight Technologies for his support. I would also like to thank Laura Levesque and everyone at Modelithics for their support and for building and testing the filter presented in this article.

REFERENCE:

1. The Modelithics Substrate Library can be requested as a free update by contacting Modelithics at support@Modelithics.com. Please mention this article with the request.

New Products

WR75 Circulators, Loads Handle High Power

THE SPACENXT KU SERIES of high-power WR75 circulators and loads are designed for use in MEO/GEO satellite-communications (satcom) systems. The components feature low loss from 10.70 to 12.75 GHz. Circulators exhibit 0.11-dB insertion loss and 20-dB minimum return loss at operating temperatures from –25 to +125°C, while loads have minimum return loss of 20 dB over the same temperature range. Circulators handle 350 W CW power; loads are rated for as much as 267 W CW power. The components are sealed for electromagnetic compatibility (EMC) and constructed with a low mass-aluminum housing with chromate finish..

SMITHS INTERCONNECT, 8851 SW Old Kansas Ave., Stuart, FL 34997, (772) 286-9300, www.smithsinterconnect.com

Directional Coupler Is Ready for Space

MODEL 101040010SQ is a space-qualified directional coupler with extremely broadband frequency range of 1 to 40 GHz. The stripline design maintains 10-dB coupling across the frequency range with coupling flatness of ±1 dB and frequency sensitivity of ±1.52 dB. The insertion loss is 1.3 dB or better from 1 to 20 GHz and 1.7 dB or better from 20 to 40 GHz. The coupler provides better than 14-dB directivity from 1 to 20 GHz and better than 10 dB from 20 to 40 GHz. The worst-case VSWR is 1.50:1 from 1 to 20 GHz and 1.70:1 from 20 to 40 GHz. The coupler, which is supplied with female 2.4-mm connectors, can handle 20 W average power and 3 kW peak power. It measures 2.00 × 0.40 × 0.65 in. and weighs just 1.3 oz.

KRYTAR, INC., 1288 Anvilwood Ct., Sunnyvale, CA 94089, (408) 872-8376, e-mail: sales@krytar.com, www.krytar.com

Dual Directional Coupler Runs 20 to 520 MHz

MODEL ZDDC-50-521+ is a dc-pass, dual directional coupler with excellent coupling and low loss from 20 to 520 MHz. Across that wide frequency range, the insertion loss is typically just 0.1 dB. It maintains 50-dB coupling with typical coupling flatness of ±0.95 dB across the full frequency range. Well-suited for commercial and military applications requiring high power-handling capability, the RoHS-compliant coupler is rated for maximum input power of 400 W at a case temperature of +85°C and maximum input power of 300 W at a case temperature of +105°C. The input/output return loss is typically 38 dB from 20 to 150 MHz and 28 dB from 150 to 520 MHz. The coupler, which has an operating temperature range of –55 to +105°C, can pass as much as 4 A dc from input to output. It's splash- and water-resistant per the IP67 immersion standard and comes in a rugged metal case measuring 3.0 × 2.154 × 0.975 in. (76.20 × 54.71 × 24.75 mm) with female Type N input and output connectors and female SMA coupled-port connectors.

MINI-CIRCUITS, P.O. Box 350166, Brooklyn, NY 11235-0003, (718) 934-4500, www.mini-circuits.com

Peel-and-Stick Antennas Cover L, S, and C bands

THE PEEL & STICK APPLIQUE antennas for unmanned-aerial-vehicle (UAV) and drone applications, including for mobile ad hoc network (MANET) radios, operate over frequency ranges within the span of 30 MHz to 10 GHz. They are less than 10 mils thick and weigh less than 1 oz. The antennas are supplied with a durable, one-time-application adhesive on one side of the radiator that attaches the antenna to a surface. The antennas are suitable for attachment to noncarbon UAVs such as those constructed of fiberglass, Kevlar, or polypropylene.

PHARAD LLC, 1340 Charwood Rd., Ste. L, Hanover, MD 21076, (410) 590-3333, FAX: (410) 590-3555, www.pharad.com

Calibration Kit Serves VNAs from 60 to 90 GHz

MODEL STQ-TO-12-U3-CKIT1 is an E-band waveguide calibration kit for vector network analyzers with a frequency range of 60 to 90 GHz. It includes two straight waveguide sections, one fixed short, one fixed impedance-matching load, one sliding load, one quarter-wavelength offset, two waveguide quick connects, 10 3/32 hex head waveguide screws, a 3/32-in. hex waveguide screwdriver, and one calibration data USB drive. The calibration kit is supplied in a wooden box.

SAGE MILLIMETER INC., 3043 Kashiwa St., Torrance, CA 90505, (424) 757-0168, FAX: (424) 757-0188, E-mail: sales@sagemillimeter.com, www.sagemillimeter.com

Power Dividers/Combiners Cover Bands to 18 GHz

A LINE OF two-way power dividers/combiners provides frequency coverage in octave and multi-octave bands from 0.005 to 18.0 GHz. The component series includes models for 500 MHz to 1 GHz, 2 to 4 GHz, 4 to 8 GHz, and 8 to 18 GHz. Performance levels from 500 MHz to 1 GHz include 20 dB minimum isolation, 1.20:1 maximum VSWR, 0.3 dB maximum insertion loss, ±0.2 dB amplitude balance, and ±2 deg. phase balance. From 2 to 4 GHz, it has 20 dB isolation between ports, 1.30:1 VSWR, 0.3 dB maximum insertion loss, ±0.2 dB amplitude balance, and ±3 deg. phase balance. From 4 to 8 GHz, the performance levels include 18 dB maximum isolation, 1.60:1 maximum VSWR, 0.6 dB maximum insertion loss, ±0.2 dB worst-case amplitude balance, and ±4 deg. worst-case phase balance. From 8 to 18 GHz, the power divider/combiner performance is 16 dB minimum isolation, 1.60:1 maximum VSWR, 1.0 dB minimum insertion loss, ±0.5 dB worst-case amplitude balance, and ±6 deg. worst-case phase balance. All units are equipped with aluminum housings and SMA female connectors and rated for 20 W average power and 1 kW peak power.

ARRA, INC., 15 Harold Ct., Bayshore, NY 11706; (631) 231-8400, www.arra.com

This index is provided as an additional service by the publisher, who assumes no responsibility for errors or omissions.

Subscription Assistance and Information:
(ISSN 0745-2993)
Microwaves & RF is published monthly. Microwaves & RF is sent free to individuals actively engaged in high-frequency electronics engineering. In addition, paid subscriptions are available. Subscription rates for U.S. are $95 for 1 year ($120 in Canada, $150 for International). Published by Informa Media Inc., 9800 Metcalf Ave., Overland Park, KS 66212-2216. Periodicals Postage Paid at Kansas City, MO and additional mailing offices. POSTMASTER: Send change of address to Microwaves & RF PO Box 2100, Skokie, IL 60076-7800. For paid subscription information, please contact Microwaves & RF at PO Box 2100, Skokie IL 60076-7800. Canada Post Publications Mail agreement No. 40612608. Canada return address: IMEX Global Solutions PO Box 25542, London ON N6C 6B2.


The sweetest & largest
assortment of
Miniatures
in the world . . .
from ARRA of course!
For your "sweet tooth" . . .
Miniature
Variable Attenuators
Bands from DC–18GHz
Some models feature:
♥ Extremely flat attenuation vs. frequency response
♥ Constant phase with △ attenuation.
The ultimate in reliability, and wear-free performance . . . achieved with ARRA's non-contacting method of attenuating.
Most units incorporate ARRA's proprietary attenuating elements which give excellent stability over a wide temperature range.
Customerized to your requirements.
Contact us at 631-231-8400 or sales@arra.com.
. . . the last word in variable attenuators
ARRA INC.
Visit our website at www.arra.com
15 Harold Court, Bay Shore, N.Y. 11706 • 631-231-8400

BUY NOW

TAKE ADVANTAGE OF FALL PROMOTIONS

Experience the **CPS2008** for FREE

For a limited time, when you purchase a 4500C Peak Power Analyzer or an RTP5000 Real-Time Peak USB Power Sensor, **get a CPS2008 for FREE.**

CPS2008 True-Average Connected Power Sensors

Trade in your power analyzer for the NEW **4500C**

15% trade in for a 4500B

10% trade in for any 4500/4400 models

4500C Peak Power Analyzer

For more information, contact your local salesperson at 973-386-9696 or visit boonton.com.

This offer cannot be combined with any other promotions. Valid until 12/31/2018.

Boonton

Leaders in RF Power Measurement for more than 70 Years